Studies of DTF and TTFV-based Donor-Acceptor Systems and Redox-Active Polymer Thin Films

by

A thesis submitted to the School of Graduate Studies in partial fulfilment of

the requirements for the degree of

MS.c

Department of Chemistry

Memorial University of Newfoundland

April 2022

St. John's Newfoundland

Abstract

1,4-Dithiafulvene (DTF) is a five-member heterocycle that has been frequently used as a redox-active molecular building block in various organic electronic materials. The combination of two DTF groups via an exo-ring C=C bond leads to formation of well-known tetrathiafulvalene (TTF), which has been extensively studied since the first discovery of its metallic conductivity. Previous research has demonstrated that DTF and tetrathiafulvalene vinylogue (TTFV)-based conjugated molecules and polymers show favored intermolecular interactions (e.g., π–π stacking and charge-transfer interactions) with electron-deficient nitroaromatic compounds (NACs), owing to the electron-donating nature of DTF and TTFV groups. Such properties can be utilized in the design of chemical sensors for detection of NACs, which are an important class of pollutants in the environment. To further understand the interplay between NACs and DTF/TTFV-containing π-systems, a group donor–acceptor ensembles containing nitrophenyl-substituted DTF and TTFV moieties have been investigated in this thesis work. Detailed synthetic methods and structure-property relationships will be discussed in the first chapter. In particular, the structural, electronic, and electrochemical redox properties were systematically examined by X-ray single crystallographic, UV-Vis absorption, and cyclic voltametric analyses, in conjunction with density functional theory (DFT) modeling. With the fundamental properties characterized and understood, a new type of TTFV-based redox-active polymer was next designed and prepared. In the second part of this project, a strategy of double-layer polymer film will be introduced. With this method, robust and redox-active TTFV polymer thin films could be efficiently generated on the

surface of glassy carbon electrodes. These modified electrodes were found to show sensitive responses to various phenolic compounds at low concentrations (10^{-8} to 10^{-7}M), suggesting promising application in rapid electrochemical sensing of phenol derivatives and related chemicals.

Acknowledgements

First of all, I would like to express my sincere thanks to my supervisor Dr. Yuming Zhao for his guidance and support during my research work and thesis writing. Yuming is a person who I always want to be. He is kind, supportive, knowledgeable, and the best teacher. He is the most helpful person that I know. I have learned so much from him in chemistry, science, and lifestyle, and this has been such a great research experience for me. I would like to thank my co-supervisor, Prof. Baiyu H. Zhang, and my supervisory committee member, Dr. Talia Jane Stockmann, for their help and guidance throughout my program. I would like to thank Dr. Jian-Bin Lin, one of the best crystallographers in Canada. Dr. Lin is very supportive, hard working, and knowledgeable. I would also like to thank my lovely Mother and my family for their encouragement and support during my entire life.

I would also like to thank my fantastic group members, Zahra Ahmadian Tabasi, Ramin Eradeh, Monther Zeird, Maryam Faghih Abdollahi, Roxana Fazli, Fatemeh Salami, Farshid Shahrokhi, as well as other research groups in the Department of Chemistry. They have helped me a lot during my program.

I would like to thank all of my friends in St. John's. They are like a family for me, and I had lots of happy times with them.

Last but not the least, I would also like to thank all the faculty members and staff at the Department of Chemistry, Memorial University for creating such a great and friendly environment for students. I sincerely thank Memorial University and NSERC for funding and support.

Contents

List of Figures

List of Schemes

List of Abbreviations and Symbols

AFM	atomic force microscopy
AIEE	aggregation-induced enhanced emission
APPI	atmospheric pressure photo-ionization
aq	aqueous
BCP	bond critical point
BN	binaphthalene
ca.	circa
calcd	calculated
CBPQT	cyclobis(paraquat-*p*-phenylene)
CCDC	Cambridge Crystallographic Data Centre
CD	circular dichroism
CDCA	chenodeoxycholic acid
CL	chemiluminescence

cm	centimeter(s)
CP	conducting probe
C-T	charge-transfer
CV	cyclic voltammetry
d	doublet
COF	covalent organic framework
D-A	donor-acceptor
DFT	density functional theory
DMF	dimethylformamide
DMSO	dimethyl sulfoxide
DNA	deoxyribonucleic acid
DNT	2,4-dinitrotoluene
DSSC	dye-sensitized solar cell
DTF	dithiafulvene or dithiafulvenyl
Et	ethyl
E_g	band gap
exTTF	π-extended tetrathiafulvalene

FTIR	fourier transform infrared
FMO	frontier molecular orbital
g	gram(s)
h	hour(s)
HOMO	highest occupied molecular orbital
HRMS	high-resolution mass spectrometry
Hz	hertz
I	current
ICT	intramolecular charge transfer
ITO	indium tinoxide
IR	infrared
ISE	isomerization stabilization energy
J	coupling constant
LUMO	lowest unoccupied molecular orbital
m	multiplet
m/z	mass-to-charge ratio
MALDI-TOF	matrix-assisted laser desorption/ionization–time of flight

MCBJ	mechanically controlled break-junction
Me	methyl
mg	milligram(s)
MHz	megahertz
min	minute(s)
mL	milliliter(s)
mmol	millimole(s)
mol	mole(s)
MOF	metal organic framework
m.p.	melting point
MS	mass spectrometry
mV	millivolt(s)
mW	milliwatt(s)
NBO	natural bonding orbital
NCI	noncovalent interaction
NICS	nucleus independent chemical shift
NIR	near-infrared

NLO	nonlinear optical
nm	nanometer(s)
NMR	nuclear magnetic resonance
NMI	*N*-methylimidazole
OFET	organic field-effect transistor
OLED	organic light-emitting diode
OPE	oligo(phenylene ethynylene)
OPV	organic photovoltaic cell
ORTEP	Oak Ridge thermal ellipsoid plot
ox	oxidation
η	power conversion efficiency
PAH	polycyclic aromatic hydrocarbon
PET	photoinduced electron transfer
PI	pyrenoimidazole
PIMNA	pyrenoimidazole coupled with naphthalene
ppm	parts per million
PV	photovoltaic

PVSC	perovskite solar cell
PXRD	powder X-ray diffraction
ϕ	quantum yield
QTAIM	quantum theory of atoms in molecules
red	reduction
RDG	reduced density gradient
s	singlet
SAM	self-assembled monolayer
SEM	scanning electron microscopy
STM-BJ	scanning tunneling microscopy break-junction
SWCNT	single-walled carbon nanotube
t	triplet
TBAF	tetrabutylammonium fluoride
TD-DFT	time-dependent density functional theory
TFA	trifluoroacetic acid
THF	tetrahydrofuran
TLC	thin-layer chromatography

TPA	triphenylamine
TPPy	tetraphenylpyrene
DLS	dynamic light scattering
TNT	2,4,6-trinitrotoluene
TTF	tetrathiafulvalene
TTFAQ	anthraquinone-type π-extended tetrathiafulvalene
TTFV	tetrathiafulvalene vinylogue
UV-Vis	ultraviolet-visible
V	volt(s)
XRD	X-ray diffraction
δ	chemical shift
ϵ	molar extinction coefficient
λ_{max}	maximum absorption wavelength

Chapter 1

Introduction

1.1 Introduction to Tetrathiafulvalene (TTF) and Derivatives

Tetrathiafulvalene (TTF), with another name of 2,2'-bis(1,3-dithiole), has been considered as the most popular and hence the most thoroughly investigated organic π-electron donor.[1–8] The TTF molecule has a simple heterocyclic structure (Figure 1.1). TTF and its derivatives show excellent π-electron-donating and electrochemical redox properties and therefore have attracted enormous attention from the synthetic community for many decades. The first synthesis of TTF was done as early as in the 1900s, but it was Fred Wudl's seminal paper[9] published in 1971 that disclosed its remarkable electronic properties and great potential in organic electronics. It is worth noting that immediately after Wudl's report, studies of similar sulfur-based π-conjugated donors were also done by other researchers, such as the synthesis of unsubstituted TTFs by Coffen[10] in 1971 and Hünig[11] in 1978. Wudl was

recognized as the pioneer who investigated the pure TTF and observed the high electrical conductivity of TTF radical cation. His work opened the door to novel "organic metals" and "organic superconductors" in years to come. The TTF-based organic metals were produced in 1973, in the form of a charge-transfer complex of tetrathiafulvalinium tetracyanoquinodimethane (TTF-TCNQ).[12,13] The first type of organic superconducting materials are known as the Bechgaard's salts,[14,15] which showed unprecedented high electrical conductivity for organic-based solids when discovered. These studies reported the ability of TTF to be reversibly oxidized to cation radical and dication at accessible potentials, which can be adjusted by TTF substitutions or structural modifications.[16,17]

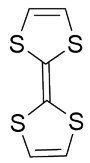

Figure 1.1: Molecular structure of TTF.

TTF has been extensively applied in the field of molecular electronics. In 1974, Aviram and Ratner[18] linked TTF to tetracyanoquinodimethane (TCAQ) as an electron-acceptor through a non-conjugated bridge to achieve a molecular rectifier. Ever since then, a variety of TTF-based intramolecular charge-transfer compounds have been prepared and some were demonstrated to act as molecular junctions.[19–22] Taking advantage of the three redox states (0, +1, +2) of TTF, molecular wires, switches, and memory devices have been developed based on TTF-containing molecular systems.[23–26] One type of molecular wires are linear polymers with π-conjugated backbones, such as oligo-(*p*-phenylene ethynylene)s (OPEs).[27–32]

It is common to use thiols as the anchoring groups for attaching molecular wires to a metal surface.[33–35] Other anchoring groups include alkylsulfides and disulfides that can also be used to bridge the interface at a metal surface/junction.[33–40] The 14-π electron tetrathiafulvalene system is non-aromatic, and it can undergo electron transfer at very low oxidation potentials to sequentially and reversibly form radical cation and dication states ($E^1_{1/2}$ = +0.37 V and $E^2_{1/2}$ = +0.67 V in dichloromethane versus the saturated calomel electrode). Scheme 1.1 illustrates the sequential oxidation reactions of TTF.

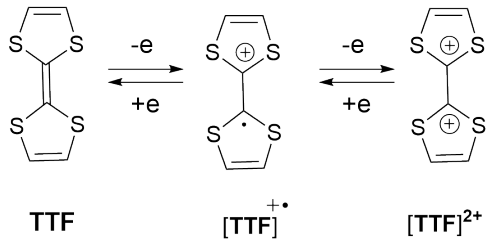

Scheme 1.1: Stepwise single-electron transfer reactions of TTF.

In contrast to the non-aromatic nature exhibited by the dithiole units in the neutral TTF, the oxidized forms of TTFV, including radical cation ($TTF^{\cdot+}$) and dication (TTF^{2+}), have one and two 6π-electron heteroaromatic 1,3-dithiolium rings, respectively (see Scheme 1.1). The gained aromaticity stabilizes the oxidized forms, rendering TTF with relatively low oxidation potentials and hence excellent electron-donating ability. Its unique redox properties make TTF a highly useful molecular building block in the development of organic π-conjugated oligomers/polymers, macrocycles, and supramolecular charge-transfer self-assemblies. Moreover, the structure of TTF can be flexibly modified to generate diverse derivatives, the chemical and redox properties of which can be controlled and finely adjusted by introducing

electron-donating and/or electron-withdrawing substituents to them. Compared with neutral TTF, its radical cation and dication show much higher degrees of π-electron delocalization, which can be readily observed in the visible region of the absorption spectrum. These features allow for the development of colorimetric sensing functions enabled by redox and electrochemical means. In the solid state, TTF derivatives can form highly ordered stacks or two-dimensional sheets through sulfur$\cdots$sulfur interactions and intermolecular π–π interactions. These properties have been utilized in crystal engineering of functional organic electronic and optoelectronic materials.

TTF shows good tolerance to a wide scope of synthetic conditions; for example, mild acids, bases, and the presence of various metal catalysts. Therefore, incorporation of TTF into various molecular and macromolecular systems can be readily done through a large number of organic reactions. Conditions that involve extremely acidic or strongly oxidizing agents are known to lead to the formation of cationic TTF species through protonation or oxidation. These reactive intermediates may further react to yield undesired by-products. It is therefore necessary to avoid using these reaction conditions in the synthesis of TTF-containing materials.

The oxidation of unsubstituted TTF undergoes sequential single-electron transfers, with two oxidation potentials at $E^1_{1/2} = +0.34$ V, $E^2_{1/2} = +0.73$ V (vs Ag/AgCl reference in MeCN). Some examples of the application of TTF in materials chemistry are shown in Scheme 1.1. In recent years, radical-enhanced molecular recognition has been the mostly applied pattern in the design of stimuli-responsive supramolecular systems and synthetic molecular machines.[41–44] Reversible pairing of stable organic radicals was employed as a popular non-covalent driving force in switchable molecular shuttles,[45] pumps,[46] muscles,[47] foldamers or host–guest complexes.[48,49] The main

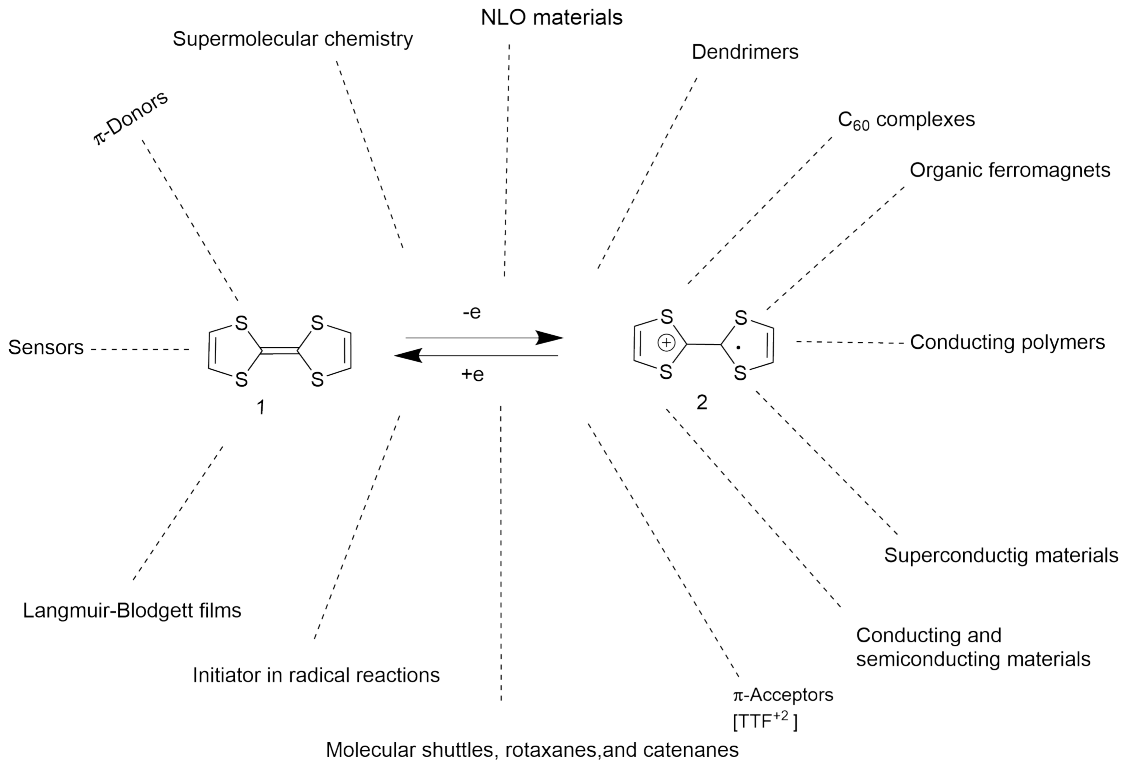

Scheme 1.2: Application of the redox-active TTF unit in molecular, supramolecular, and materials chemistry.

building blocks for these molecular devices are TTF and its derivatives, owing to the propensity of their radical cations for forming intriguing mixed-valence dimers through non-covalent interactions.[50–53] Mixed-valence TTF radical cation dimers are scarcely seen in the solution phase under ambient conditions, mainly because of their poor stability.[54–56] However, the formation of mixed-valence TTF dimer is a desirable precondition for the development of stimuli-responsive molecular and supramolecular systems. Stabilized mixed-valence dimers of TTF can be achieved through two approaches: (i) connecting two TTF groups through an appropriate covalent linkage[57,58], and (ii) confinement of two TTF molecules within a supramolecular host.[57,59] Stoddart and co-workers succeeded in preparing stable TTF dimers in mechanically

interlocked molecules like rotaxanes[60] or catenanes.[61,62] It is possible to form stable mixed-valence radical cation TTF dimers in the solution phase through modifications of monomer's π-conjugation patterns[63] to increase dispersive interactions within the dimers. However, there is a common drawback related to such a π-extension strategy; that is, the (opto)electronic characteristics of TTF are dramatically changed. For instance, the oxidation potentials or absorption bands are shifted as a result of π-extension.[63,64] Moreover, π-extension may also lead to variation of the chemical nature of these materials.[65–67]

The desirable TTF synthon for building functional supramolecular systems should constantly maintain (i) useful (opto)electronic features, (ii) adequate stability for its intermolecular mixed-valence and radical cation dimer, and (iii) tunability for redox and stimuli-responsive performances. In recent years, active studies have been performed to incorporate TTF into 24-crown-8 macrocycles, aiming at developing supramolecular host systems for complexation with cationic guests and understanding their interplays with TTF oxidation potentials.[68–70]

1.1.1 Synthesis and Properties of TTFs

TTFs in general can be classified into two categories–simple TTFs and extended TTFs (ex-TTFs). The structures of ex-TTFs may be derived from extensions on the side chains of dithiole rings or both dithiole rings that are linked together by a π-conjugated spacer. Precursors need to be carefully selected in synthetic planning. Scheme 1.3 outlines the common synthetic routes for preparing the TTF skeleton.

TTFs can be synthesized via a variety of reactions, among which the phosphite-

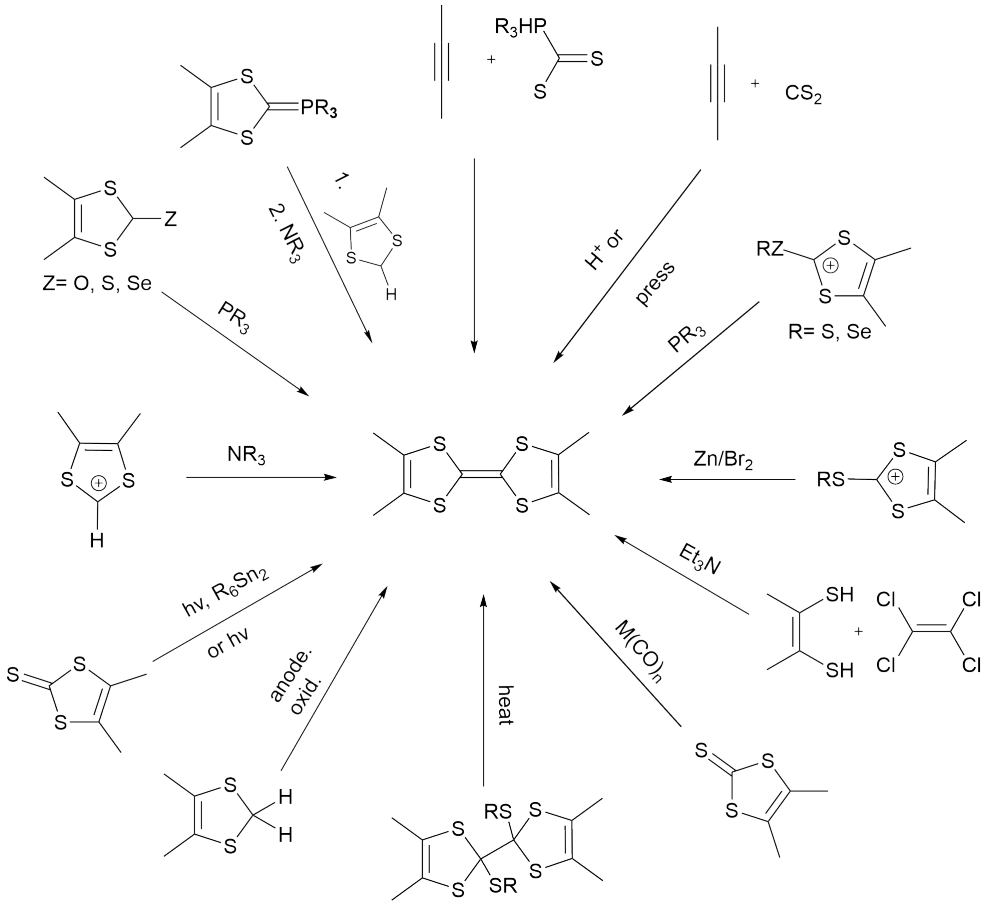

Scheme 1.3: Synthetic methods for preparation of TTF skeleton.

promoted olefination of 1,3-dithiole-2-thiones is the most frequently used one. The reaction of 1,3-dithiole-2-thione with a trialkyl phosphite under heating leads directly to the formation of TTF products. An exemplar reaction is illustrated in Scheme 1.4A. This method is particularly suitable for the synthesis of TTFs with a symmetric substitution pattern. However, it is incapable of making TTFs with unsymmetric substitutions. The reaction between a 1,3-dithiole-2-thione and a 1,3-dithiole-2-one as shown in Scheme 1.4B can produce unsymmetrically substituted TTF products. To ensure good yields for the phosphite-promoted olefination reactions, high-temperature conditions are preferred. On the other hand, high temperatures may negatively

impact the synthesis of TTF derivatives that are not thermally stable. To mitigate this problem, a Wittig-type reaction is commonly used as an alternative olefination approach (Scheme 1.4C).

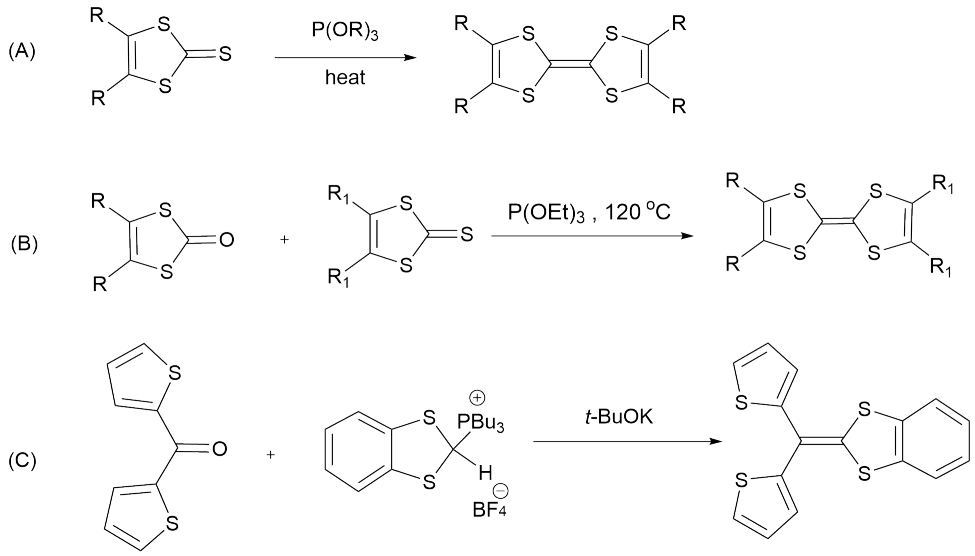

Scheme 1.4: Synthetic methods for symmetrical and unsymmetrical TTF derivatives.

1.1.2 π-Extended TTFs

Attachment of diverse groups to the skeleton of TTF leads to new classes of π-extended TTF derivatives. Numerous ex-TTFs exhibit excellent electron-donating properties as well as electrochemical redox activity. To create TTF analogues with extended π-units, a commonly adopted strategy is to linearly lengthen the vinyl bridge in the parent TTF structure by inserting various conjugated π-units between the two dithiole heterocycles (see Figure 1.2A). Another way to produce ex-TTFs is to fuse aromatic rings with the two dithiole units (Figure 1.2B) or with the central π-bridge of TTF (Figure 1.2C).

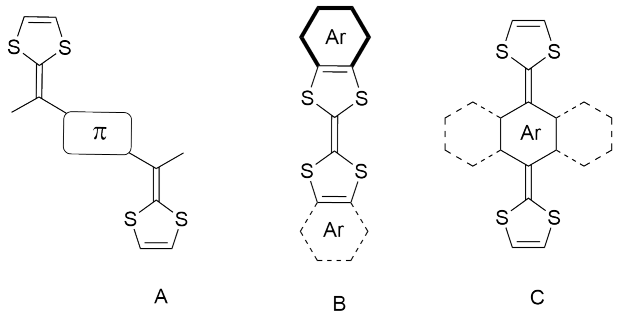

Figure 1.2: Illustration of three ways of extending the π-backbone of TTF. (A) Linear π-extension, (B) annulation of dithioles, and (C) fusion with an aromatic central core.

Insertion of a quinoid unit between the dithiole units has been widely used to generate novel ex-TTF derivatives with enhanced redox activity.[71] TTF is an electron-donating scaffold that can generate a radical cation ($TTF^{\cdot+}$) and dication (TTF^{2+}) in a stepwise manner. Mixed-valence (MV) states are formed in the radical cation of TTF as well as the dimer of a radical cation TTF and a neutral TTF.[72–82] These MV-state materials offer great opportunities for investigating intramolecular and intermolecular electron-transfer mechanisms.[83–86] In this respect, extension of the 1,3-dithiole-2-thione-4,5-dithiolate group has resulted in several adaptable TTF-based building blocks, including self-assembled frameworks, luminescent substances, single molecule magnets, organic solar cells, semiconductors, and redox-switchable systems.[87–98] There have been numerous studies on TTF analogues with extended π-conjugated systems, in which the length of the spacer that bridges the redox-active units plays a vital role in controlling the conductivity mechanism and related charge-transfer properties.[99–101] Investigations on furano- and pyranoanhydride-based π-extended TTFs have been carried out recently. Electron coupling among the donor–acceptor (D—A) scaffolds leads to better control over the MV states. Based on the

Robin–Day classification, there are three types of organic MV compounds depending on the extent of electron coupling element (H_{ab}) among two redox centers. Class I is referred to the MV compounds in which the interaction is quite small. The existence of medium interaction between two redox cores leads to class II MV. Class III is accompanied by strong interaction and full delocalization of the charge over the whole system. The main feature of the organic π-conjugated MV systems is the intervalence charge-transfer (IV-CT) band that can be modulated through molecular tailoring, through which molecular materials with new optical and electrical characteristics can be developed.

Connecting two TTF moieties through a π-conjugated bridge has been a popular design motif for the preparation of organic conductors.[102–104] The electronic properties of these materials are greatly dependent on the degrees of intra- and intermolecular electronic interactions among oxidized and neutral TTFs. TTF dimers can possibly show five redox states, including 0, +1, +2, +3, and +4. These redox states have been discovered in compounds, in which two TTF moieties are fused with a central benzene or pyrazine ring.[105] The two TTF units act as electrochemically independent redox centers. Relatively weak Coulombic interactions occur between the cations of TTF if the two TTFs are oxidized at similar potentials. The electronic interactions were probed by spectroscopic analysis, showing that the bridge mediates electronic communications between the units. Otsubo, Iyoda, and co-workers[106–108] reported that when two TTFs were linked by ethynediyl and buta-1,3-diyndiyl, they behaved as electrochemically self-reliant redox centers. However, the electronic spectra of the generated radical cations (TTF-bridge-$TTF^{\cdot+}$) showed intramolecular IV-CT absorption bands along with a broad absorption band near 1300—1400 nm.[107] When

two TTFs are linked through a cross-conjugated tetraethynylethene (TEE) spacer (e.g., **1-1**, Figure 1.3), they act as autonomous redox centers that can be oxidized at the same potential during cyclic voltammetric analysis (i.e., simultaneous two-electron oxidation).[109–111]

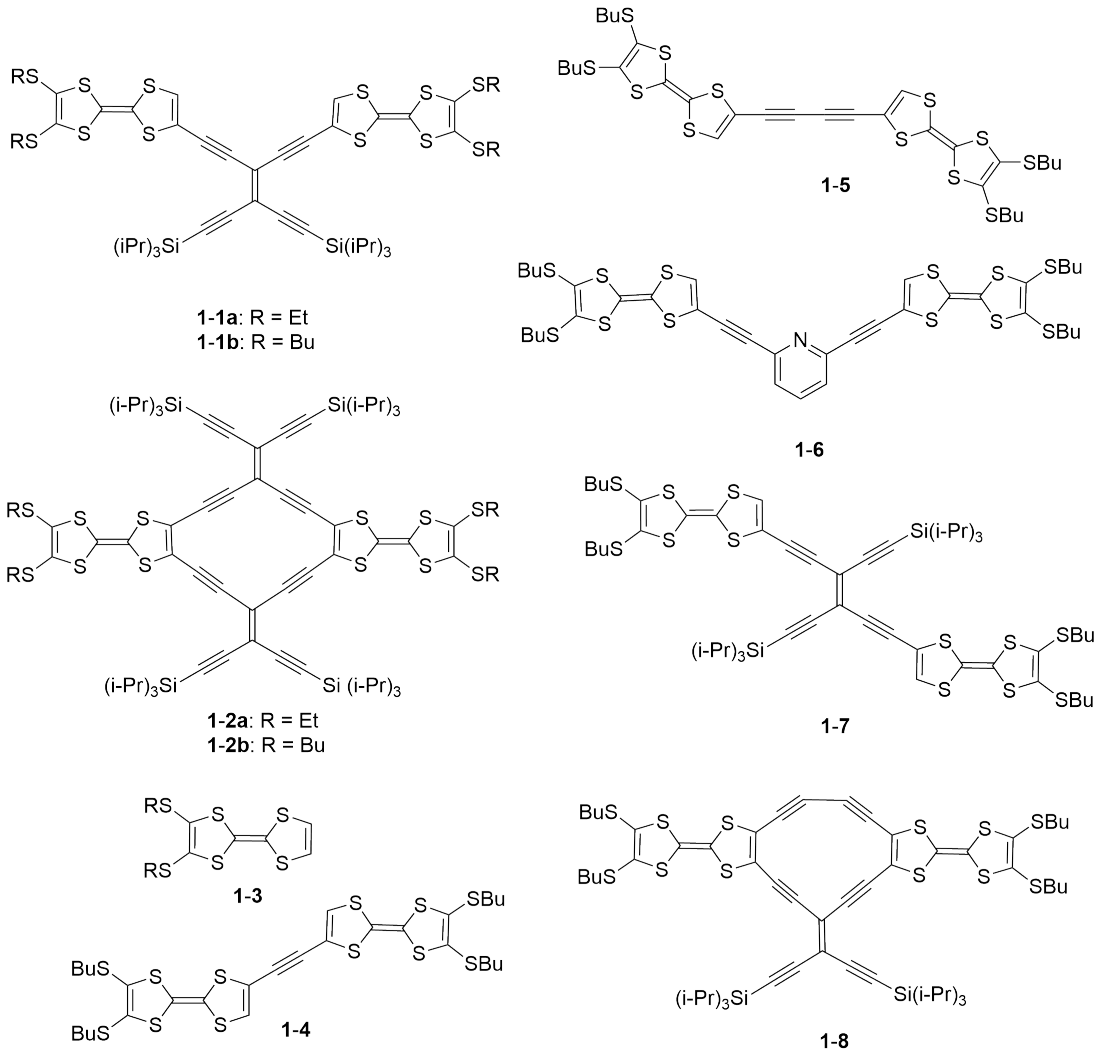

Figure 1.3: TTF dimers with linear or cross-conjugated bridging units.

If two TTFs units are connected through two tetraethynylethene (TEE) bridges in a cyclic structure, such as the extended radialenes **1-2** shown in Figure 1.3, electronic

communications occur between two TTFs. This was evidenced by the observation of two separate redox waves in its cyclic voltammogram (two steps of oxidation).[111] Moreover, a low-energy IV-CT absorption band was seen at 2257 nm, which was related to the intermediate radical cation. Rapta and co-workers[112] clearly revealed the effects of acyclic versus cyclic bridging units through cyclic voltammetric and EPR/UV–vis–NIR spectroelectrochemical analyses. They synthesized and examined a number of cyclic and acyclic acetylenic scaffolds that carry two TTF units (Figure 1.3). The bridge that separates two TTF moieties was changed systematically from the linear conjugated ethyne, butadiyne and tetraethynylethene (*trans*-substituted) units to cross-conjugated tetraethynylethene unit with acyclic and cyclic motifs. The cyclic structures (radialenes) consist of both *endo*- and *exo*-cyclic double bonds. The interactions between the two TTF moieties in each of these compounds were analyzed by cyclic voltammetric, UV–vis–NIR absorption, and EPR analyses. The electron-accepting features related to the acetylenic cores were also evaluated by electrochemical means. Low and co-workers[113,114] demonstrated that how the rotamers could influence the electronic coupling in bis-TTF/ruthenium complexes that are linked via oligoynediyl spacers. They prepared and characterized a series of TTF dimers as presented in Figure 1.3.

More examples of bis-TTF derivatives reported in the literature are shown in Figure 1.4. Simple bis-TTF **1-9**[115] and arylene/heteroarylene bridged bis-TTFs **1-10**, **1-11**,[115] **1-12** and **1-13**[116] were found to show two-electron oxidation in PhCN. However, the insertion of a Ru center between two TTF acetylides in complex **1-14**[117] led to a splitting of the two-electron oxidation potentials for the first and second TTF units (by 110 mV). The one-electron oxidation of the Ru metal center was also

observed experimentally. There is a strong communication between the two TTF units in **1-14**, which can be attributed to the Ru center and the bulky ligands. As such the two TTF moieties prefer a co-planar conformation.[117] Through direct fusion of the dithiole rings of two TTF, such as compound **1-15**,[118] or through pyrazine or benzene ring fusion (**1-16**, **1-17**), two TTF units can be covalently linked to show considerably enhanced electronic communications.[118]

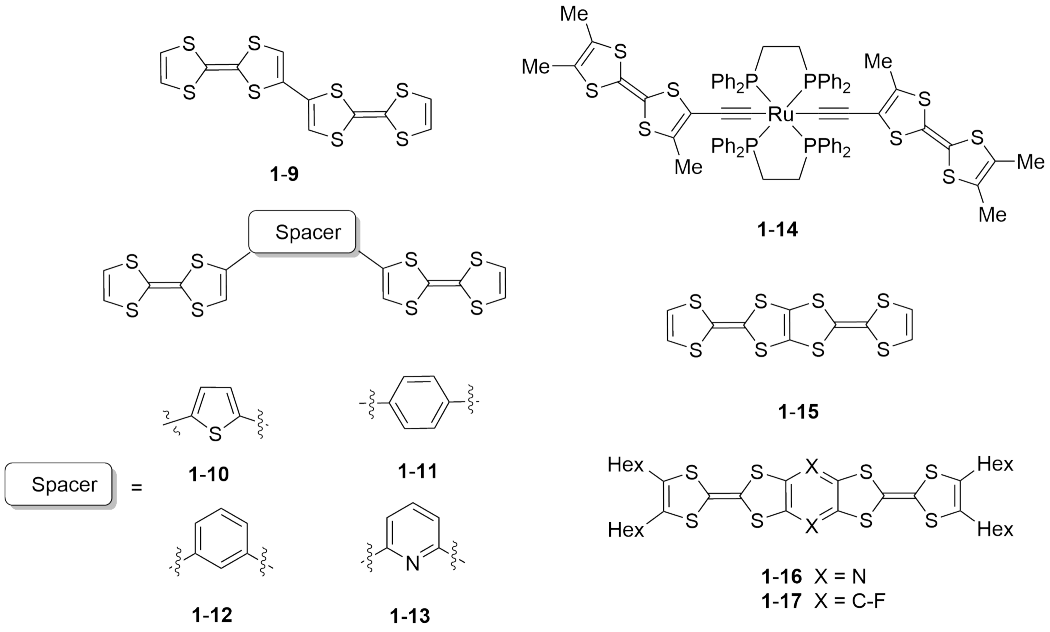

Figure 1.4: Representative bis-TTFs reported in the literature.

In 2017, Liu and co-workers[119] reported two novel tetrakis-(DTF) functionalized spiro[fluorene-9,9'-xanthene] (SFX) derivatives, namely SFX-DTF1 and SFX-DTF2 (Figure 1.5). Their studies indicated that these compounds show significant hydrophobic hole-transporting properties. The hole mobility exhibited by these compounds were attributed to the incorporation of DTF end groups at the 2,2′-, 7,7′- and 2,3′,6′,7-positions of the SFX core. Structurally, these compounds can be

viewed as spiroannulated ex-TTFs. It has been suggested that this type of exTTFs would be useful as dopant-free hole-transporting materials (HTMs) in perovskite solar cells (PVSCs).

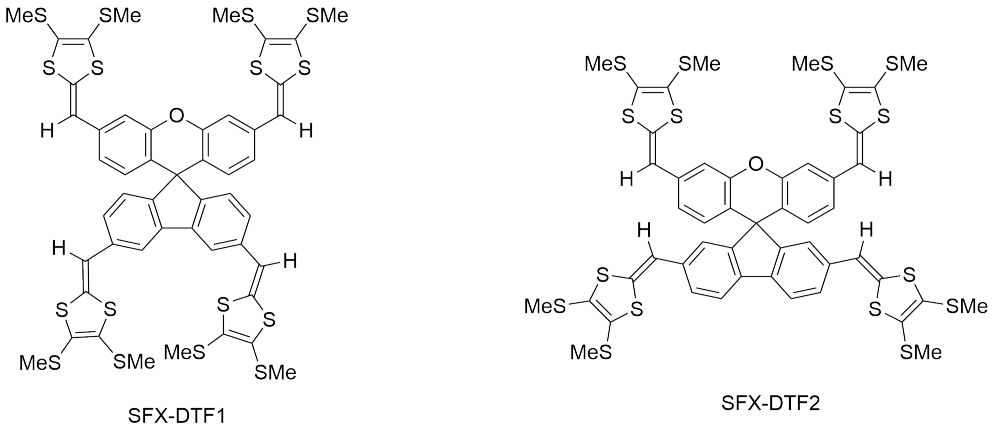

Figure 1.5: Spiroannulated ex-TTFs developed by Liu *et al.*

Fujioka and co-workers[120] in 2016 reported that Vilsmeier–Haack type formylation on different 6-aryl-1,4-dithiafulvenes could be useful for the preparation of various π-electron donors, especially dendralene-type donors along with aromatic rings incorporated through applying the formylated products as precursors. Electrochemical properties of these π-electron donors were characterized. They presented 1,3-dithiol-2-ylidene units on **1-18** or **1-20** using the Horner–Wadsworth–Emmons (HWE) reaction or trialkyl phosphite-mediated olefination reaction, which lead to different novel π-extended TTF donors, monoaryl-substituted TTF vinylogues **1-21**, heteroaromatic ring inserted [3]dendralene derivatives with triple 1,3-dithiol-2-ylidenes **1-23**, and their TTF-fused analogues (Figure 1.6). Electrochemical characteristics of the new π-electron donors have been also investigated by cyclic voltammetry.

Pritam and co-workers reported three classes of D–A π-extended chromophores,

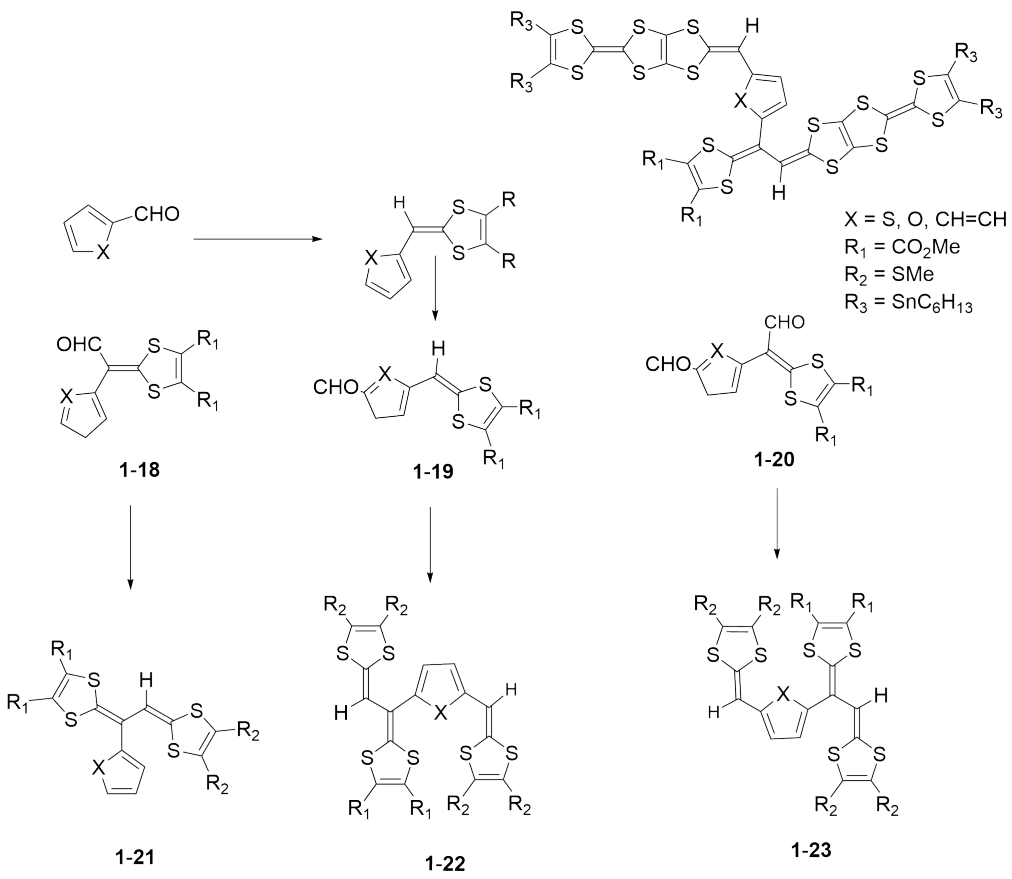

Figure 1.6: Synthetic routes to extended TTF systems.

in which both anhydride- or imide-based π-acceptors and TTF/DTF donors were incorporated. Large π-surfaces, including benzoperylene or coronene derivatives, which were quite insoluble in ordinary solutions were attached to the TTF/DTF donors for the first time.[121] Moreover, they described the first tri- and tetra-DTF substituted PDMA acceptors. Alkyl chains were linked to the TTF/DTF or imide units to give good solubility. The donor units resulted in the formation of radical cations ($D^{\cdot+}$), while the π-extended acceptor formed the radical anions ($A^{\cdot-}$) through chemical oxidation/reduction reactions under ambient conditions. The radical anions also gained stabilization through the large π-surface of the TTF/DTF moieties.

These radical anions exhibited UV-Vis-NIR absorption properties. It was also found that some of these chromophores show NIR fluorescence, with λ_{max}^{em} extending up to about 740 nm. Additionally, certain TTF/DTF-appended chromophores showed excited-state solvatochromism (**1-26** and **1-28**). The π-acceptors with anhydride functionalities showed lower reduction potentials than those with imide groups. Increasing the number of donor groups, on the other hand, made the systems much easier to be oxidized. Remarkably, some *trans*-TTF-fused molecules formed MV states in the mid infrared (MIR) region (**1-24, 1-25, 1-27**, Figure 1.7). These systems, owing to their multi-state redox activity, panchromism, and NIR to MIR optical absorption properties, have been applied in the preparation of multi-stimuli-responsive and switchable molecular materials.[122,123]

1.1.3 Application of TTF in Functional Molecular Devices

In recent years, radical-enhanced molecular recognition has been applied as a popular strategy for the development of stimuli-responsive supramolecular systems and synthetic molecular machines. Reversible pairing of stable organic radicals is a widely used mechanism in the operations of switchable molecular shuttles, pumps, muscles, foldamers, and host–guest complexes.[23–32] TTF and its derivatives have found extensive application in this area, since their radical cations tend to form intermolecular mixed-valence radical-cation dimers. As discussed before, TTF is an excellent π-electron donor. The electrochemical redox properties of TTF can be widely used in various fields, including organic conductors, superconductors, photovoltaic cells, field effect transistors, sensors and biosensors, solar cells, and

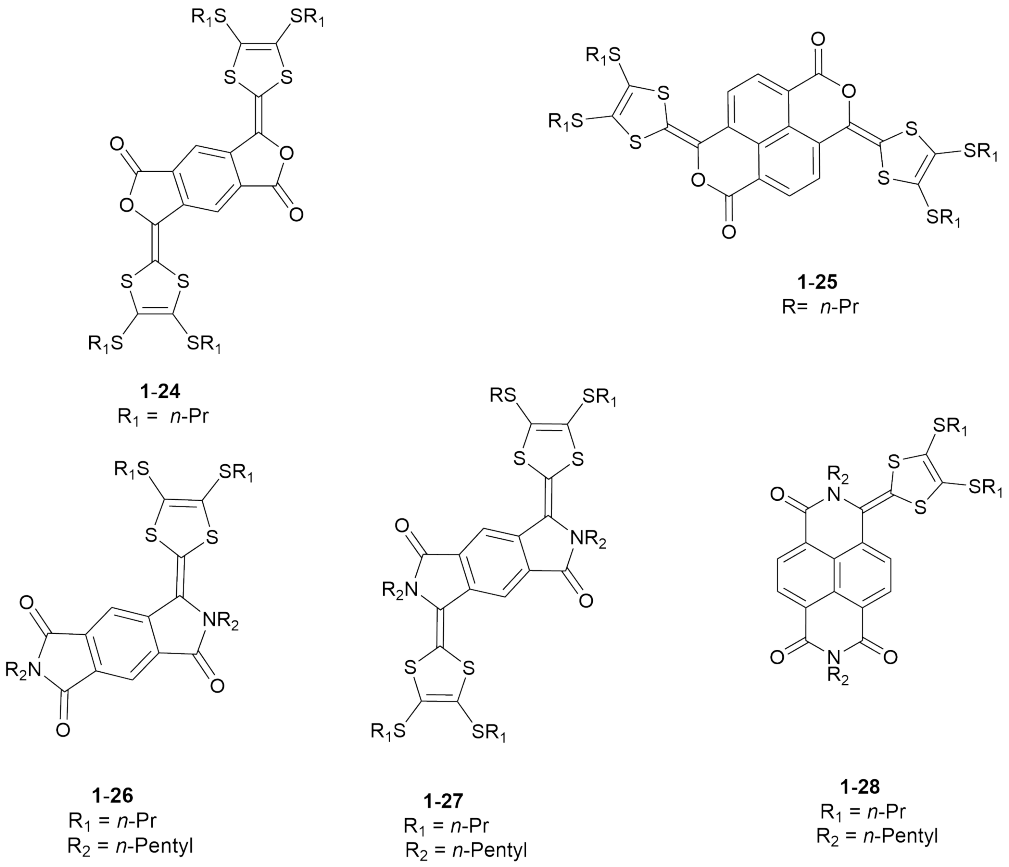

Figure 1.7: Selected examples of TTF/DTF-appended D–A chromophores.

more prominently as polymeric electrooptic materials, molecular devices and single-electron donors in catalysis. TTF and derviatives can show C-T and π-interactions with a variety of π-conjugated molecules with complementary electronic nature and molecular shapes. Therefore they are particularly useful in supramolecular chemistry and molecular devices. In the following sections, a brief literature review concerning recent application of TTFs and ex-TTFs in materials chemistry is provided.

1.1.3.1 TTF Derivatives as Chemosensors

Several applications can be derived from the electrochemical and redox properties of TTF derivatives such as creation of molecular sensors, amplification of redox-

fluorescent switches, redox-controlled gels, and molecular tweezers and clips.[124–128] The use of TTFs as redox-active components in electrochemical sensors has been pursued for decades. A wide range of sensing functions have been developed, especially sensors for metal cations.[129] By using different types of linkage groups, TTF cores can be covalently linked to receptor groups to form sensor systems. In these sensors, the TTF unit functions as a reporter, signaling redox currents and/or potential changes in response to the binding of analytes and receptors. For example, the TTF-crown ether hybrids shown in Figure 1.8 were designed as selective sensors for different metal ions. The crown ether groups act as the receptors, providing binding cavity to selectively capture metal ions. When a metal cation is bound to the crown ether, an enhanced inductive effect is transduced to the TTF unit, which reduces the electron density of TTF. The oxidation potential of the TTF core is in turn increased, which can be detected by various voltammetric methods. In this way, sensitive detection and quantification of certain metal ions can be achieved. The Becker group pioneered in designing two TTF derivatives, crown ether-annulated or tethered TTFs, as cation sensors.[130,131] Crown ethers are not easy to synthesize and require ultra-high dilution and certain conditions to accomplish satisfactory yields. Crown-TTF systems also show low solubility as a result of their limited conformational flexibility. To circumvent these problems, Bryce and co-workers developed TTF sensors that carry more flexible podand receptors rather than crown ethers (see Figure 1.9). With these modifications, the podant-TTF sensors achieved better solubility and exhibited selectivity for certain transition metal ions.

Podand ligands are acyclic analogues of crown ethers. They provide binding sites for specific transition metal ions.[132,133] The structural flexibility makes the synthesis

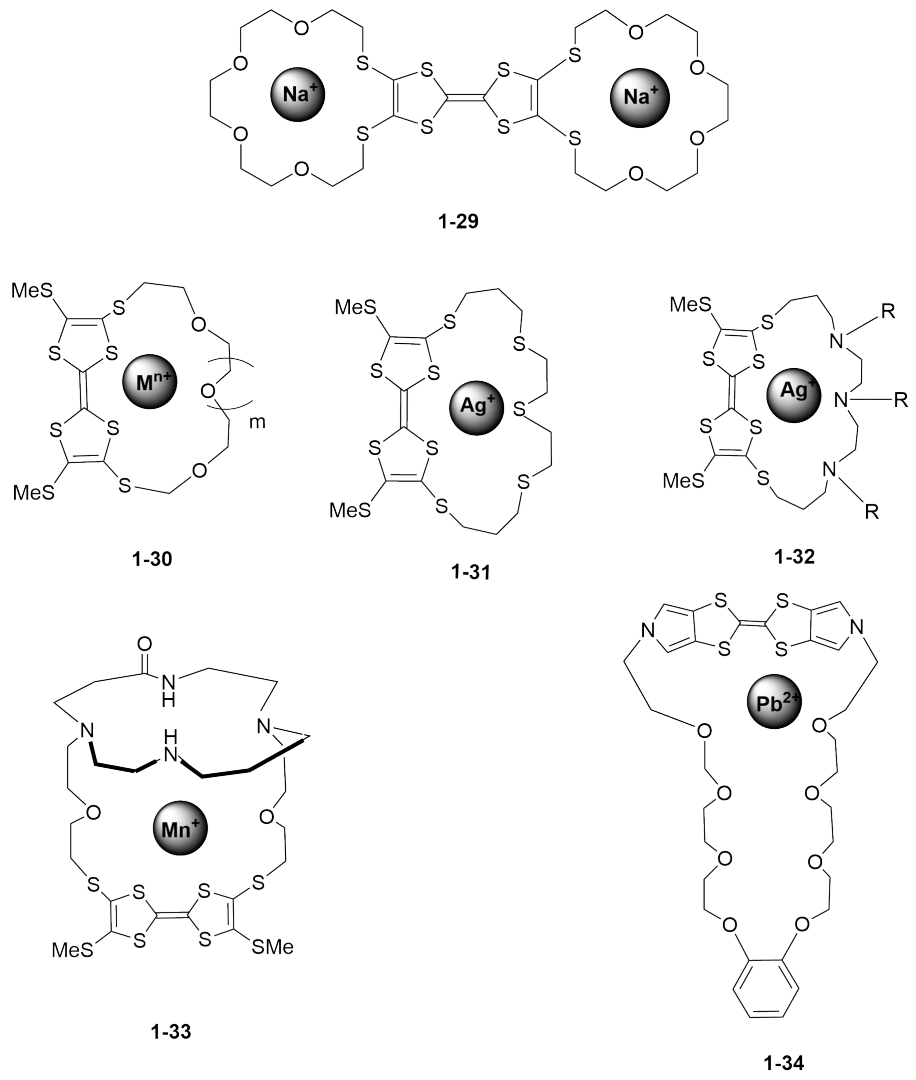

Figure 1.8: Examples of crown-annulated or tethered TTFs as metal cation sensors.

of TTF-podant systems more convenient and cost-effective than TTF-crown ethers. Podand receptors show different binding properties and selectivity as compared to crown ether receptors. As a result, the podand-TTF sensors complement instead of replace the crown-TTF sensors. TTF can also be combined with the calix[4]arene system to generate cation sensors. Calix[4]arene is a good cation receptor that has a rigid backbone and a three-dimensional inner cavity. Calix[4]arene can effectively

bind with various metal ions with strong affinity and defined stoichiometry. In this respect, sensors containing a calix[4]arene receptor tends to show very good sensing performance for metal ions. Figure 1.10 shows an example of a TTF-calix[4]arene hybrid that can be used to detect sodium cation effectively.[134,135]

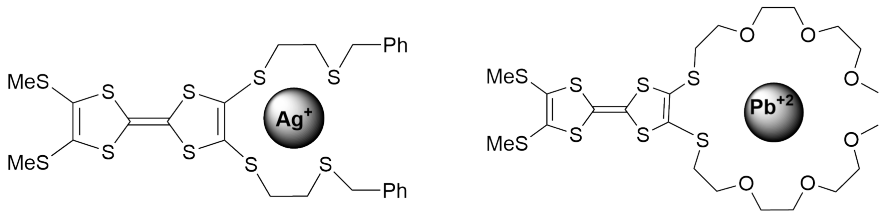

1-35 1-36

Figure 1.9: Examples of TTF-podand systems as transition metal ion sensors.

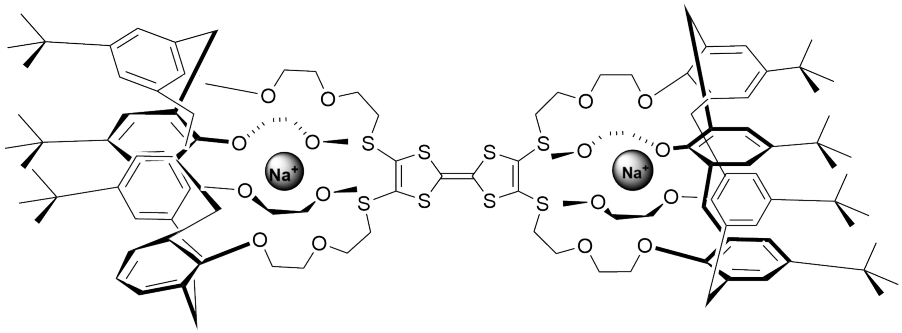

1-37

Figure 1.10: A bis(calix[4]arene)-TTF compound as a robust sodium cation sensor.

Most aryl-substituted TTFV derivatives exhibit a pseudo-*cis* conformation that facilitates the construction tweezer-like receptors or supramolecular hosts. A class of phenyl-acetylenic TTFVs has been investigated by the Zhao group via cross-coupling and cycloaddition reactions, taking advantage of the convenient reactivity of the alkynyl groups attached. Click chemistry has become the most important synthetic

strategy in modern materials chemistry, since Sharpless first introduced this concept in the late 1990s. In 2013, the Zhao group designed and synthesized molecular tweezers **1-38** (Figure 1.11) by using a click reaction between an alkynyl-substituted TTFV and an azido-phenylbornate precursor using the Cu-catalyzed alkyne-azide coupling (CuAAC) conditions.[136] The two phenylboronic acid groups in this tweezer were designed to act as efficient receptors for saccharides, while the redox-active TTFV central unit acted as an electrochemically active indicator for monitoring the binding events of saccharides with **1-38**. Electrochemical sensing function towards a range of monosaccharides was achieved under physiological conditions. Through a similar CuAAC strategy, a class of arene-substituted TTFV molecular tweezers was also generated by the Zhao group. Compound **1-39** is an example of these compounds (Figure 1.11). It was found to selectively bind with C_{70} fullerene in the presence of a large excess of C_{60} fullerene (> 1000 fold).[137] Fluorescence spectroscopic titration revealed that binding of **1-39** with C_{70} fullerene produced a fluorescence enhancement caused by the anthracene fluorophores on the molecule. This type of molecular tweezers can be used as highly sensitive fluorescence sensors for fullerenes, with the responsiveness of the fluorescence being determined by the arene fluorophores connected to the TTFV unit.

Several types of chemosensors based on TTFs are also noteworthy, including those for neutral and anionic chemical species, for example, the anthryl-TTF derivatives **1-40** shown in Figure 1.12. These compounds were prepared and used for the detection of singlet oxygen as chemiluminescent traps.[138,139] As a cytotoxic chemical, singlet oxygen is very important for the survival of live cells.[62,63] Sensitive detection methods for singlet oxygen are therefore highly desirable. The anthryl unit is a

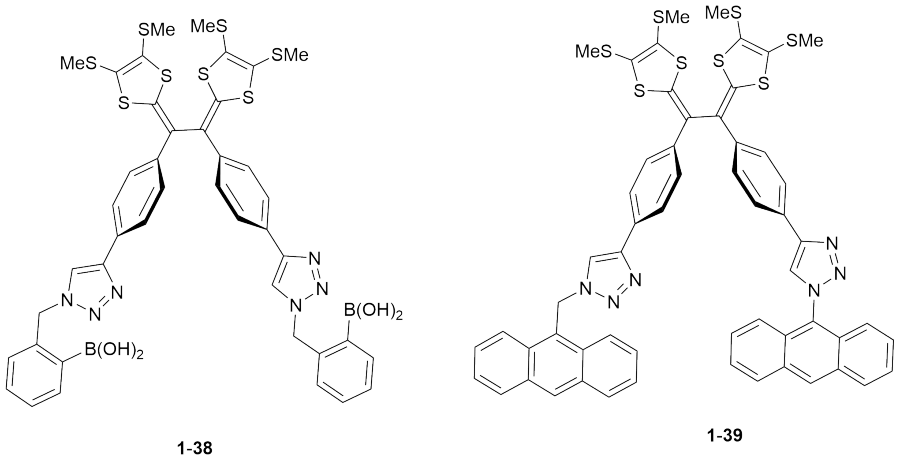

Figure 1.11: TTFV-based molecular tweezers **1-38** and **1-39**.

luminophore that reacts with singlet oxygen in the structures of **1-40a-c**. In response to singlet oxygen trapping, the TTF group transfers electrons as a strong electron donor. Photo-induced electron transfer (PET) is the key process in the sensing mechanism. Singlet oxygen reacts with the anthryl group of **1-40** to yield strong chemiluminescence, switching the fuorescence quantum yield from $\Phi = 0.0039$ to $\Phi = 0.21$. In contrast, other reactive oxygen species, such as H_2O_2, OCl^-, and O_2 did not induce the same magnitude of fluorescence response. It has also been demonstrated that the introduction of electron-rich TTF to the 9-position of anthracene can greatly increase its reactivity to singlet oxygen as revealed by the observed chemiluminescence changes.

The proposed sensing mechanism consists of three steps, as shown in Scheme 1.5. First, the electron-donating TTF unit of **1-41** activates the anthracene moiety to trap singlet oxygen, yielding an unstable endoperoxide **1-42**. The subsequent breakdown of the peroxide intermediate results in the excitation of the anthracene moiety. By oxidizing the electron-rich TTF moiety, the molecule is transformed into a cationic

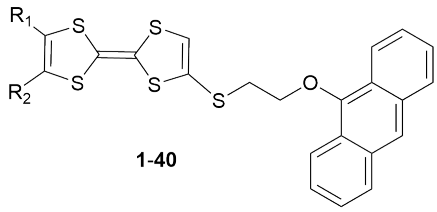

40a: $R_1 = R_2 = SMe$
40b: $R_1 = SCH_2CH_2O$-Anthryl; $R_2 = H$
40c: $R_1 = R_2 = S(SCH_2CH_2O)CH_2CH_2OH$

Figure 1.12: Anthryl-TTF derivatives for sensing of singlet oxygen.

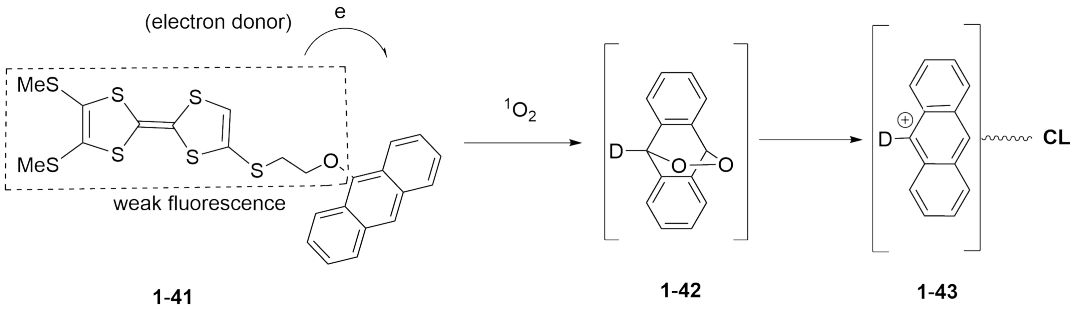

Scheme 1.5: Possible mechanism for strong chemiluminescence (CL) resulting from the interactions of sensor **1-41** with singlet oxygen.

form. As a consequence of such a tandem reaction, the generation of the final cationic species leads to chemiluminescence.

For the detection of saccharides, sensors made of TTF, anthracene, and phenylboronic acid units were developed; for example, compounds **1-44** and **1-45** in Figure 1.13.[64–66] In these two chemosensors, the anthracene moiety acts as a fluorophore for fluorescence signaling. Phenylboronic acid serves as a saccharide receptor, since it is able to complex with the 1,2- or 1,3-diol groups in saccharides to form boronate esters in water. TTF in these sensors works as a mediator to regulate the fluorescence of anthracene. Without binding with saccharides, the fluorescence of these sensors is quenched due to a PET mechanism, in which the TTF donor transfers electrons to the

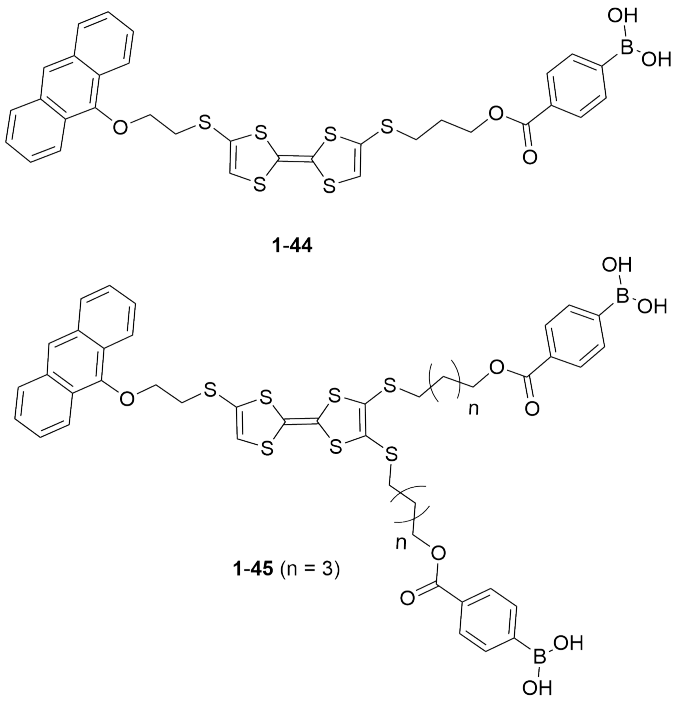

Figure 1.13: TTF-anthracene systems functionalized with phenylboronic acid groups as selective fluorescenc sensors for saccharides.

anthracene unit upon photoexcitation. When the sensors are bound to saccharides, the electronic properties of the boron center are changed. In particular, the boronate group is a stronger acceptor than boronic acid due to increased Lewis acidity. As a result, the PET pathway from TTF to boronate dominates, making the fluorescence of the anthracene unit turned on. The detailed mechanism for the sensing function is explained in Scheme 1.6. Sensor **1-44** displayed an excellent selectivity for D-fructose, while sensor **1-45** was more selective for D-glucose. The results indicated that the number of boronic acid receptors attached to the anthrancene-TTF backbone has a significant effect on saccharide selectivity.

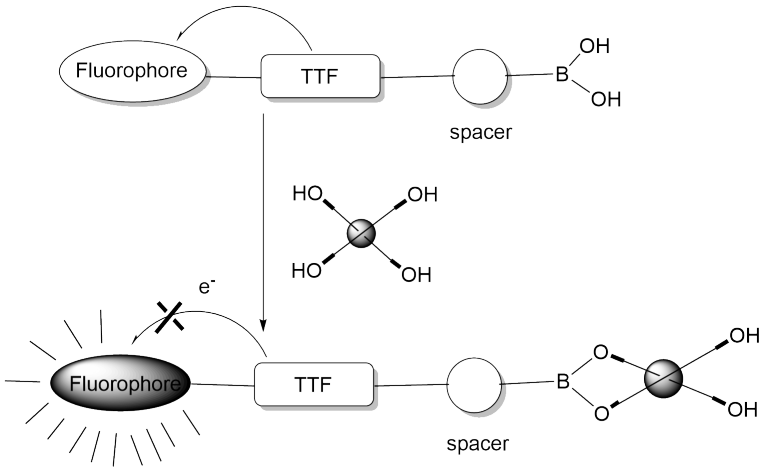

Scheme 1.6: TTF-anthracene systems functionalized with phenylboronic acid groupsas fluorescence turn-on sensors for saccharides.

1.1.3.2 TTF Derivatives as Molecular Machines and Switches

The reversible redox behavior of TTF derivatives makes them useful switchable building blocks for advanced molecular devices. It is possible to modify and fine-tune the redox properties of TTFs at the molecular level and apply them to molecular switches and machines.[140–142] A change in color (such as a transition from pale yellow to deep green or blue) generally indicates the oxidation of TTF to its cationic states. Zhou *et al.*[143] investigated the colorimetric properties of a class of chiroptical molecular systems, in which TTF groups are covalently linked to chiral binaphthyl units. It is known that axially chiral binaphthalene molecules produce strong circular dichroism (CD) signals that can be easily detected.[144] It has been demonstrated that changes in the oxidation states of the two TTF units resulted in either attractive or repulsive interactions between them. Consequently, the dihedral angle of the binaphthalene molecule varies to give detectable CD signal changes (Scheme 1.7).

Scheme 1.8 illustrates the mechanism for the redox-controlled dihedral angle

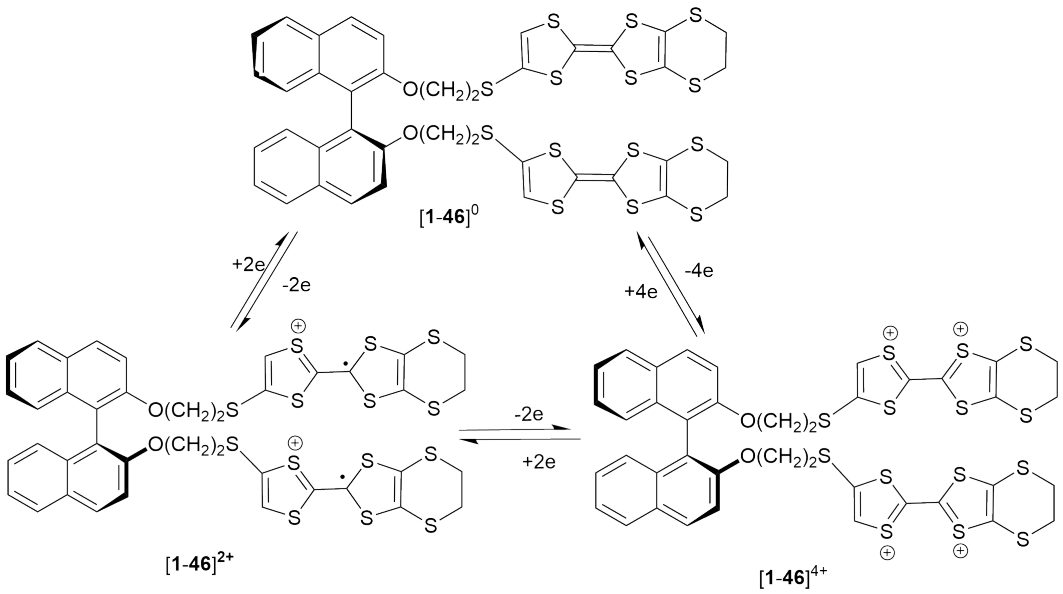

Scheme 1.7: Illustration of the three states of compound **1-46** associated with its oxidation and reduction.

changes through tuning the oxidation states of TTF. In the first step, each TTF is oxidized to its radical cation. At this point, intramolecular attraction between the two radical cations draws them closer and reduces the dihedral angle between two naphthalene rings. As the TTF units are further oxidized, two dicationic TTF units are formed. Coulombic repulsion occurs between them, causing an increase in the dihedral angle between two naphthalene rings.

Redox-controlled fluorescent switches have been achieved by TTF-fused porphyrin systems, for example, compounds **1-48**, **1-49**, and **1-50** in Figure 1.14. In these compounds, the fluorescence of porphyrin units is quenched by adjacent TTF donors. Upon oxidation, the TTF units lose their electron-donating ability, and the electron transfer from TTF to porphyrin is inhibited. As a consequence, these TTF-fused porphyrins exhibit increased fluorescence when oxidized.

The Stoddart group designed a rotaxane-type molecular machine (shuttle) **1-51**,

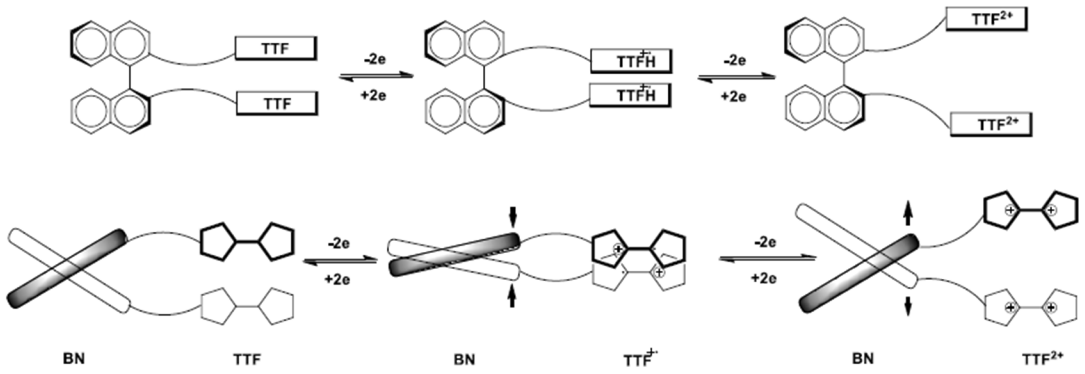

Scheme 1.8: Schematic illustration of the three states of **1-47** showing different dihedral angles after oxidation of TTF units (BN: binaphthalene unit).

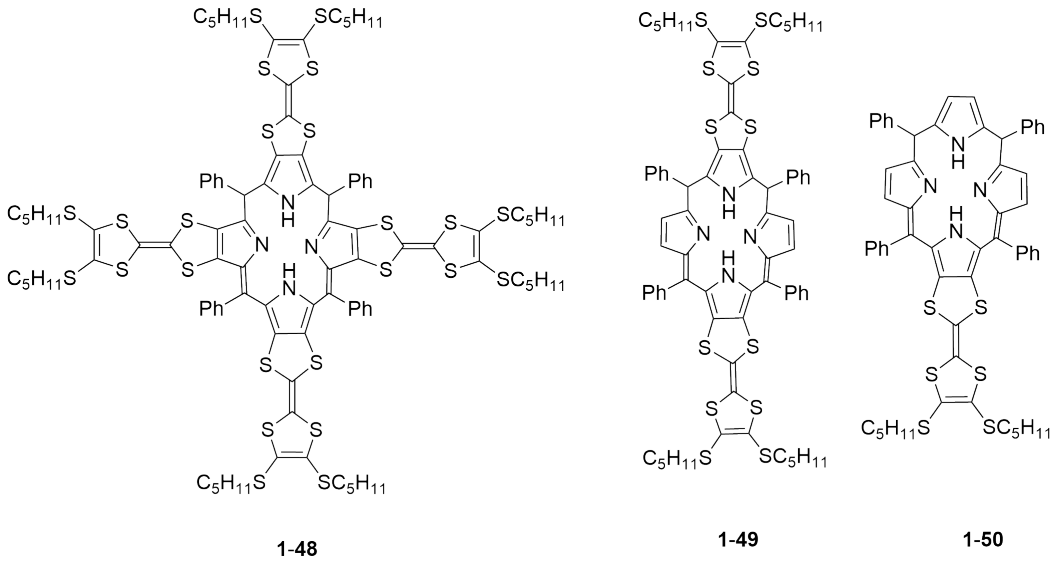

Figure 1.14: TTF-porphyrin-based redox fluorescent switches.

which employs TTF as a key functioning unit (see Figure 1.15).[145,146] As a result of the oxidation or reduction of TTF moieties through chemical or electrochemical processes, the redox-bistable rotaxane underwent controlled and reversible motions. The working principle of this molecular machine is based on the chemistry of host-

guest recognition.[147] As shown in Figure 1.15, the rotaxane system contains two $CBPQT^{4+}$ rings circling around a molecular wire that carries two TTF and two naphthalene stations. When the TTF stations are in the neutral state, the $CBPQT^{4+}$ rings are drawn closer to them through charge-transfer interactions as the TTF unit is a better electron donor than the naphthalene group. When the two TTF groups are oxidized, the $CBPQT^{4+}$ rings are pushed away by electrostatic repulsion and move toward the naphthalene units. The motion of $CBPQT^{4+}$ rings in this molecular shuttle can be controlled by the redox processes taking place on the TTF units.

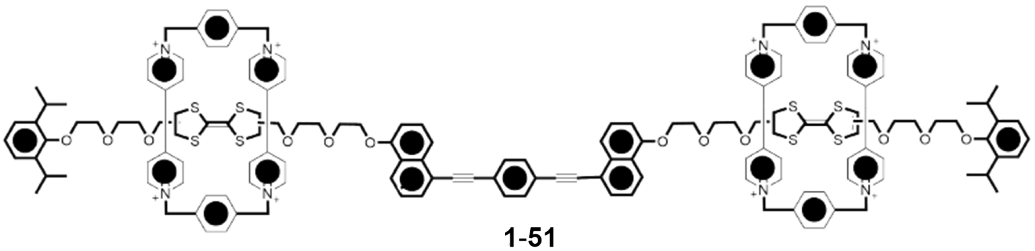

1-51

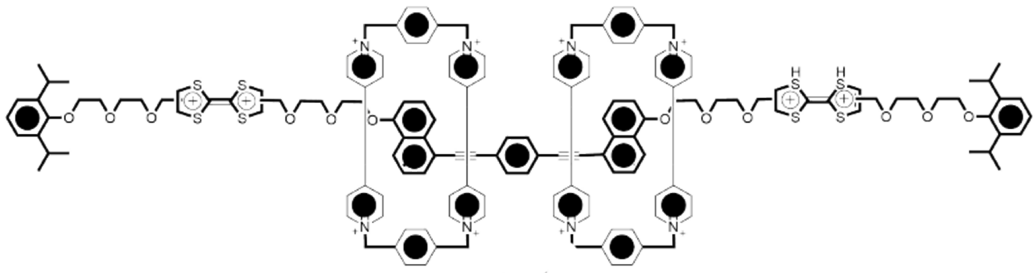

1-52

Figure 1.15: Rotaxane **1-51** as a redox-controlled molecular machine.

1.2 Introduction to 1,4-Dithiafulvene (DTF)

1,4-Dithiafulvene (DTF) is a significant organic electron-donating functional group, which is the half structure of TTFV (Scheme 1.9). In general, DTFs can be functionalized by π-insertion and/or π-annulation to generate what are known as π-extended TTFs or ex-TTFs. Many of DTF derived materials show intriguing electronic and semiconducting properties. Like TTF derivatives, DTF-functionalized π-conjugated materials have also found wide applications in organic electronic and optoelectronic devices.

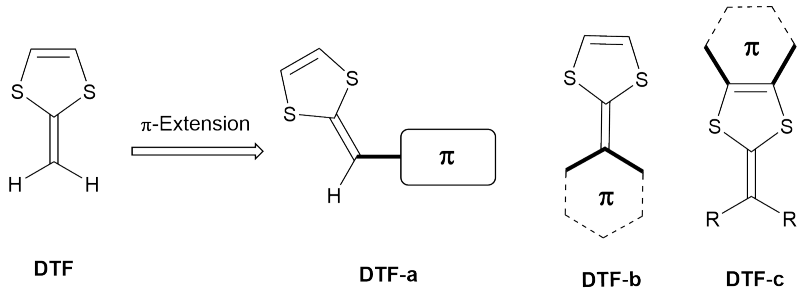

Scheme 1.9: General strategies for integrating the DTF unit into various π-conjugated systems.

1.2.1 Electron-donating Properties of DTF

As an electron-rich heterocycle, DTF is capable of releasing an electron upon oxidation. There have been some theoretical investigations on the thermochemical and structural properties of 2-methylene-1,3-dithiole, which is the unsubstituted DTF.[148,149] Based on nucleus independent chemical shift calculations (NICS) and isomerization stabilization energy calculations (ISE), unsubstituted DTF was suggested to be a

good π-electron donor.[150] However, unsubstituted DTF is unstable and therefore cannot be easily obtained for experimental analysis. Through π-conjugation, DTF can be substituted and linked with other functional groups in order to gain improved stability and enriched electronic properties.

Extension of the DTF structure leads to new opportunities for improving chemical stability, redox activities, and electronic properties. Three different approaches can be used to incorporate a DTF group into conjugated molecular systems (Scheme 1.9). The 1,3-dithiole ring may either be directly connected to a π-conjugated unit or be linked to the unit via covalent linkages on the vinylidene position.[151] The DTF derivatives investigated in this thesis work is characterized by the motif where the DTF group is linked to a π-conjugated arene group at vinylidene position.

1.2.2 Synthetic Methods for DTF-Functionalization

The first DTF was synthesized by Kirmse and Horner in 1958.[152] They used 4-phenyl-1,2,3-thiadiazole **1-53** to produce a biradical intermediate **1-54** through photolysis. Some of the intermediate then turned into thiokene **1-55**. The combination of **1-54** and **1-55** gave diphenyl-substituted DTF **1-56** as a final product (Scheme 1.10). As this approach did not exhibit stereoselectivity and gave a low yield, it was not accepted as an effective method for DTF synthesis.

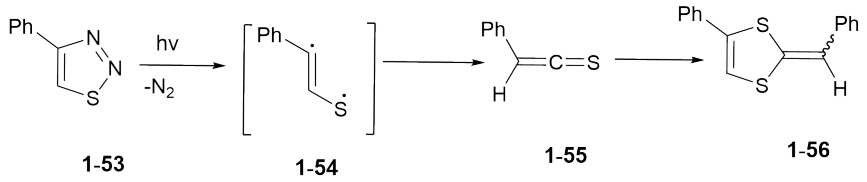

Scheme 1.10: Formation of DTF through photolysis of 1,2,3-thiadiazole.

Later, the Wittig-type olefination reaction was developed as a more useful synthetic method. In 1971, Hartzler devised a process for obtaining dithiols substituted with phenyls (i.e., 2-benzylidene-1,3-dithioles).[153] It consists of two steps. The cycloaddition of aliphatic phosphine with acetylene **1-58** first forms phosphorane intermediate **1-59**, which then undergoes the Wittig reaction with its benzaldehyde counterpart to produce the final product **1-60**. A new approach involving protonation of dithiol-2-yl phosphonium intermediates with HBF_4 has been described by Cava and co-workers (Scheme 1.11).[154] In basic conditions, the phosphonium salts can be converted into Wittig reagents, which can then react with a variety of aldehydes and ketones to generate olefinated compounds. A number of different phosphonate reagents and phosphonium salts have been described for DTF functionalization on various π-conjugated systems via the Wittig-type olefination reaction.

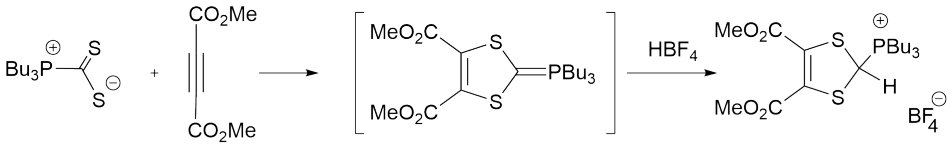

1-57 **1-58** **1-59** **1-60**

Scheme 1.11: Synthesis of 1,3-dithiol-2-yl phosphonium tetrafluoroborate.

In 2007, Bryce and co-workers[155] developed another method, often referred to as phosphite-promoted olefination. This reaction occurs by reacting an aldehyde or ketone directly with 1,3-dithiole-2-thione under normal heating conditions in the presence of excess $P(OMe)_3$ or $P(OEt)_3$ (Scheme 1.12).

Over the past decade, phosphite-mediated olefination reactions have gained increasing popularity in the synthesis of DTF derivatives, mainly due to the following

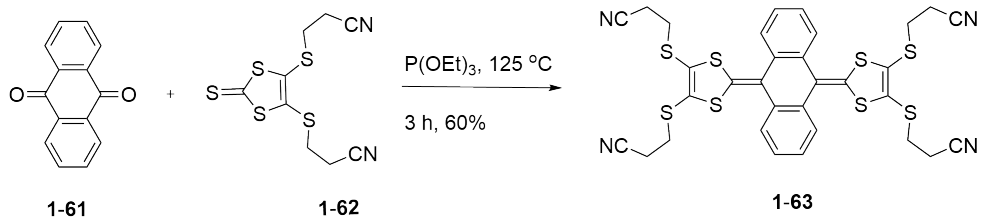

Scheme 1.12: DTF functionalization through the phosphite-promoted olefination reaction.

reasons. First, it is an easy reaction that requires only one step. Second, a variety of π-conjugated aldehydes and ketones can be used as starting materials. Third, the 1,3-dithiole-2-thione precursor can be readily synthesized and tailored to meet desired properties. Scheme 1.13 describes the mechanism of the phosphite-promoted olefination reaction.

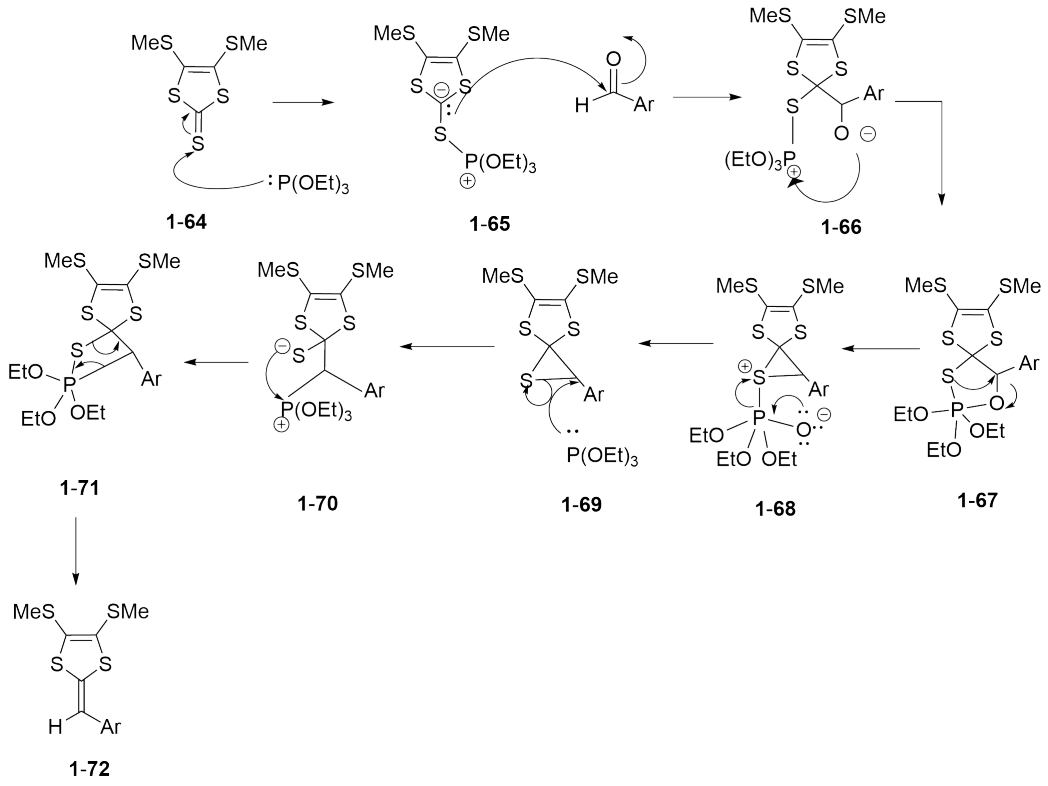

Scheme 1.13: Reaction mechanism for the phosphite-promoted olefination reaction.

Apart from the above-mentioned methods, the double S-vinylation procedure may also be used to achieve post-olefination functionalization.[156,157] For instance, 1,2-benzenedithiol can undergo DTF functionalization (Scheme 1.14), when reacted with a *gem*-dihalovinyl system under certain conditions. DTF product **1-75** is characterized by its extended benzo-*d*[1,3]dithiole structure. Some difficult DTF syntheses have been successfully handled by using this method, while other approaches such as phosphite-promoted olefinations and Wittig-type methods fail to deliver desired products. Morin and Nielsen, for example, reported that the reaction can be applied to generate highly efficient DTF-functionalization of large polycyclic aromatic hydrocarbon (PAH) cores under extremely mild conditions.[158,159]

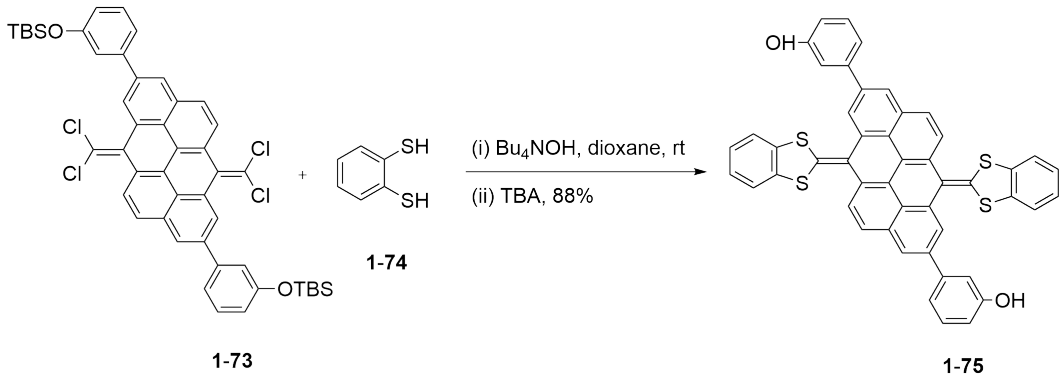

Scheme 1.14: Post-olefination functionalization through double S-vinylation.

1.2.2.1 Synthetic Methods for 1,3-Dithiole-2-thiones

In order to prepare a wide range of derivatives of DTFs and TTFs, 1,3-dithiole-2-thiones are often used as starting materials since they can be readily functionalized with a wide variety of side groups. A number of different DTF products have been synthesized in this thesis by phosphite-promoted olefination. Scheme 1.15 presents

the structure of a 1,3-dithiole-2-thione **1-80** synthesized by this method.

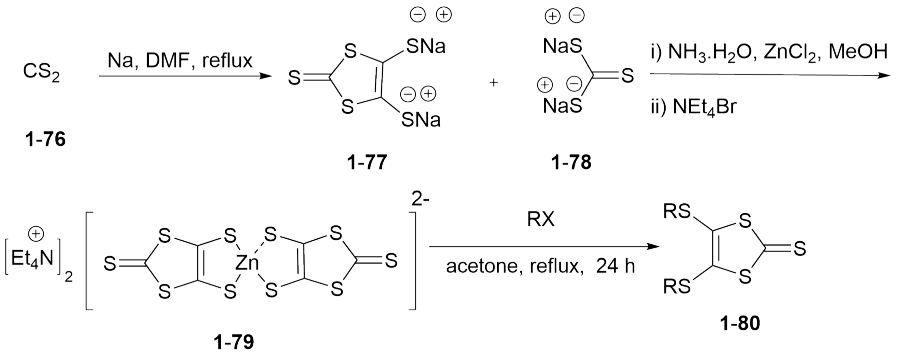

Scheme 1.15: Synthetic route for 1,3-dithiole-2-thione **1-80** involving the reduction of CS_2 with Na as the key step.

A wide range of 1,3-dithiole-2-thiones can be prepared in large quantities at relatively low costs using this method. In the synthesis, CS_2 is treated with an alkali metal (e.g., Na or K) . Alkali metals act as reducing agents and convert CS_2 to 1,3-dithiole-2-thione-4,5-dithiolate **1-88**. This transformation can be explained by the mechanism illustrated in Scheme 1.16.[160] The first step in this mechanism is the reduction of CS_2 by Na metal, which forms radical anion **1-82**. Then the radical anion reacts with a second radical anion to yield dithiolate **1-83**. The dithiolate anion is chelated with zinc (II) cation to generate a stable salt of ammonium zincate **1-79**. The zinc salt **1-79** can react with an electrophile appropriate to the desired structure of 1,3-dithiole-2-thione to yield the thione compound **1-80**.

There are also other synthetic methods available for the preparation of 1,3-dithiole-2-thiones in addition to those described previously. Scheme 1.17 provides a concise summary of these synthetic methods.

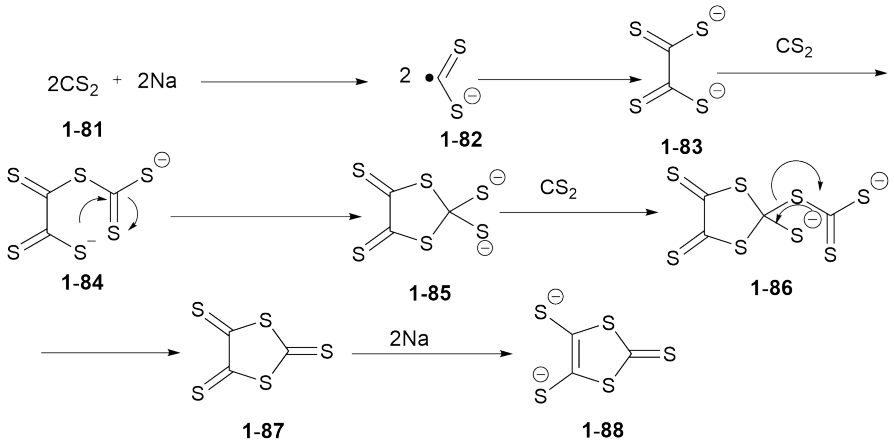

Scheme 1.16: Reaction mechanism for 1,3-dithiole-2-thione **1-80** involving the reduction of CS_2 with Na as the key step.

1.2.3 Chemical Properties and Redox Activity of DTFs

DTF is an electron-rich heterocycle that readily forms to a radical cation when oxidized. In 1957, Kirmse and Horner[152] published a study on the oxidative dimerization reaction of DTF. This reaction involved oxidizing DTF **1-89** to yield a reddish-violet salt **1-90**. Further studies in 1974 offered evidence for oxidation of diaryl-substituted DTFs (Scheme 1.18) and provided indicative structure data derived from elemental analysis and UV-Vis absorption measurements. They proposed that the radical cation **1-92** was formed in the following step of oxidation. Then, a stable dication salt was formed by dimerization of two intermediate radical cations. An aryl group attached to the DTF vinyl position aids in the formation of radical cation intermediates, in turn producing a stable dication product, and the presence of the vinyl proton facilitates elimination, which leads to the product known as a tetrathiafulvenyl vinylogue (TTFV).

The DTF dimerization reaction can be promoted by several oxidants, including

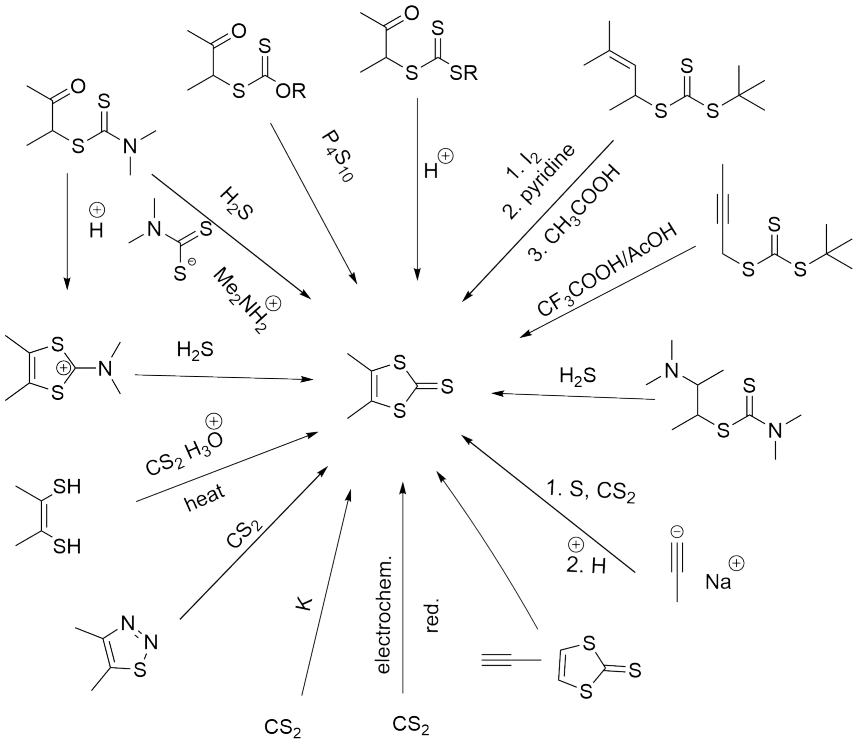

Scheme 1.17: Synthetic methods for 1,3-dithiole-2-thiones.

$(BrC_6H_4)_3SbCl_6$,[161,162] I_2,[163,164] Br_2,[165,166] and $AgBF_4$.[167–169] DTF dimerization reactions can also be induced by electrochemical conditions, resulting in the formation of numerous TTFV products.[166,170–172] Hapiot *et al.*[173] conducted a comprehensive study of the oxidative dimerization mechanism of DTF through cyclic voltammetric (CV) analysis in 1996. According to their proposed mechanism, a radical cation **1-92** is generated through a fast electron transfer followed by the rapid formation of a dication dimer **1-93** (Scheme 1.19). The next step entails abstracting the two hydrogens from vinylidene, completing the double elimination reaction to produce TTFV **1-94**, which is readily oxidized to produce a stable TTFV dication at a lower potential than the starting material DTF.

Several other reactivities for DTF have been reported in the literature. Details

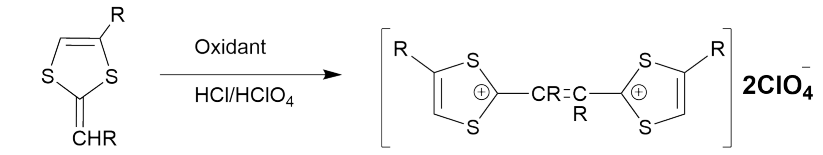

1-89a R = Ph
1-89b R = *p*-tol
1-89c R = 4-Cl-C_6H_4
1-89d R = 4-OMe-C_6H_4

1-90a R = Ph
1-90b R = r-tol
1-90c R = 4-Cl-C_6H_4
1-90d R = 4-OMe-C_6H_4

Scheme 1.18: Oxidative dimerization of DTFs.

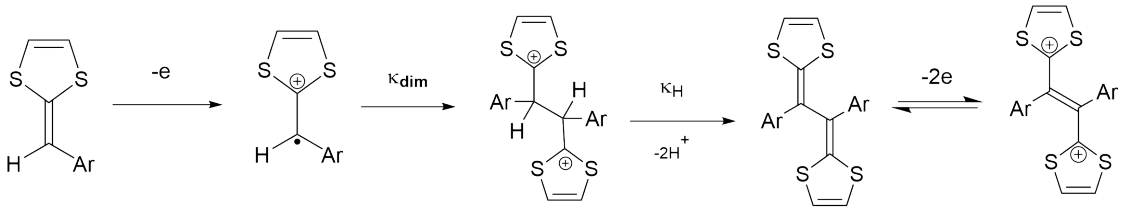

1-91 **1-92** **1-93** **1-94** **1-95**

Scheme 1.19: Mechanism for DTF oxidative dimerization

are provided in Scheme 1.20.[165] DTF vinylidene proton is usually displaced by different electrophilic groups in the majority of reaction mechanisms. In 1951, Hartzler suggested that benzylidenedithioles (i.e., phenyl-DTFs) were quasi-aromatic compounds due to their resonance properties.[153] The C=C bond on the exo-ring position can be substituted in a variety of ways, including bromination,[174] addition to a diazonium salt, nitrosylation,[175] or formylation with oxalyl chloride.[176]

The activated C=C bond of DTF can possibly undergo cycloaddition reactions.[177] Furthermore, a photo-oxidative cleavage reaction can also occur in the presence of DTF and C_{60} fullerene.[161,178] The photoexcitation of C_{60} induces the formation of singlet oxygen, which then interacts with the C=C bond, cleaving DTF into the related aldehyde and 1,3-dithiol-2-one. Researchers from the Zhao group have recently identified certain properties of DTF that are unique. When phenyl-DTF is substituted

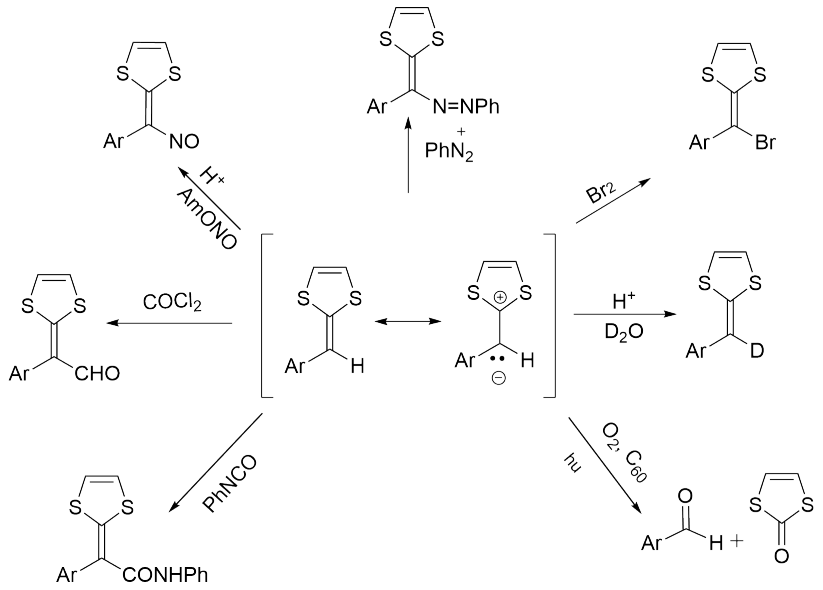

Scheme 1.20: Summary of the reactivities of DTFs with various electrophiles.

with an *ortho*-substituent such as CH_3 or Br, the presence of iodine can promote oxidative coupling reaction, leading to unusual products such as compounds **1-97** (Scheme 1.21).

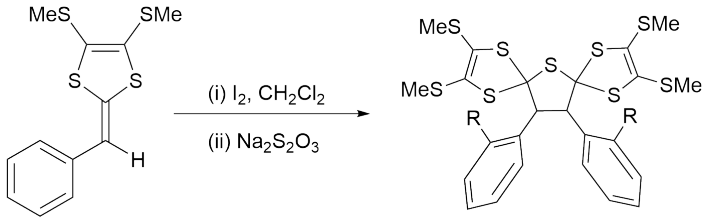

1-96a R = CH_3
1-96b R = Br

1-97a R = CH_3
1-97b R = Br

Scheme 1.21: An unusual oxidative dimerization of phenyl-DTFs with *ortho*-substituents.

In the above reaction, the *ortho*-substituted group is believed to inhibit the deprotonation step in the oxidative dimerization process. As a result, the protonated dication intermediate reacts with $Na_2S_2O_3$ during the workup step to provide a bis-

spiro-tricyclic product, **1-97**. As a result of resonance effects, the π-extended aryl groups, which are linked to a DTF, may stabilize the radical cation intermediate and become resistant to the process of oxidative dimerization.

There is another type of substitution reaction that DTF can undergo. As shown in Scheme 1.22, 1-naphthyl or 9-anthryl-substituted DTF **1-98** reacts with a 1,3,4-thiadiazole-2-thiol **1-99** in the presence of iodine. The reaction mechanism begins with the oxidation of DTF **1-98**. The resulting DTF radical cation further reacts with a 1,3,4-thiadiazole-2-thiol to form a thiadiazolyl-substituted product **1-100** in good yield.[179]

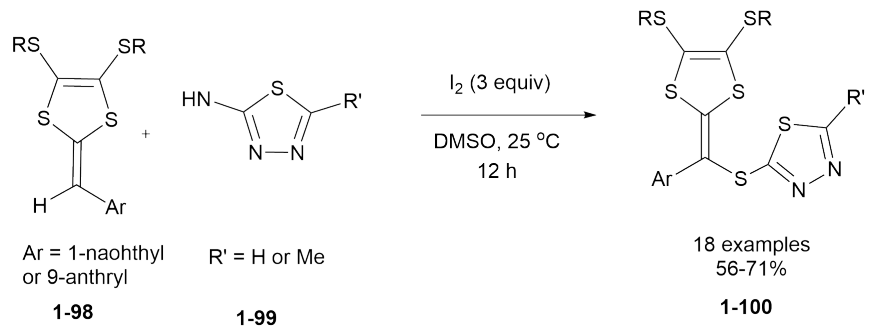

Scheme 1.22: Iodine-mediated oxidative vinylic C(sp^2)–H sulfenylation.

An intramolecular alkynedithiolium cycloaddition reaction was serendipitously observed by Zhao's group. As shown in Scheme 1.23, a bis(DTF)-substituted phenylacetylene derivative **1-101** was treated with iodine, with the intention of making TTFV-based conjugated oligomers or polymers. Nevertheless, a bis(indenothiophene) **1-102** was observed as the most significant product of this reaction.[180] Another cyclized product, **1-103**, was formed after treatment of **1-101** with a strong acid, TFA. Experimental results indicated that the protonation of the vinylic carbon is a criti-

cal step in this type of reaction. Density functional theory (DFT) analysis revealed that the reaction begins with protonation of the vinylic carbon, yielding a dithiolium cation intermediate that further reacts with the *ortho*-alkynyl group to form an intramolecular cycloaddition product.[181]

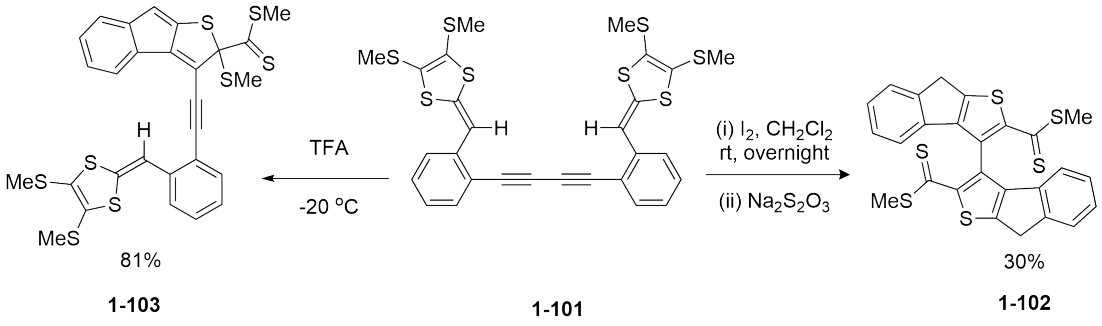

Scheme 1.23: Intramolecular alkynyl-dithiolium cycloaddition reactions.

1.3 Recent Progress in DTF and TTFV Functionalized Organic Materials

1.3.1 Organic Solar Cells

Optoelectronic performance of the π-conjugated systems, to which DTF is attached, can be enhanced by the DTF functional group. In 2008, Leriche and co-workers[182] prepared six different triphenylamines (TPAs) functionalized with DTF (Figure 1.16). These compounds were investigated as active materials in organic field-effect transistors (OFETs) and photovoltaic devices.

According to this study, compound **1-104** exhibits a higher hole mobility compared to the other compounds listed in Figure 1.16, because of its stronger π-

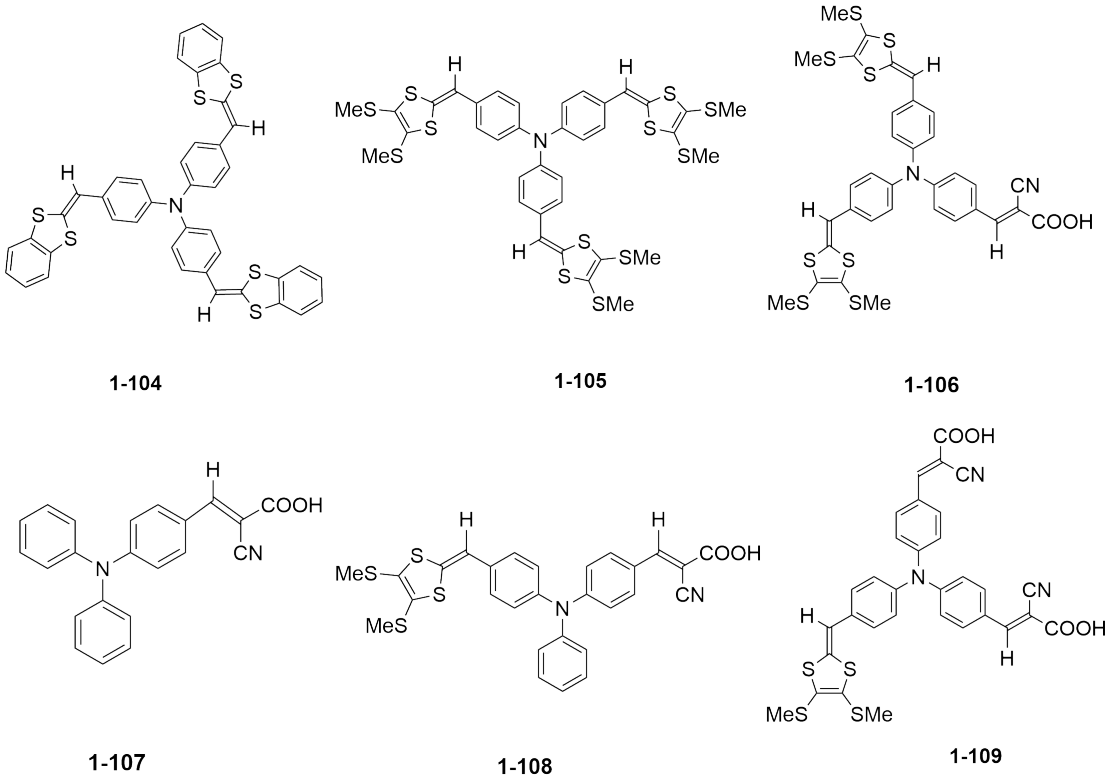

Figure 1.16: DTF-functionalized triphenylamines for solar cell devices.

stacking in the solid state. Compound **1-104** was also used together with C_{60} fullerene in fabrication of a bulk heterojunction (BHJ) solar cell. The resulting solar cell showed an acceptable conversion efficiency; however, the device did not demonstrate sufficient stability.

The DTF–A-type metal-free organic sensitizers were synthesized by Yang and co-workers[183] in 2012 for the preparation of dye-sensitized solar cells (DSSCs) (Figure 1.17). Increasing the length of the π-bridge results in improved performance for devices based on DTF sensitizers. In terms of power conversion efficiency (η) of 8.29% for compound **1-108** (Figure 1.16), which is the highest value among others. Comparison of these compounds with metal-based sensitizers indicated that organic DSSCs with high performance based on DTF-functionalized dye molecules are likely

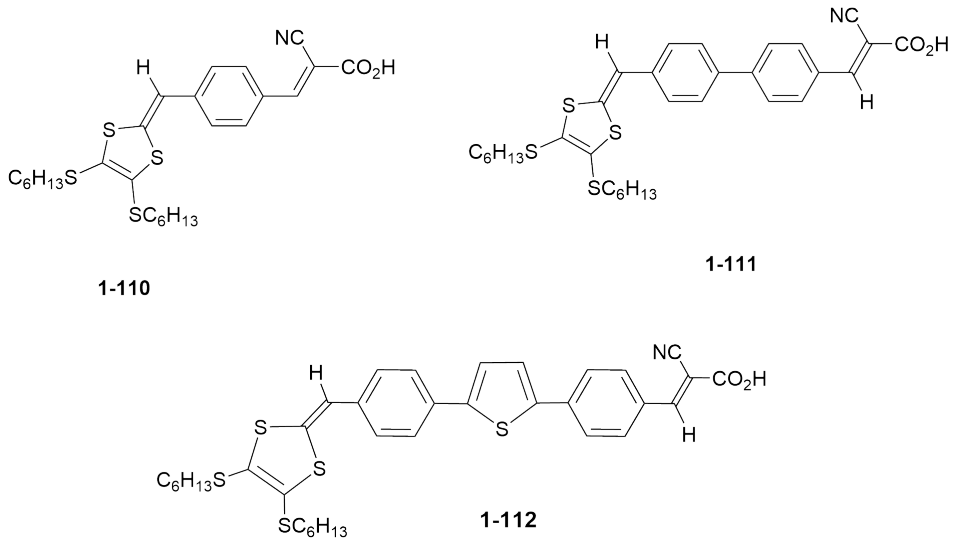

Figure 1.17: DTF-unit as a donor for high-efficiency dye-sensitized solar cells.

to be developed in the future (the power conversion efficiency(η) for the Ru-based N719 is 8.76%. A significant amount of research has been conducted in this area.

Guo and co-workers[184] recently reported that dye sensitized solar cells incorporating DTF functionalized systems were highly efficient. In this study, they synthesized two V-shaped dye compounds (**1-113**, **1-114**, Figure 1.18) that were later co-adsorbed on TiO_2 with chenodeoxycholic acid (CDCA) to obtain a high (η) 9.04%. DSSC systems were functionalized with the same DTF/(2-cyanoacetic acid strategy as star-shaped TPA systems so that they could meet high performance requirements.

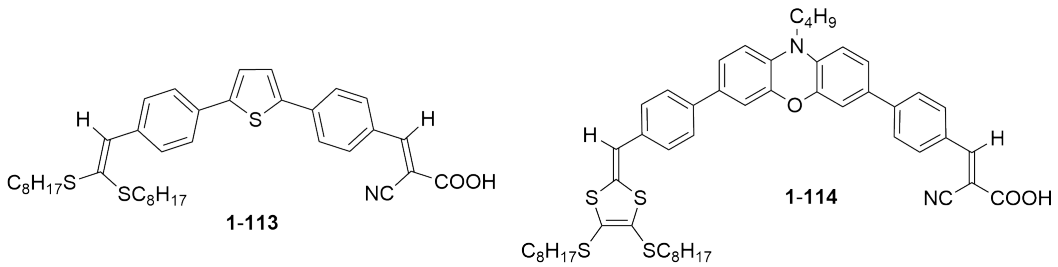

Figure 1.18: V-shaped DTF-functionalized dyes for high-performance DSSCs.

Wang and co-workers[185] designed and synthesized a spiro[uoren-9,9'-xanthene] molecule functionalized with dithiafulvenyl (**1-115** and **1-116**, Figure 1.19). In their study, two substances were found to have the potential to be applied as hole-transporting materials in perovskite solar cells (PVSCs). Because of the beneficial S–S contact in the solid state, the DTF group resulted in high hole mobility and excellent air stability. It was found that compound **1-115** had a hole mobility approximately five times greater than compound **1-116**. The researchers concluded that the DTF positions on the spiro[uorene-9,9'-xanthene] structure can impact device performance to a significant extent.

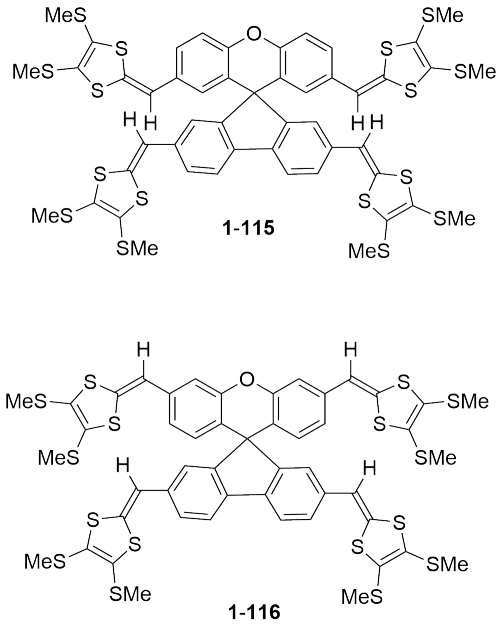

Figure 1.19: DTF-functionalized spiro[uorene-9,9'-xanthene]s as hole-transporting materials for PVSCs.

1.3.2 Molecular Wires

Molecular wires composed of linear π-conjugated oligomers and polymers can be used for a variety of applications, including nanoscale electronics and optoelectronic devices.[186–190] TTF-based charge transfer complexes have been extensively applied in making crystalline materials that contain TTF and acceptors oriented in separated stacks. The polymer composites that consist of TTF charge transfer complexes have been synthesized and examined as transparent conductive materials. The TTF radical cation is able to act as an acceptor and the neutral TTF and TTF radical cation composition can also form mixed-valence complexs. The formation of self-assembly stacking can be considered as a driving force for molecular switches regarding to mechanical movement.[191]

TTF also is considered as a key compound for construction of nanodevices and nanosensors.[192–194] TTF can interact with transition metal ions to yield charge transfer complexes. Previous research measured the charge transfer properties of TTF complexed with various transition metal ions, including (Cu(II), Fe(III), Ru(III), Rh(III), and so forth. Evaluation of their conductivities in the powdery forms has been reported.[195–197]

A number of DTF-functionalized oligo(phenylene ethynylene)s (OPEs) have been synthesized by Nielsen and co-workers (Figure 1.20).[198–202] These oligomers were subjected to conductive probe (CP) atom force microscopic (AFM) measurements on self-assembled monolayers (SAMs) and mechanically controlled break-junction experiments on single molecules in order to understand their molecular wire behavior and related structure-property relationships.[203,204]

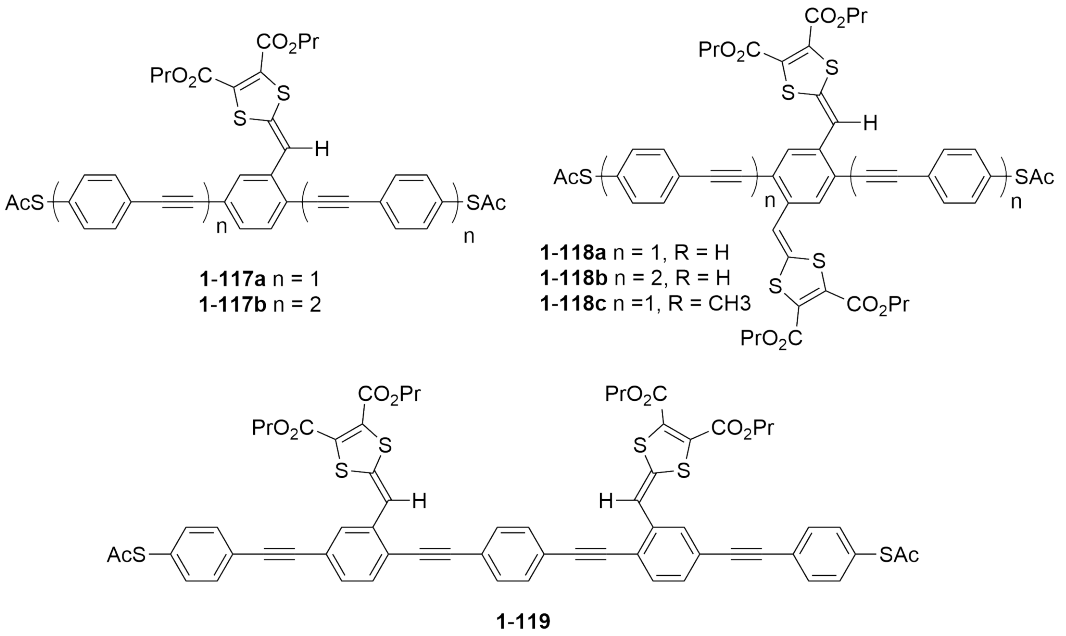

Figure 1.20: DTF-functionalized OPEs as molecular wires.

CP-AFM analysis of these OPE wires showed that the molecular conductivity increases as the number of DTF groups orthogonally arranged increases along the wires. In contrast, DTF groups result in a decrease in the probability of junction formation as well as insignificant effects on the conductance of a single molecule, which was indicated by single-molecule measurements using STM-BJ and MCBJ. Other factors, such as the structure of the interfacial layer, are also important. On the other hand, it is a very challenging task to measure molecular conductance. According to a study by Lissau *et al.*,[205] a group of A-substituted OPE wires with linear and cross-conjugated structures has been investigated. Two DTF-functionalized OPEs were characterized and compared (**1-120** and **1-121**, Figure 1.21). According to the MCBJ measurement with gold contacts, both compounds displayed remarkably broadened conductance peaks. The conductance histograms of compounds **1-115** and **1-116** were different, since **1-120** exhibits linear conjugation and **1-121** shows cross

conjugation.

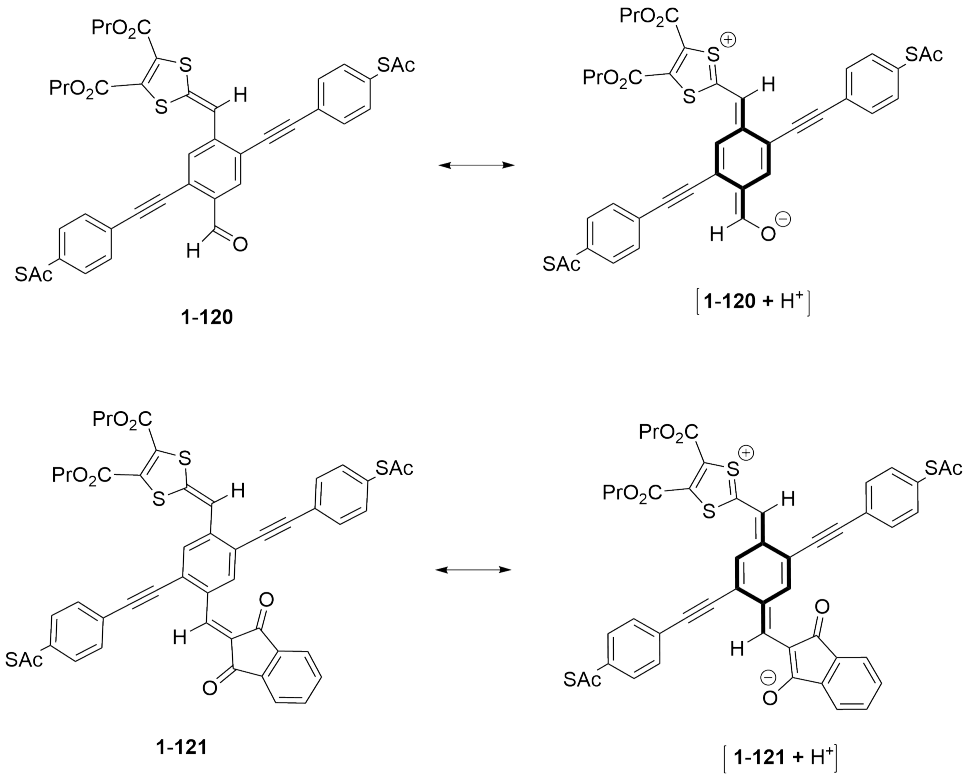

Figure 1.21: Cruciform-shaped D–A substituted OPE molecular wires.

Petra and co-workers[206] prepared label-free biosensors based on functionalized TTF–Au wires in combination with microfluidic techniques. The TTF-Au wires were prepared through bottom-up synthesis and functionalized with various molecules in order to achieve label-free sensing functions for catecholamines and human IgG (Schemes 1.24 and 1.25).

.

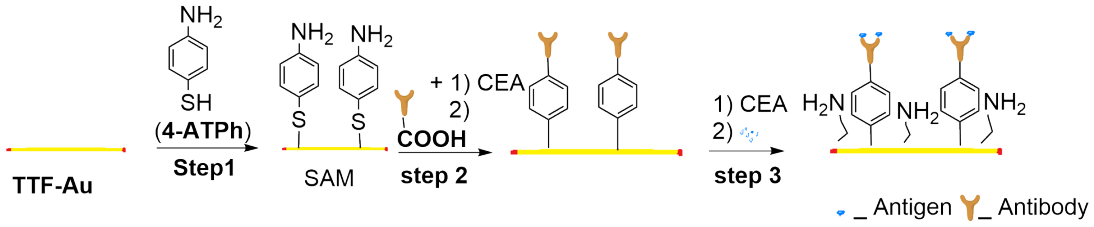

Scheme 1.24: Functionalization of the TTF–Au wire for immunoassay. Step 1: SAM of 4-ATPh. Step 2: immobilization of the capturing antibody (anti-human IgG) by using EDC/NHS. Step 3: (1) blocking the unreacted wire surface by CEA and (2) antigen (human IgG) binding.

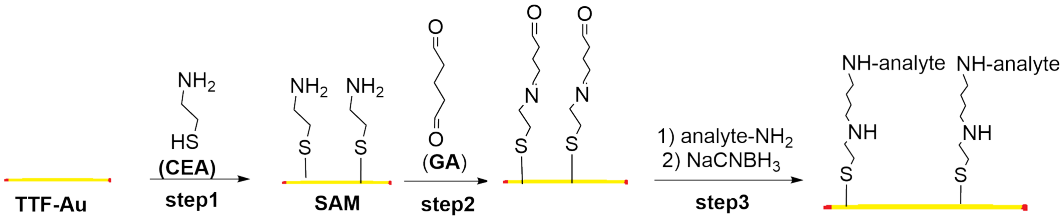

Scheme 1.25: Functionalization of the TTF–Au wire for the amine sensing. Step 1: formation of the CEA self-assembled monolayer (SAM) by the Au–S bond. Step 2: binding of GA to form a Schiff base. Step 3: (1) binding of analytes with the amino group (analyte-NH_2) and (2) treatment with $NaCNBH_3$ to form a stable secondary amine.

1.3.3 DTF Building Blocks for Redox-active Sensors

As discussed before, DTF can undergo oxidative coupling to form a C–C bond. Based upon this reactivity, polymers, oligomers, and even macrocyclic molecules can be synthesized using various DTF-substituted molecules as precursors. Hascoat and co-workers[173] in 1997 reported that the oxidative coupling of a bis(DTF) compound **1-122** yielded macrocyclic products **1-123a** and **1-123b** (Scheme 1.26).

In 2016, Mohammadreza and co-workers[207] reported the synthesis of a TTFV-

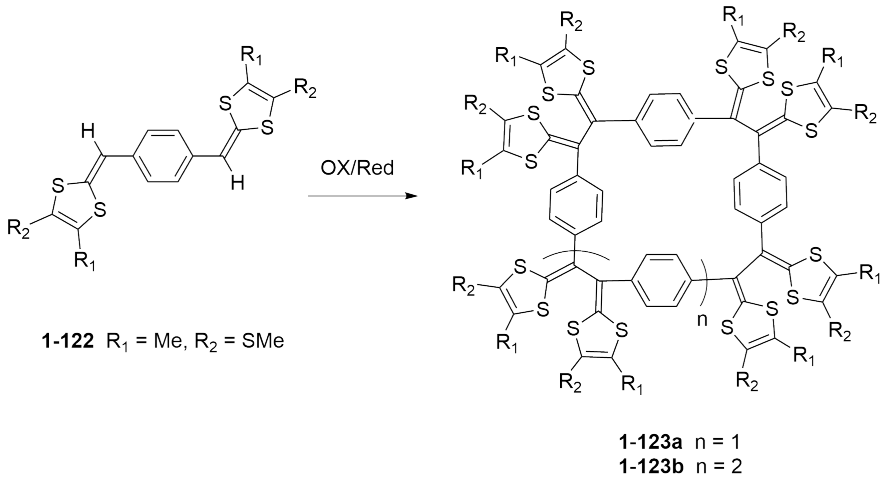

Scheme 1.26: Preparation of TTFV macrocycles through DTF oxidative coupling.

pyrene macrocycle **1-125** through oxidative coupling of bis(DTF)-pyrene **1-124** (Scheme 1.27) There are two steps involved in the synthesis. In the first step, the monomer **1-124** was oxidized using iodine. The reaction was stopped after approximately 45 minutes, yielding a mixture of monomer and dimer. Mechanical grinding was carried out on the mixture in the presence of iodine to yield macrocycle **1-125** with an impressive 37% yield. The reaction time has a major role to play in the synthesis of this macrocycle. Further studies have revealed that macrocycle **1-125** can serve as an effective supramolecular host for nitrobenzene. According to molecular modeling studies, the DTF groups in the structure assists in the binding of macrocycle **1-125** with electron-deficient aromatics. This observation encouraged Mohammadreza to synthesize a class of multivalent DTF-functionalized polyarene building blocks **1-126** and **1-127** (Figure 1.22) for preparation of redox-active polymer thin film sensors, which are highly sensitive to nitrobenzene explosives.[208]

After the multi-cycle cyclic voltammetric scans of the octa-DTF compound **1-122**, a stable microporous cross-linked polymer thin film was created on the

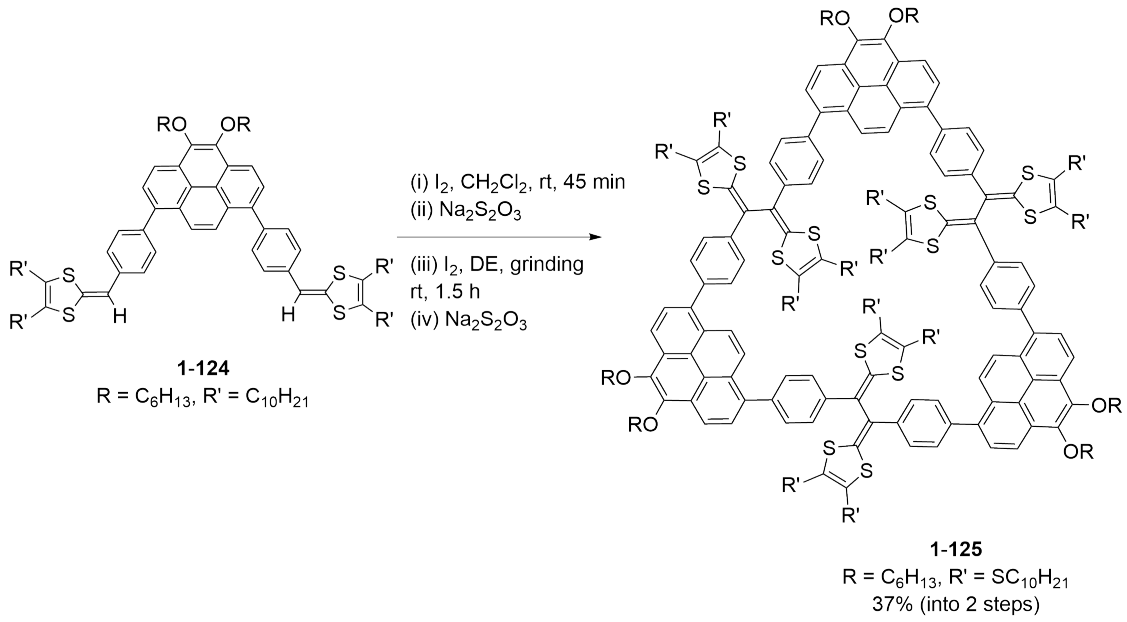

Scheme 1.27: Preparation of TTFV macrocycles under oxidative conditions.

working electrode surface. The thin film formed on the working electrode surface exhibited sensitive electrochemical response to nitrobenzene at low concentrations. Nevertheless, the thin film sensors showed limited durability and stability.

In 2019, a double-layer strategy was proposed and tested by Zhao's group in order to improve the stability of cross-linked polymer thin films.[209] Shahrokhi and Zhao published a report on the synthesis of a TTFV-pyrene derivative **1-128** (Figure 1.23). Through electropolymerization of a DTF-substituted phenylacetylene precursor, a durable redox-active polymer thin film was generated on the surface of a working electrode. This polymer thin film surface was next modified with DTF-substituted dendrimer **1-128** through electropolymeization, which deposited another layer of polymer thin film. This double-layer thin film sensor showed excellent sensitivity and selectivity for TNT among other nitrobenzene derivatives.

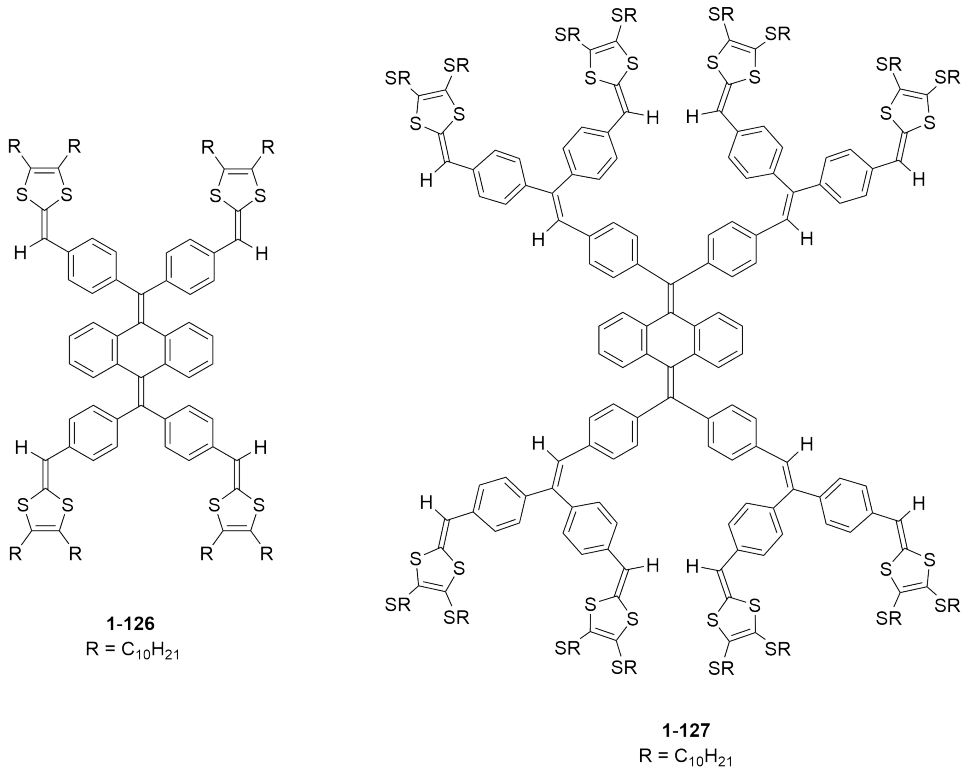

Figure 1.22: Multivalent DTF-endcapped dendrimers.

1.4 Objectives and Organization of This Thesis Work

The performance of the DTF-modified polymer thin film sensors work well in organic solvents, but they are not compatible with aqueous media. When they are placed in water, voltammetric scans would lead to quick detachment of the thin films from the working electrode, resulting in a complete lose of sensing function. It is likely that the hydrophobic nature of the polymer films play an important role in its incompatibility with water. Moreover, these polymer films only showed electrochemical sensing properties for electron deficient aromatic compounds, such nitrobenzene and its derivatives. Further structural modifications are warranted in order to expand the

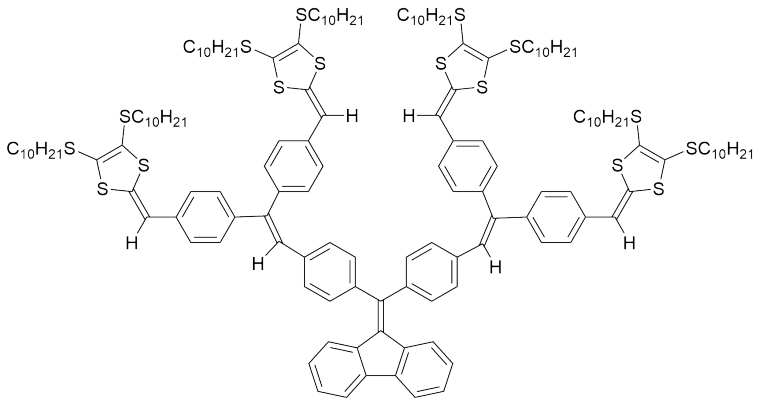

Figure 1.23: Structure of tetra(DTF)-substituted fluorene-cored phenylene vinylene dendrimer **1-125**.

sensing scope of this type of polymer thin films.

The major goal of this MSc dissertation is to develop new DTF and TTFV-based molecular materials for both fundamental studies and applications in optoelectronic devices (e.g., electrochemical sensors). There are two major research projects that have been conducted in this MSc thesis work, dealing with the synthesis and characterization of functionalized π-conjugated DTF and TTFV-based molecular materials. In the synthetic work, a series of reactions, including phosphite-promoted olefination, alkylation, and oxidative coupling were carried out to newly prepared DTF and TTFV derivatives that are subsituted with various donor/acceptor groups. Following the synthesis, advanced instrumental analyses were applied such as NMR, mass spectrometry, IR, UV-Vis absorption spectroscopy, X-ray single crystallography, and cyclic voltammetry (CV), to systematically examine their structural, electronic, and redox properties. Fundamental structure-property relationships and potential applications in electrochemical sensing for aromatic pollutants (e.g. phenol and

phenol derivatives) have been revealed based on the experimental studies. Detailed results of these studies are outlined in the following two chapters.

Chapter 2 describes a comprehensive study of the properties of a series of nitro and methoxy-substituted DTF and TTFV derivatives with focuses placed on understanding their electronic absorption, redox, X-ray single crystallographic, and supramolecular properties. Our studies unravel the effects of donor/acceptor-substitution on the electronic absorption, electrochemical redox, and solid-state supramolecular self-assembling properties of these DTF and TTFV systems.

Chapter 3 focuses on the design and synthesis of a new family of DTF-end-capped redox-active 1,3-diphenoxypropane, in which a new bola-type bis(DTF) compound and its mono-DTF-substituted precursor were synthesized and characterized in this work. Crystallographic and UV-Vis absorption spectral analyses have clearly showed their molecular conformations, solid-state packing, and electronic transition properties. The flexible structure of the bola-bis(DTF) was clearly identified as a key factor that causes significant changes in redox potentials compared to rigid structures counterparts. This result provides a new design concept for for DTF and TTFV-based redox-active molecular devices, including electrochemical sensors. A double-layer thin film was generated through sequential electropolymerization of a structurally rigid bis(DTF) and the bola-bis(DTF) on a glassy carbon electrode. Systematic electrochemical analyses showed that they can act as electrochemical sensors for electron-rich phenol and phenol derivatives. These results point to potential application in sensing emerging organic contaminants in the environment, for example, phenolic industrial wastewater or pollution from cannabis industry. Experimental work in these two chapters have met success, resulting in one research

articles published in a peer-reviewed scientific journal and one submitted manuscript under peer-review. In both papers, the author of this thesis is the first author, who made major contribution to the experimental work and data analysis. The author also actively participated in the manuscript preparation in collaboration with her supervisor and other co-workers. So, Chapters 2 and 3 of this thesis are formatted in a paper-based structure. Chapter 4 describes a summary of this thesis work. Based on the results of this thesis work, future research directions are suggested.

Chapter 2

Donor/Acceptor Substituted Dithiafulvenes and Tetrathiafulvalene Vinylogues: Electronic Absorption, Crystallographic, and Computational Analyses

The contents of this chapter were published as a full article on *New J. Chem.* **2021**, *45*, 11918–11926. Contributions of authors are described below:

Azadeh Afzali is the first author, who conducted all the experimental work and data collection. She also contributed to the manuscript preparation and editing.

Maryam F. Abdollahi is a PhD student in the Zhao group. She conducted the DFT computational analysis reported in this article. Prof. Baiyu H. Zhang is the co-supervisor of Azadeh Afzali, who contributed to developing the project, manuscript editing, and securing funding support to this work. Prof. Yuming Zhao is the supervisor of Azadeh Afzali and helped her design and develop this project. In this article, he acts as the corresponding author, who wrote the manuscript, participated in data analysis, and handled the manuscript submission.

2.1 Introduction

1,4-Dithiafulvene (DTF) is a five-member heterocycle (see Figure 2.1) that has been frequently used as a redox-active molecular building block in various organic electronic materials.[210,211] Being non-aromatic in its neutral state, DTF can be readily converted into an aromatic dithiolium cation through oxidation. As such DTF exhibits very good $\pi-$electron donating properties.[115,212–214] The combination of two DTF groups via an exo-ring C=C bond yields the well-known tetrathiafulvalene (TTF), which has been one of the most studied organic molecules ever since the metallic conductivity of TTF salts was first discovered by Wudl and co-workers in the early 1970s.[215,216] Nowadays, a vast array of TTF-based molecules and its $\pi-$extended analogues (exTTFs) has been documented and their appealing applications in advanced molecular electronic and optoelectronic materials and devices are still attracting unabated research interest and efforts.[217–220]

Among various ex-TTFs, the class of vinyl-extended TTF, namely tetrathiafulvalene vinylogue (TTFV), has been under active investigation over the past two

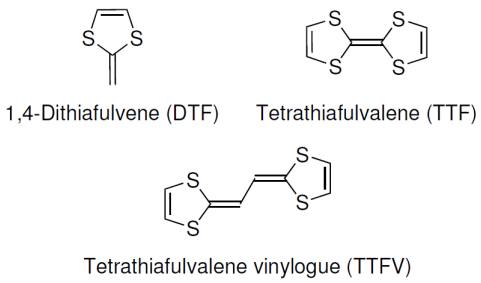

Figure 2.1: Molecular structures of DTF, TTF, and TTFV.

decades.[221] A DTF group can be directly bonded to an arene group (e.g., phenyl), forming a redox-active π-system that is prone to a facile oxidative dimerization reaction.[212–214] As outlined in Figure 2.1, the DTF group upon oxidation releases one electron to generate a reactive radical cation that dimerizes quickly to form a diphenyl-substituted TTFV product. Since TTFV is a better electron donor than DTF, the dimerization reaction eventually leads to a stable TTFV dication before a reductive workup step is implemented. It is worth noting that neutral diphenyl-TTFV and its dication show dramatically different conformations.[222–228] Taking advantage of the excellent redox-activity and unique redox-controlled conformational switching properties of TTFV, various TTFV-based molecular tweezers, conjugated polymers, and macrocycles have been developed to explore their applications in chemical sensing and supramolecular chemistry.[221,228–238] Our group recently reported that a TTFV-pyrene-based macrocycle showed fluorescence turn-on sensing properties for nitrobenzene,[142] while some DTF-TTFV dendrimers exhibited high selectivity and sensitivity in terms of electrochemical recognition/detection of 2,4,6-trinitrotoluene (TNT).[143,144] Nitroaromatic compounds (NACs) have been widely used in explosives, dyes, pesticides, and pharmaceutical feedstocks. Detection and sensing of this type of compounds have important implications in the fields of mining industry, military, na-

tional security, and environmental control.[145–147,239] In our previous work, the sensing performance of TTFV-based materials for nitrobenzenes was ascribed to $\pi-\pi$ interactions between the electron-deficient nitroaromatic ring and the electron-rich dithiole ring of DTF and TTFV groups. In particular, the π-stacking of two aromatic rings with opposite electronic nature has been known to result in intermolecularcharge-transfer[148] that in turn modifies photophysical properties and redox activity.[149,150] To deepen the knowledge for the design of DTF and TTFV-based chemosensors for NACs, fundamental understanding of the interplay between dithiole and nitrobenzene, both covalently and noncovalently, warrants systematic investigations.

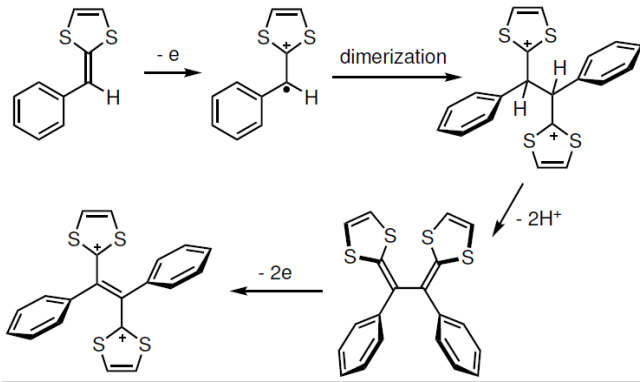

Figure 2.2: Oxidative dimerization mechanism of phenyl-substituted DTF.

In the literature, $\pi-\pi$ interactions of nitrobenzenes with arenes have been investigated mainly by the computational modeling approach.[151] X-ray crystallographic analysis is a powerful analytical tool that can cast in-depth insight into the details of the noncovalent interactions taking place in the solid state.[152] However, X-ray analysis cannot be easily applied to address the topic of nitrobenzene/dithiole noncovalent interactions, mostly due to the difficulty in obtaining good-quality co-crystals of nitrobenzene with DTF or TTFV compounds. To circumvent this problem, we en-

visioned that molecular donor–acceptor ensembles containing nitrophenyl, DTF, and TTFV moieties could serve as suitable model compounds to obtain this knowledge. These compounds allow the electronic interactions between the electron-donating dithiole and electron-withdrawing nitrophenyl groups to be analyzed. Furthermore, their crystallization can lead to good-quality single crystals for diffraction analysis in order to disclose the detailed properties of noncovalent interactions between nitrobenzene and dithiole. Aiming at this goal, we prepared nitrophenyl-substituted DTF and TTFV derivatives **3** and **4** (Figure 2.3). Additionally, electron-rich methoxyphenyl-substituted DTF and TTFV derivatives **7** and **8** were also prepared as counterparts in order to better understand the electronic substitution effects on aromatic $\pi - \pi$ interactions[153] through comparative analyses. Previously, a nitro-substituted phenyl-DTF was reported by Katz *et al.* to show strong second-order nonlinear optical susceptibility.[154] Okada and co-workers recently employed a nitrophenyl-DTF to prepare donor–π–acceptor dyes.[155] The synthesis of certain methoxy-substituted phenyl-DTF and related TTFV derivatives has been documented.[212,224,240,241] Nevertheless, systematic comparative analysis of these donor/accetpor-substituted DTF and TTFV systems have not yet been reported in the literature. The following describes a comprehensive study of the properties of a series of nitro and methoxy-substituted DTF and TTFV derivatives with focuses placed on understanding their electronic absorption, redox, X-ray single crystallographic, and supramolecular properties.

2.2 Results and Discussion

2.2.1 Synthesis of donor/acceptor-substituted DTF and TTFV derivatives

The synthesis of *para*-nitrophenyl and *para*-methoxyphenyl-substituted DTF and TTFV model compounds followed our previously reported procedures.[242] As shown in Figure 2.3, to prepare phenyl-DTF derivatives **3** and **7**, we conducted the phosphite-promoted olefination reactions[243] between 1,3-dithiol-2-thione **2** with *para*-nitrobenzaldehyde (**1**) and *para*-methoxybenzaldehyde (**6**), respectively. These olefination reactions proceeded smoothly at elevated temperature (100–120 °C) for 3 h. Nitrophenyl-substituted DTF **3** was obtained in a modest yield of 46%, and it appears as a red-colored crystalline solid after purification. Compound **3** was found to slowly decompose during a certain period of time when stored under ambient conditions. In contrast, methoxyphenyl-substituted DTF **7** is a colorless solid with good stability. The limited stability of **3** is therefore deemed to be the reason for its lower yield in comparison with that of *para*-methoxy-substituted DTF **7** (85%), although the two olefination reactions were run under very similar conditions. It is likely that the strongly electron-withdrawing effect of the nitro group enhances the reactivity of vinyl group of **3** towards molecular oxygen to cause decomposition.

DTF derivatives **3** and **7** were subsequently subjected to iodine-induced oxidative dimerization reactions, affording corresponding TTFV products **4** and **8** in similar yields (ca. 50–55%). Like its DTF precursor, nitrophenyl-substituted TTFV **4** is a dark red solid with limited stability. Methoxyphenyl-substituted TTFV **8**, however,

appears as a yellow-colored solid with a much better stability. All the DTF and TTFV compounds were successfully recrystallized to form good-quality single crystals through carefully controlled solvent(CH_2Cl_2)/non-solvent (hexane) diffusion at room temperature. It is noteworthy that during the recrystallization of **4**, a trace amount of yellow-colored single crystals was collected. X-ray structural analysis proved that it is a bis-spiro byproduct **5** (Figure 2.3. Similar side products were observed in the oxidative dimerization of phenyl-DTFs, where the phenyl group carries substituents at its *ortho*-position.[228,242] The central thia-bridged five-member ring of **5** results from the nucleophilic attack by $Na_2S_2O_3$ during the reductive workup step. The formation of **5** indicates that less *ortho*-hindered but more electron-deficient phenyl can also induce this side reaction by enhancing the electrophilicity of the TTFV unit.

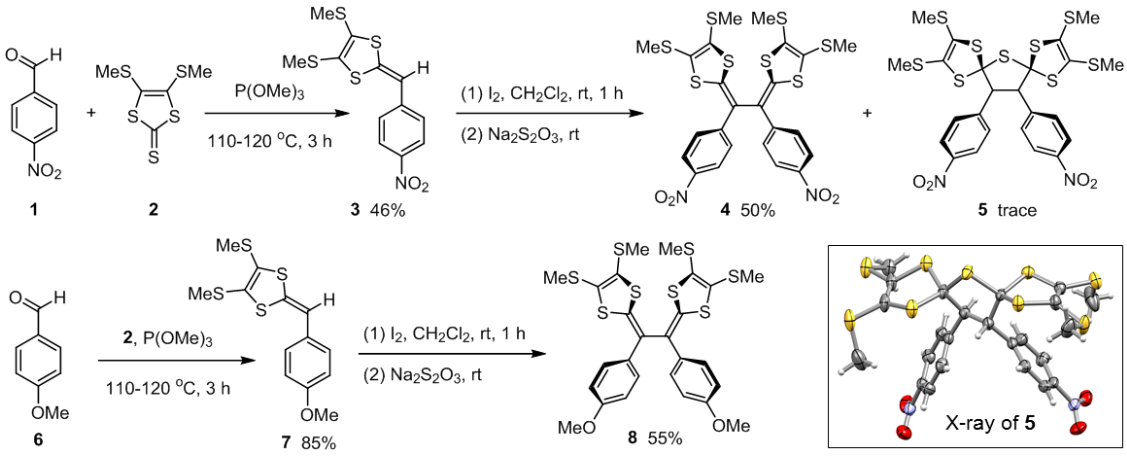

Figure 2.3: Synthesis of *para*-nitrophenyl and *para*-methoxyphenyl-substituted DTF and TTFV model compounds. Inset: X-ray structure of compound **5** (CCDC 2077632).

2.2.2 Comparative study of the electronic properties of donor / acceptor-substituted DTF and TTFV derivatives

The electronic properties of *para*-nitrophenyl and *para*-methoxyphenyl-substituted DTF and TTFV derivatives were investigated by UV-Vis absorption and cyclic voltammetric (CV) analyses. As shown in Figure 2.4, the UV-Vis spectrum of nitrophenyl-substituted DTF **3** shows significant low-energy maximum absorption band (λ_{max}) at 449 nm, which can be mainly ascribed to the HOMO→LUMO transition according to density-functional theory calculations (see the Appendix for detailed TD-DFT results). The λ_{max} of methoxyphenyl-substituted DTF **7** appears at 341 nm, which is substantially blueshifted than that of **4**. The cut-off wavelength of the low-energy band of **3** is observed at 522 nm, which corresponds to an optical bandgap (E_g) of 2.37 eV. The (E_g) of DTF **7** is calculated as 3.05 eV according to the cut-off wavelength at 406 nm in its UV-Vis spectrum. Clearly, the direct $\pi-$conjugation between the electron-donating dithiole and electron-withdrawing nitrophenyl units of **3** results in a very strong electron push–pull effect and hence a relatively narrow optical bandgap. The donor (methoxy) substitution, on the other hand, does not influence the degree of $\pi-$electron delocalization as much as the acceptor (nitro) substitution.

The UV-Vis spectrum of nitrophenyl-substituted TTFV **4** shows a low-energy absorption band at the same wavelength as that of its DTF precursor **3**. This is because the molecule of **4** takes a twisted conformation that prohibits effective $\pi-$electron communications between the two phenyl-DTF segments in the molecule. As such, the degree of $\pi-$electron delocalization of TTFV **4** is nearly the same as that

of DTF **3**, albeit the $\pi-$framework of **4** is much larger in size than DTF **3**. Similar results can be found when comparing the UV-Vis spectra of nitrophenyl-substituted TTFV **8** and its DTF precursor **7**. Again, the twisted TTFV conformation can be used to rationalize these outcomes. In is interesting to note that the absorption band of bis-spiro compound **5** is substantially blueshifted to 264 nm in comparison to its TTFV counterpart **4**. Obviously, the disruption of $\pi-$conjugation between the dithiole and nitrophenyl moieties exerts a pronounced effect of lowering the degree of $\pi-$electron delocalization.

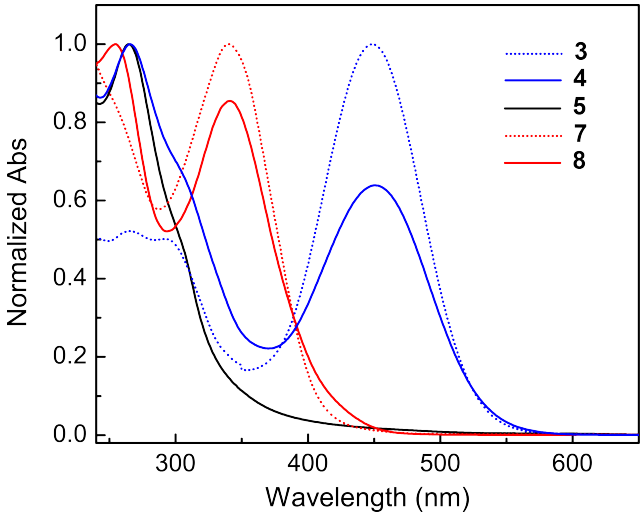

Figure 2.4: UV-Vis absorption spectra of compounds **3**–**5**, **7**, and **8** in CH_2Cl_2 at room temperature.

The electrochemical redox properties of the DTF and TTFV derivatives are investigated by multi-cycle CV analyses. As shown in Figure 3.10A, both the nitrophenyl and methoxyphenyl-substituted DTFs (**3** and **7**) show quasi-reversible redox wave pairs in their voltammogram. It is interesting to note that the cathodic and anodic potentials of nitrophenyl-substituted DTF **3** are more positive than

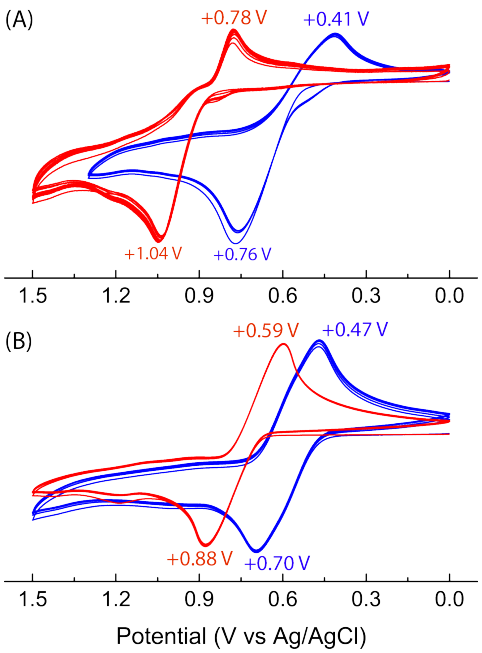

Figure 2.5: Cyclic voltammograms of (A) DTF derivatives **3** (red trace) and **7** (blue trace), and (B) TTFV derivatives **4** (red trace) and **8** (blue trace).

those of methoxyphenyl-substituted DTF **7**. The significant differences in redox potentials testify to a strong electronic substitution effects on the π-electron density of DTF, which is in good agreement with the data of UV-Vis analysis. Multi-cycle CV scans of the two DTF derivatives show no significant changes in their CV profiles. Previously reported phenyl-DTFs usually show an apparent growth of a redox wave couple after the first cycle of CV scans, as a result of the formation and accumulation of oxidatively coupled products (TTFVs) on the working electrode during the CV scans.[244,245] However, this is not the case for DTFs **3** and **7**. It is noteworthy that the cathodic peak appearing the reverse scan of DTF **3** (at +0.78 V) is significantly more positive than that of its TTFV counterpart **4** (+0.59 V). Comparison of the CV data of DTF **3** and DTF **4** thus confirms that the quasi-reversible features revealed by the voltammogram of **3** are mainly due to the single-

electron transfer (oxidation/reduction) processes occurring on the DTF moiety, and there is no significant deposition of oxidatively dimerzed product (i.e., TTFV **4**) on the working electrode during the multi-cycle CV scans of **3**. It is likely that the strong electron-withdrawing effect of nitro group reduces the reactivity of the radical cation of **4** towards dimerization under the electrochemical conditions.The redox potentials of methoxyphenyl-substituted DTF **7** and TTFV **8** are quite similar. The separation of anodic and cathodic peaks for TTFV **8** is narrower than DTF **7**, indicating a higher degree of reversibility. The qausi-reversible redox wave pair in the voltammogram of **7** can be assigned to single-electron transfer on the DTF moiety, while the redox wave pair in the voltammogram of TTFV **8** is attributed to simultaneous two-electron transfers. The multi-cycle CV scans of DTF **7** does not show the characteristic growth of TTFV redox couple. It is reasoned that the electron-donating methoxy group provides stabilization to the radical cation of DTF **7**, which in turn makes its dimerization reaction rate on the working electrode slower than the CV scan rate applied.

2.2.3 X-ray single crystallographic properties

The X-ray single crystal structure of nitrophenyl-DTF **3** is shown in Figure 2.6. In the crystalline state, the molecule of **3** adopts a fully planar π-conjugated conformation, which facilitates the electron push-pull interactions between nitrophenyl and dithiole groups. The crystal packing contains slipped face-to-face π-stacks (see Figure 2.6A), where adjacent molecules of **3** are in an antiparallel orientation with close intermolecular distances of 3.43 Å and 3.48 Å, respectively. Such an arrangement

allows the electron-donating dithiole group to interact with the electron-withdrawing nitrophenyl group intermolecularly. Of note is that in the adjacent pair of molecules, the benzylic carbon atoms show a close intermolecular distance of 3.39 Å (highlighted in Figure 2.6B), which is slightly shorter than the van der Waals diameter of carbon.

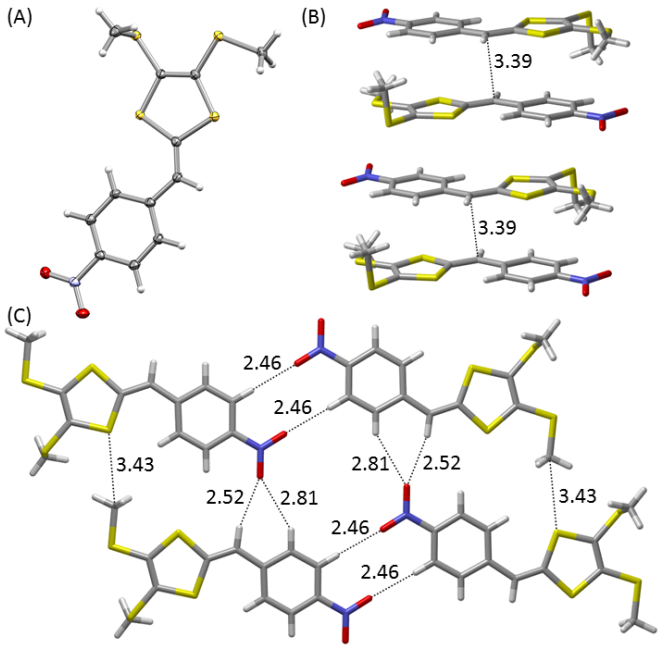

Figure 2.6: (A) ORTEP drawing (50% ellipsoid probability) of *para*-nitrophenyl-DTF **3**. (B) Crystal packing diagrams of **3** showing (B) slipped face-to-face π-stacking, and (C) edge-to-edge interactions. Selected intermolecular distances are highlighted in Å (CCDC 2077629).

The two methyl groups of DTF **3** show different orientations with respect to the conjugated molecular plane; one is nearly co-planar, and another is perpendicular. The co-planar methyl group encounters more steric crowding with the dithiole ring of the same molecule; however, intimate intermolecular S$\cdots$C contacts can be observed between the co-planar methyl and a dithiole sulfur atom of the adjacent

molecule (Figure 2.6C) with a S···C distance of 3.43 Å. This interaction brings about stabilizing effects due to favored donor–acceptor orbital interactions; that is, the lone pair orbital of the dithiole sulfur atom (donor) to interact with the antibonding orbital of the C–S bond (acceptor). The nitro group in DTF **3** facilitates intermolecular hydrogen bonding interactions as well. As shown in Figure 2.6C, the nitro oxygen atoms show close contact with the edges of adjacent molecules, forming O···H hydrogen bonds with distances from 2.46 Å to 2.81 Å. Overall, the solid-state packing of nitropheny-DTF **3** is organized by π-stacking, S···C contact, and hydrogen bonding interactions.

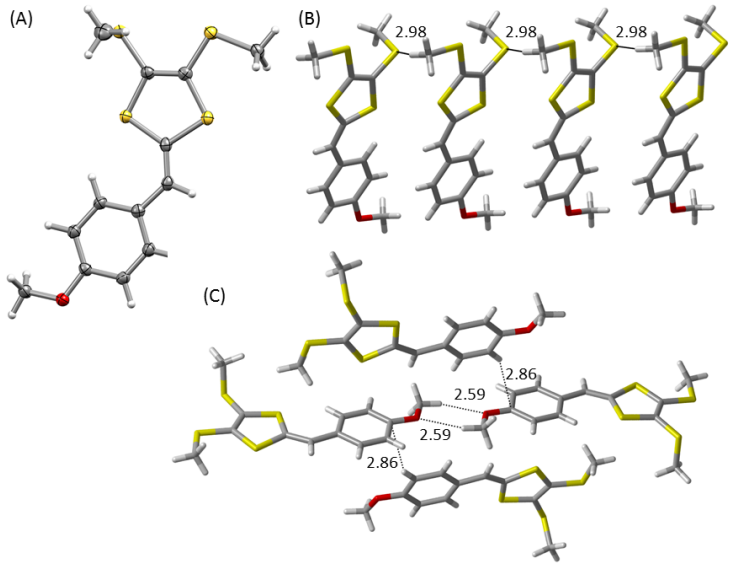

Figure 2.7: (A) ORTEP drawing (50% ellipsoid probability) of *para*-methoxyphenyl-DTF **7**. (B) Crystal packing diagrams of **7** showing (B) slipped face-to-face π-stacking, and (C) edge-to-edge interactions. Selected intermolecular distances are highlighted in Å (CCDC 2076928).

The X-ray structure of methoxyphenyl-DTF **7** is depicted in Figure 2.7. Like its

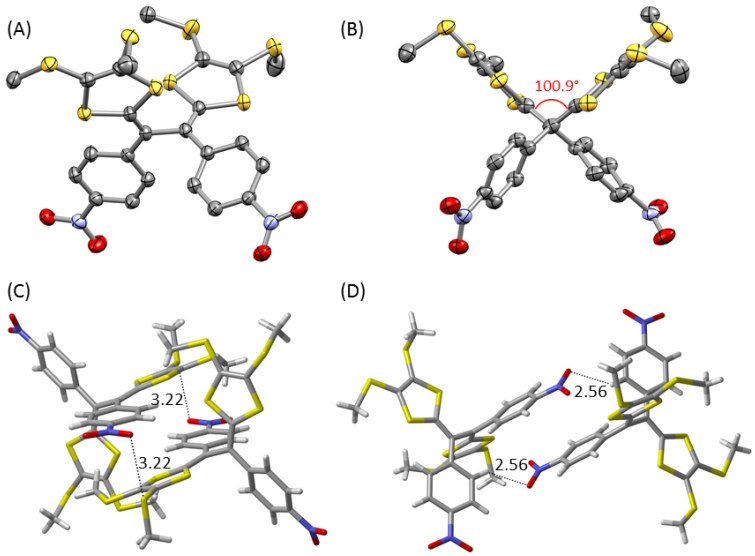

Figure 2.8: (A) and (B) ORTEP drawings (50% ellipsoid probability) of *para*-nitrophenyl-TTFV **4** viewed from different perspectives (hydrogen atoms are not shown for clarity). Crystal packing motifs of **4** driven by (C) intermolecular O···S and (D) O···H interactions. Selected intermolecular distances are highlighted in Å (CCDC 2077631).

counterpart **3**, the π-framework of **7** retains a fully planar conformation to attain a maximum degree of π-conjugation. The packing of **7** in the crystal structure is dominated by intermolecular S···H, O···H, and CH···π interactions as highlighted in Figure 2.7B/C. There is no significant π-stacking observed in the crystal structure, which can be rationalized by the electron-donating methoxyphenyl and dithiole rings in **7** that are repulsive to one another when they are arranged face-to-face. The contrasting packing motifs between **3** and **7** indicate that the electron-rich dithiole unit only favors stacking with electron-deficient nitrobenzene, which accounts for the observed selective binding of NACs with certain dithiole-containing systems.[207,208]

The X-ray structure of nitrophenyl-substituted TTFV **4** shows a twisted confor-

mation due to the significant steric crowding among the arene groups in the molecule (Figure 2.8A/B). It is worth noting that the dihedral angle between the two vinyl units in **4** is 100.9°, rendering the molecule a cruciform-shaped conformation as can be clearly viewed in Figure 2.8B. Such a conformation disfavors intermolecular face-to-face π-stacking among the arene groups in the crystal packing. On the other hand, the electron-withdrawing nitro group gives rise to attractive intermolecular O$\cdots$S interactions with adjacent SCH_3 group, which draws the dithiole ring to a close proximity to the nitrobenzene unit (Figure 2.8C). In a sense, these types of interactions can be ascribed to the "chalcogen bonding interactions",[243,246–249] which could account for the supramolecular binding of NCAs with various TTFV-based systems.[207,208,250] Moreover, significant intermolecular O$\cdots$H interactions can be seen between closely positioned nitro oxygen and phenyl proton (Figure 2.8D).

The molecules of methoxyphenyl-substituted TTFV **8** in the single crystal show two slightly different molecular structures (Figure 2.9A). Both show cruciform-shaped conformations similar to that of TTFV **4**, but the dihedral angle between the two vinyl units in each of the molecules (81.9° and 95.7°, respectively) is smaller than that of **4**. The two molecules of **8** show close CH$\cdots\pi$ contacts among the methoxy and phenyl rings, which serve as the main noncovalent forces assembling the crystal packing of **8**. As shown in Figure 2.9B, there are four molecules of **8** in the unit cell. Unlike the packing of TTFV **4**, the crystal structure of **8** does not show significant intermolecular interactions between the dithiole and methoxyphenyl rings. The results further corroborate that electron-rich dithiole only favors to interact with electron-deficient arenes such as nitrobenzene.

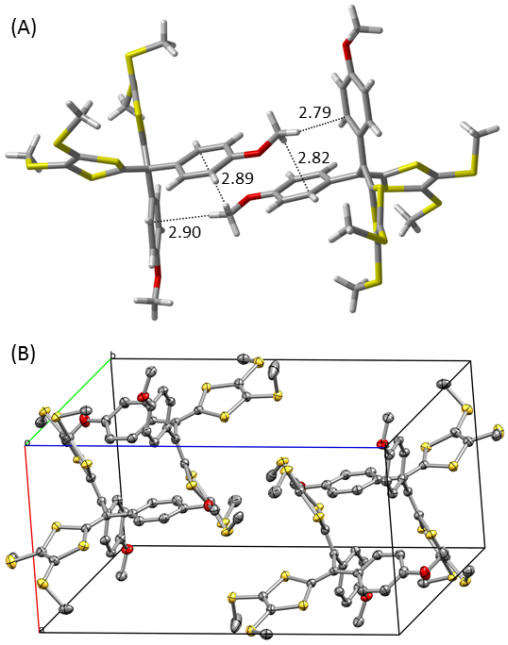

Figure 2.9: (A) X-ray structures of two molecules of *para*-methoxyphenyl-TTFV **8** with intermolecular CH$\cdots\pi$ interactions highlighted in Å. (B) ORTEP drawing (50% ellipsoid probability) of the molecules of **8** packed in the unit cell. Hydrogen atoms are not shown for clarity (CCDC 2077628).

2.2.4 DFT computational analysis

2.2.4.1 Molecular electrostatic potential and frontier molecular orbital properties

To further understand the electronic properties of *para*-nitrophenyl and *para*-methoxyphenyl substituted DTF and TTFV derivatives, density functional theory (DFT) calculations were carried out. We first examined the electron density and frontier molecular orbital (FMO) properties of these compounds in the gas phase. As shown in Figure 2.10A, the molecular electrostatic potential (MEP) plot of nitrophenyl-substituted DTF **3** shows that the nitro oxygen atoms possess the highest

negative electrostatic potentials, while the regions around the methyl, vinyl, and phenyl hydrogens exhibit significant positive electrostatic potentials. Such a charge distribution pattern is in line with the intermolecular edge-to-edge interactions in the crystal packing (see Figure 2.6A). In contrast to **3**, the MEP plot of methoxyphenyl-substituted DTF **7** reveals a high degree of electron density over the phenyl ring and dithiole group, which accounts for their disinclination towards co-facial π-stacking in the crystal packing. The most positive electrostatic potentials of **7** are located around the methoxy and thiomethyl groups. The observed S$\cdots$H and edge-to-edge contacts in the crystal packing of **7** (Figure 2.7C and D) are also in line with the charge distribution properties disclosed by the MEP plot.

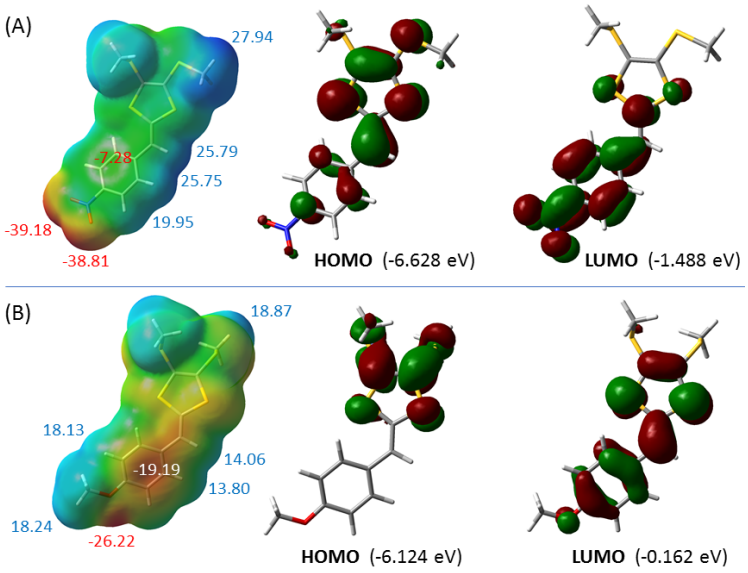

Figure 2.10: Plots of MEP surfaces and frontier molecular orbitals for DTF derivatives (A) **3** and (B) **7**. Maximum and minimal potentials on the MEP surfaces are highlighted (in kcal/mol). Calculations done at the M06-2X/Def2SVP level of theory.

The highest occupied molecular orbital (HOMO) of nitrophenyl-substituted DTF

3 is mainly distributed on the electron-rich dithiole unit, and its lowest unoccupied molecular orbital (LUMO) is more concentrated on the electron-withdrawing *para*-nitrophenyl moiety (Figure 2.10A), indicating a high degree of π-electron delocalization. For methoxyphenyl-substituted DTF **7**, the HOMO is solely contributed by the dithiole group, whereas the LUMO is extensively distributed across the π-conjugated phenyl-dithiole framework. The HOMO energy of **3** is lower than that of **7** by 0.504 eV. Since the oxidation potential can be correlated to the HOMO energy,[251] such a significant difference in the HOMO energies of **3** and **7** concurs with the results of their CV analysis; that is, the anodic peak of **3** in its cyclic voltammogram is more positively shifted by 0.26 V relative to that **7** (see Figure 3.10A).

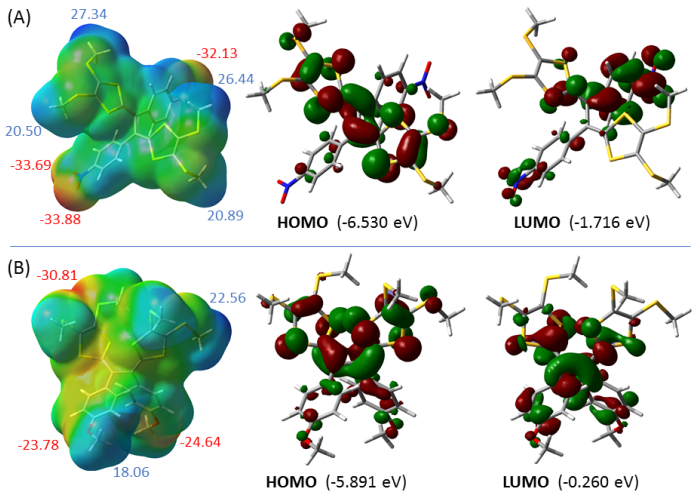

Figure 2.11: Plots of MEP surfaces and frontier molecular orbitals for TTFV derivatives (A) **4** and (B) **8**. Maximum and minimal potentials on the MEP surfaces are highlighted (in kcal/mol). Calculations done at the M06-2X/Def2SVP level of theory.

The MEP and FMO properties of TTFV derivatives **4** and **8** are depicted in Figure

2.11. Similar to its DTF precursor, the nitro oxygens of TTFV **4** hold the strongest negative electrostatic potentials, while the edges of electron-deficient phenyl groups show positive potentials as well. Intermolecular attractions between nitro oxygens and phenyl edges therefore constitute the major driving forces in the crystal packing of **4** (see Figure 2.8D). The HOMO of **4** is distributed along the two dithiole rings and the vinyl bridges between them. The LUMO is mainly located on one of the nitrophenyl group. Compared with DTF **3**, the HOMO of **4** is more delocalized and its energy is higher than that of **4** by 0.098 eV. This result is in line with that of the first oxidation potential of TTFV **4**, which is about 0.16 V lower than that of DTF **3** as determined by CV analysis. The phenyl rings in methoxyphenyl-substituted TTFV **8** do not appear to be as electron-rich as that of DTF **7**. The conformation of TTFV **8** shows a relatively large twist angle between the phenyl and dithiole groups due to significant steric crowding. As such, the electron-pushing effect from the dithiole to the phenyl ring is attenuated. The MEP plot of **8** shows that the most negative potentials appear around the methoxy oxygen atoms, and the thiomethyl and methoxy groups possess the most positive potentials. Relative to its DTF precursor **7**, the HOMO of **8** is also more delocalized and its energy is therefore lower than that of **7** by 0.233 eV. The LUMO of **8** is mainly distributed along the dithiole and vinyl moieties. The phenyl rings of **8**, however, make a much smaller degree of contribution to the LUMO in comparison to its DTF precursor **7**.

2.2.4.2 π-Stacking properties of DTF 3

To quantitatively examine the face-to-face π-stacking properties between electron-rich dithiole and electron-deficient nitrophenyl groups, a π-stacked dimer of nitrophenyl-

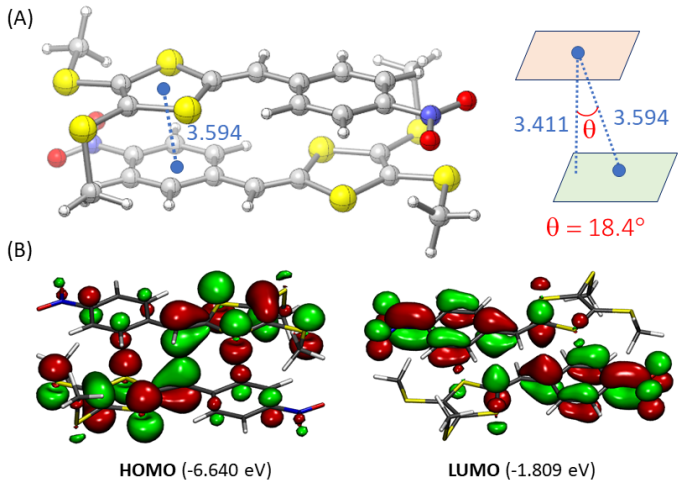

Figure 2.12: (A) Optimized geometry of a dimeric assembly of DTF **3** in the slipped face-to-face stacking mode. Intercentroid and interfacial and distances are highlighted in Å. (B) Plots of frontier molecular orbitals of the dimer of **3**. Calculations done at the M06-2X/Def2SVP level of theory.

substituted DTF **3** was modelled in the gas phase by DFT calculations (Figure 2.12A). The geometry of this dimer (referred to as π-dimer herein) shows a parallel displaced stacking mode similar to that observed in the crystal packing (see Figure 2.6B). It is worth noting that in the gas phase, the π-dimer structure shows an interfacial distance of 3.411 Å, which is close to the van der Waals diameter of carbon (3.40 Å). The distance between the centroid positions of the dithiole and phenyl rings that show direct π-stacking is 3.594 Å. With these two distances, the degree of parallel displacement can be reflected by a pitch angle ($\theta = 18.4°$) as shown in Figure 2.12A. It is worth noting that the geometry of the π-dimer is similar to that of two closely packed molecules of **3** in the crystal structure. In the crystal packing, two adjacent molecules of **3** show an interfacial distance of 3.28 Å, an intercentroid dithiole–phenyl distance of 3.79 Å, and a pitch angle of 30.2°. Compared with

the gas-phase π-dimer, the interfacial distance in the crystal packing is shortened slightly and the degree of slippage between the dithiole and phenyl rings is increased. The variation can be explained by the intermolecular edge-to-edge attractions in the crystal packing. The interaction energy (ΔE_{int}) of the π-dimer is calculated to be -22.64 kcal/mol, rendering the π-stacking mode an important cohesive force in the solid-state packing of nitrophenyl-substituted DTF **3**. For organic conjugated materials, $\pi - \pi$ interactions among aromatic rings play a vital role in their electronic properties; especially, the charge transfer process.[252] Usually, close stacking distance and short displacement are conducive to good orbital overlap and hence facilitates intermolecular charge transport.[253] In this sense, the slipped face-to-face stacking mode of the π-dimer of **3** should be beneficial for the development of efficient organic charge-transport materials. To assess the effects of π-stacking on the electronic properties. The frontier molecular orbitals of the π-dimer are computed (see Figure 2.12B). Compared with the individual molecule of **3**, the HOMO energy of the π-dimer is lowered by 0.012 eV, and the LUMO energy is lowered by 0.321 eV. The results indicate that face-to-face π-stacking exerts a more significant effect on the LUMO properties, which in turn would lead to enhanced electron affinity for the crystal of **3**. The computational results for the π-dimer of **3** thus point to a promising prospect for experimentally exploring the charge-transport properties of the single crystal of DTF **3**.

2.3 Conclusions

In conclusion, we have conducted a comprehensive study on the electronic, structural, and crystallographic properties of *para*-nitrophenyl and *para*-methoxyphenyl-substituted DTF and TTFV derivatives. The electron-rich dithiole and electron-deficient nitrophenyl can form donor/acceptor push-pull systems through π-conjugation, resulting in lowered electronic bandgaps and considerably shifted oxidation potentials. Their significant intramolecular charge-transfer properties can be useful for various organic optoelectronic applications. X-ray single crystallographic analyses have shown the detailed supramolecular self-assembling behavior in the solid state. Various noncovalent forces come into play to influence the solid-state packing motifs of these DTF and TTFV derivatives. Of particular note is the crystal packing properties of the nitrophenyl-substituted DTF **3**, in which an antiparallel face-to-face stacking mode exists in its crystal structure. DTF calculations revealed that the molecules of compound **3** favor forming a face-to-face stacked π-dimer in the gas phase, in which the electron-rich dithiole and electron-deficient nitrophenyl rings show attractive interactions. The π-dimer structure shows a slight degree of change in the crystal packing, indicating that this $\pi - \pi$ interacting mode can be retained as a dominant noncovalent force in the solid-state assembly. Computational modeling studies demonstrated that the π-stacking of **3** leads to enhanced intermolecular orbital interactions to narrow the HOMO–LUMO gap. Such properties are beneficial for improving charge transport performance in the solid state and hence make **3** a good candidate in the application of organic semiconducting devices. In contrast to **3**, nitrophenyl-substituted TTFV **4** do not show significant intermolecular $\pi - \pi$ interac-

tions due to its highly twisted molecular conformation. Electron-rich methoxyphenyl substituted DTF **7** and TTFV **8** do not show $\pi - \pi$ interactions either in their crystal packing. Therefore, the molecular conformation and electronic nature are two key factors to consider in the design of face-to-face stacked crystals of aromatic compounds. Overall, the findings reported in this studies offer a fundamental understanding on the interactions of NACs with electron-rich dithiole ring, which is useful for further exploring NACs related molecular sensors and supramolecular hosts.

2.4 Experimental section

2.4.1 Materials and instrumentation

All starting materials and reagents were acquired from commercial sources and used directly without purification. All reactions were carried out in standard, dry glassware. Evaporation and concentration have been conducted with a rotary evaporator. Flash column chromatography was performed with 240-400 mesh silica gel, and thin-layer chromatography (TLC) was carried out with silica gel F254 covered on plastic sheets and visualized by UV light. Melting points (m.p.) were measured using an SRS OptiMelt melting point apparatus and are uncorrected. ^{1}H and ^{13}C NMR spectra were measured on a Bruker Avance III 300 MHz multinuclear spectrometer. Chemical shifts (δ) are reported in ppm downfield relative to the signals of the internal reference $SiMe_4$ or residual solvents ($CHCl_3$: $\delta_H = 7.24$ ppm, $\delta_C = 77.2$ ppm). Coupling constants (J) are given in Hz. Infrared spectra (IR) were recorded on a Bruker Alfa spectrometer. High-resolution APPI-TOF MS analysis was done

on a GCT premier Micromass Technologies instrument. UV-Vis absorption spectra were measured on a Cary 6000i spectrophotometer.

Cyclic voltammetric (CV) analysis was carried out in a standard three-electrode setup controlled by a BASi Epsilon potentiostat. Glassy carbon electrode was used as the working electrode, and its surface was polished by 1.0 micron alumina prior to standard CV scans. A Pt wire was used as the counter electrode, and the reference electrode was Ag/AgCl (3.0 M NaCl). All CV experiments were performed in CH_2Cl_2 and/or CH_3CN media with Bu_4NBF_4 as the electrolyte.

2.4.2 Synthetic procedures

Synthesis of DTF 3. (4-Nitrobenzaldehyde), **4** (0.604 g, 3.992 mmol), compound **2** 4,5-bis(methylthio)-1,3-dithiole-2-thione (0.904 g, 3.992 mmol), and $P(OMe)_3$ (8 mL). The mixture was heated at 120 °C for 3 h with an oil bath. After that, the reaction mixture was subjected to vacuum distillation at the same temperature to quickly remove unreacted $P(OMe)_3$. The residue was purified through silica gel flash column chromatography using hexanes/CH_2Cl_2 (7:3, v/v) as the eluent. The separation resulted in two products. Compound **3** (0.62 g, 1.88 mmol,46%) as a red crystalline solid. m.p: 136.1–138.1 °C; ^{1}H NMR (300 MHz, $CDCl_3$) δ 8.23 (d, J = 15 Hz, 2H), 7.31 (d, J = 15 Hz, 2H), 6.52 (s, 2H), 3.80 (s, 3H), 2.47(d, J = 5 Hz 6H), 2.43 (s ,6H), 2.41 (s, 6H); ^{13}C NMR (75 MHz, $CDCl_3$) δ 144.4, 142.4, 140.0, 128.7, 126.6, 124.2, 111.8, 23.9, 19.1, 18.9, ppm; FTIR (neat) 3084, 2915, 1586, 1548, 1494, 1479, 1317, 1102, 725, 852,742, 681 cm^{-1}; HRMS (APPI, positive) m/z calcd for $C_{12}H_{11}NO_2S_4$ 329.9766, found, 329.9766 $[M + H]^+$.

Synthesis of TTFV 4 Compound**3** (0.500 g, 1.598 mmol) iodin (0.92 g, 3.624mmol) and CH_2CL_2 (10ml) were added to a 100 mL round-bottom flask. The reaction mixture was stirred under N_2 at room temperature for 5 min. Then (60 mL) of the aqueous solution of saturated$Na_2S_2O_3$ was added to the reaction and the mixture was kept stirring for another 15 min. The mixture was poured into a separatory funnel, and the aqueous layer was separated and extracted with CH_2Cl_2 twice. The organic layers were combined and dried over $MgSo_4$. After filtration and concentration under gentle heating and reduced pressure, the resulting residue was subjected to silica gel column chromatography using hexanes/CH_2Cl_2 (hexanes/CH_2Cl_2) (9:1, v/v) as the eluent. to give compound 4 (0.41 g, 0.414 mmol, 55%) crystalline solid . m.p.: 131.9–132.8 °C; ^{1}H NMR (300 MHz, $CDCl_3$) δ 8.18 (d, 9.1H, 4H), 7.51 (d, J = 9.1 Hz, 4H), 2.48 (s,6H),2.40(s,6H), 2.39 (s, 6H) ppm; ^{13}C NMR (75 MHz, $CDCl_3$) δ 148.35, 148.18, 144.60, 142.52, 141.17, 132.06, 129.98, 127.13, 126.38, 126.19,124.94, 124.44, 123.13, 120.94, 81.30, 67.53, 19.19, 19.05, 18.93 ppm; FTIR (neat) 3073, 2919, 2441, 1587, 1505, 1464, 1330, 1189, 1106, 1013, 1963, 848, 702 cm^{-1}; HRMS (APPI, positive) m/z calcd for $C_{24}H_{21}N_2O_4S_8$ 656.9262, found, 656.9264 $[M+H]^+$. A trace amount of compound of **5** was also obtained from the reaction as and yellow crystalline solid during recrystalization of 4. ;^{1}H NMR (500 MHz, $CDCl_3$) δ 8.04 (d, J = 8.9 Hz, 4H), 7.55 (d, J = 8.2 Hz, 4H), 2.27 (s, 6H), 1.94 (s, 6H), ^{13}C NMR (75 MHz, $CDCl_3$) δ146.84, 138.80, 129.21, 124.70, 121.77, 63.45, 29.93, 28.93, 17.43 ppm; FTIR (neat) 3359, 2920, 2851, 1520, 1345, 1261, 1103, 1016, 881, 857, 801, 697 cm^{-1}.

Synthesis of DTF 7. 4-Methoxybenzaldehyde**(6)** (6) (1.05 g, 7.74 mmol), 4,5-bis(methylthio)-1,3- dithiole-2-thione**(2)** (3.50 g, 15.486 mmol), and $P(OMe)_3$ (8.0

mL) were added to a 50 mL round-bottomed flask. The flask was placed in an oil bath and heated at 120°C for 3 h. After that, the reaction mixture was subjected to vacuum distillation at the same temperature to remove unreacted P(OMe)3. The residue was subjected to silica gel column chromatography (hexanes/ CH_2Cl_2, 7: 3) to give pure compound**7** (2.19 g, 6.96 mmol, 85%) as a white crystalline solid; m.p 60.8–61.2 °C; ^{1}H NMR (500 MHz, $CDCl_3$) δ 7.15 (d, J = 8.7 Hz, 2H), 6.89 (d, J = 9 Hz, 2H), 6.42 (s, 1H), 2.42 (s, 3H), 2.40(s, 3H); ^{13}C NMR (75 MHz, $CDCl_3$) δ 157.78, 129.24, 128.87, 128.15, 126.97, 123.93, 114.95, 113.99, 55.31, 18.91, ppm; FTIR (neat) 2962, 2912, 2837, 1556, 1501, 1305, 1283, 1024, 996, 900, 836 cm^{-1}; HRMS (APPI, positive) *m/z* calcd for $C_{13}H_{14}OS_4$ 313.9922, found, 313.9931[M + H]$^+$.

Synthesis of TTFV 8. Compound**7** (0.500 g, 1.59 mmol), iodine (1.02 g, 4.00 mmol), and CH_2Cl_2 (10ml) were added to a 100 mL round-bottom flask. The reaction mixture was stirred under N_2 at room temperature for 5 min. Then 60 mL of the aqueous solution of saturated $Na_2S_2O_3$ was added to the reaction and the mixture was kept stirring for another 15 min. The mixture was poured into a separatory funnel, and the aqueous layer was separated and extracted with CH2Cl2 twice. The organic layers were combined and dried over $MgSO_4$. After filtration and concentration under gentle heating and reduced pressure, the resulting residue was subjected to silica gel column chromatography (hexanes/CH_2Cl_2, 9:1) to give compound**8** (0.26 g, 0.414mmol, 55%) as a pale yellow crystalline solid. m.p 105.7–106.4 °C; ^{1}H NMR (500 MHz, $CDCl_3$) δ 7.35 (d, 9.0H, 2H), 6.87 (d, J = 8.9 Hz, 2H), 3.83 (s,3H), 2.43(s,3H), 2.42 (s, 2H) ppm; ^{13}C NMR (75 MHz, $CDCl_3$) δ 158.6, 133.3, 128.1, 127.8, 124.9, 124.5, 113.9, 58.5, 29.2, 23.8, 19.6 ppm; FTIR (neat) 2924, 2857, 1728, 1671, 1600, 1252, 1174, 1028, 828 cm^{-1}; HRMS (APPI, positive) m/z calcd for $C_{26}H_{2702}S_8$

626.9772, found, 626.9810 $[M+H]^+$.

Chapter 3

Studies of a Bola-Type Bis(dithiafulvene) System: Synthesis, Crystal Structure, and Electrochemical properties

The contents described in this chapter have been submitted to *New J. Chem.* as a full article that is under peer-review. Contributions of authors are described below:

Azadeh Afzali is the first author, who conducted all the experimental work and data collection. She also contributed to the manuscript preparation and editing. Zahra A. Tabasi is second author, who contributed to data analysis and manuscript writing. Prof. Baiyu H. Zhang is the co-supervisor of Azadeh Afzali, who contributed to developing the project, manuscript editing, and securing funding support to this work. Prof. Yuming Zhao is the supervisor of Azadeh Afzali and helped her design

and develop this project. In the submitted manuscript, he acts as the corresponding author, who conducted the DFT/TD-DFT calculations, MD/MM simulations, wrote the manuscript, participated in data analysis, and handled the manuscript submission.

3.1 Introduction

1,4-Dithiafulvene (DTF) is a five-memebered heterocyclic structure with remarkable electronic and electrochemical properties.[254?,255] A significant member in the family of DTF derivatives is the phenyl-substituted DTF, which features a facile oxidative coupling reactivity through a radical dimerization mechanism (Figure 3.1).[256,257] It is worth noting that this reaction not only offers an efficient C–C bond forming strategy for extending the structure of DTF, but serves as the most commonly used synthetic method for making another class of redox-active organic compounds, namely tetrathiafulvalene vinylogues (TTFVs).[258] As shown in Figure 3.1, TTFV is an intriguing π-extended analogue of the well-known organic donor, tetrathiafulvalene (TTF).[259,260] Diaryl-substituted TTFVs not only show reversible redox activities at relatively low potentials, but undergo dramatic conformational changes along with their redox processes. Owing to its rich electronic properties and redox activity, DTF has been widely used as a functional molecular building block in a wide range of molecular devices, such as molecular wires,[261,262] molecular receptors,[263–266] chemical sensors,[267–269] nonlinear optical phores,[270–273] and high-performance chromphores for dye-sensitized solar cells,[274–280] and so on.

It is noteworthy that a large number of bis- and poly(DTF)-substituted compounds have been synthesized and reported in the literature, serving as reactive build-

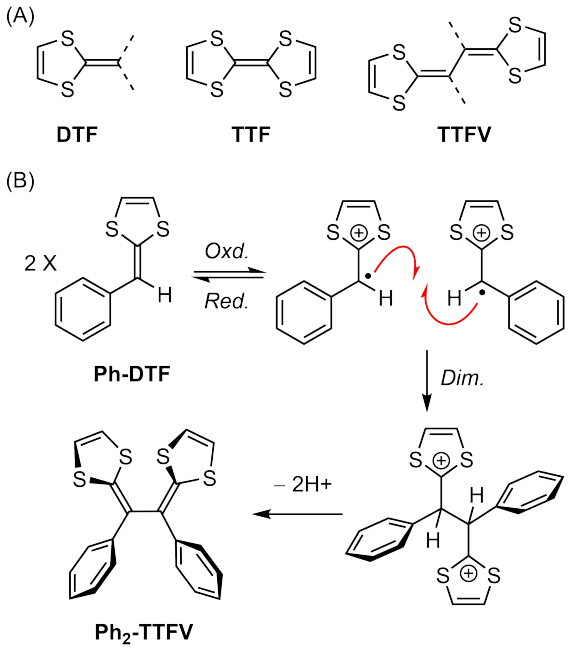

Figure 3.1: (A) Molecular structures of DTF, TTF, and TTFV. (B) Oxidiative dimerization of phenyl-subsitututed DTF.

ing blocks for construction of complex polymeric and macrocyclic structures.[281–288]

Previously, we, have extensively examined the type of DTF–π–DTF molecular structures, in which the central linkages are structurally rigid π-conjugated systems.[262,284–290] These compounds can be viewed as "molecular dumbbells" or "molecular wedges" depending on the shape of the π-linker (see Figure 3.2). When subjected to oxidative coupling conditions, their molecular rigidity predisposed them to form linear conjugated oligomers, polymers, and shape-persistent macrocycles, depending on the structural and electronic nature of the π-linkages. Bis(DTF) compounds with a flexible and non-conjugated central linker, on the other hand, give a different class of derivatives herein called "bola-bis(DTF)s" (Figure 3.2). The term "bola" is used due to the resemblance of the molecular shape to the throwing weapon, known as a bolas, which is made of two or more balls interconnected by a soft cord and designed for cap-

turing animals by entangling their legs. In contrast to their structurally rigid cousins, bola-bis(DTF)s have been rarely investigated in the literature. The only known examples of bola-bis(DTF)s are those reported by Hapiot and workers in 2007.[291,292] In their work, a series of bis(DTF) derivatives that contain flexible polyoxyethyl linkers with varying lengths were synthesized and characterized by electrochemical analysis. When subjected to electrochemical polymerization, these compounds yielded conducting polymer thin films with quickly switchable redox states.[291] Chemical oxidation of them resulted in crown ether-type macrocyclic ligands, which showed potential application in metal ion recognition.[292] Clearly, the bola-bis(DTF) derivatives could be as useful as rigid DTF–π–DTF systems in development of redox-active polymeric materials and molecular devices. Nevertheless, there has been no further studies on such systems after Hapiot's work. To address this deficiency, we conducted a systematic study of a newly designed flexible bola-bis(DTF) compound, focusing on disclosing fundamental molecular structural, solid-state packing, electronic absorption, and electrochemical properties. Moreover, we have employed the bola-bis(DTF) in combination with a rigid DTF–π–DTF to form a hybrid polymer thin film through stepwise electrochemical polymerizations. This new type of polymer film exhibited intriguing electrochemical responsiveness to phenol and phenol derivatives, which can be useful in the application of environmental sensing. Detailed results of our studies are reported in the following sections.

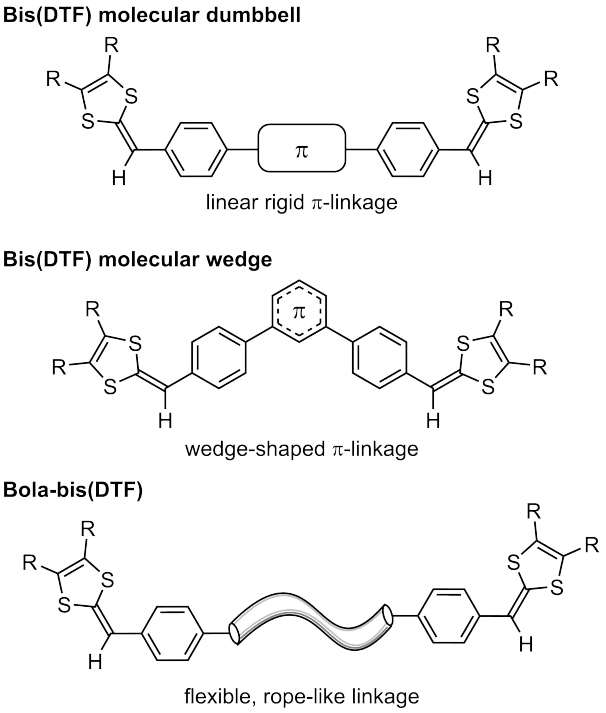

Figure 3.2: Bis(DTF)-substituted molecular building blocks with different molecular shapes and rigidity.

3.2 Results and Discussion

3.2.1 Synthesis

Figure 3.3 outlines the synthesis our designed bola-bis(DTF) **5**. The synthesis began with a double *O*-alkylation reaction between 4-hydroxybenzaldehyde (**1**) and 1,3-dibromopropane in DMF at 100 °C using K_2CO_3 as the base. The reaction proceeded for 12 hours to yield a dibenzaldehyde product **3** in 80% yield. This intermediate contains a 1,3-diphenoxypropane moiety that was intended to serve as the flexible linker for the target bola-bis(DTF). Compound **3** was subsequently subjected to an phosphite-promoted protocol[293] with 1,3-dithiole-2-thione **4** and $P(OMe)_3$. This reaction involved two steps of olefination, yielding a mono-olefinated intermediate

6 first and then the bola-bis(DTF) product **5**. It was observed that both **5** and **6** showed limited stability at high temperature. Therefore the reaction temperature was controlled between 100 to 120 °C to avoid significant thermal decomposition of the intermediate and product. The control of reaction time is also critical. The highest yield (46%) of bola-bis(DTF) **5** was obtained at a reaction time of 3 hours. Longer reaction time led to a lowered yield of **5**. Under the optimal conditions, a significant amount of intermediate **6** remained unconsumed, which could be readily separated and purified through silica flash column chromatography in an isolated yield of 25%. The acquisition of intermediate **6** is actually beneficial for the following characterization studies, since it provides a counterpart of bola-bis(DTF) **5** and hence allows better understanding of structure-property relationships through comparative analyses.

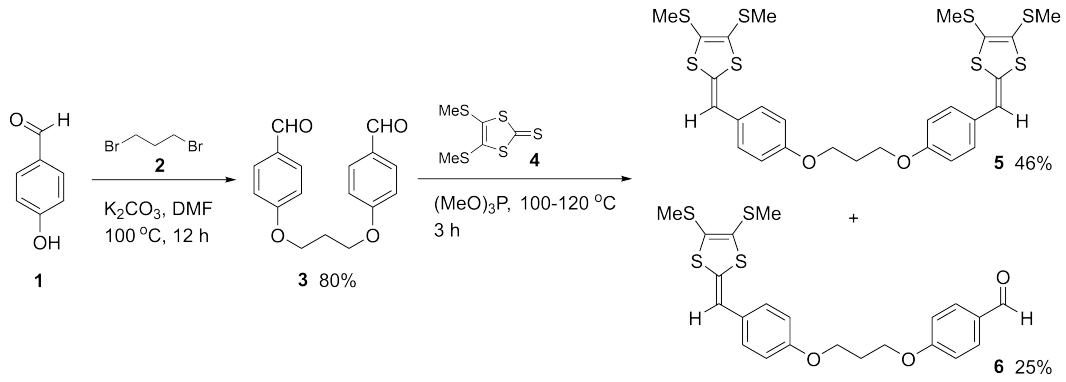

Figure 3.3: Synthesis of bola-bis(DTF) **5** and related intermediate **6**.

3.2.2 Molecular structural and solid-state packing properties

The molecular structures and purity of compounds **5** and **6** were confirmed by NMR, IR, and MS analyses (see Appendix for details). Both compounds are yellow-color

solids with reasonable stability under ambient conditions. Good-quality single crystals of these two compounds were successfully grown by a solvent/non-solvent diffusion method. In this method, pure **5** or **6** was first dissolved in a proper amount of CH_2Cl_2. On the top of the solution was gently added a layer of hexane, which slowly diffused into the layer of CH_2Cl_2 by gravity to induce single crystal growth at room temperature. The obtained single crystals of **5** and **6** were then subjected to single crystal X-ray diffraction (SCXRD) analysis to elucidate their molecular structures and solid-state packing properties.

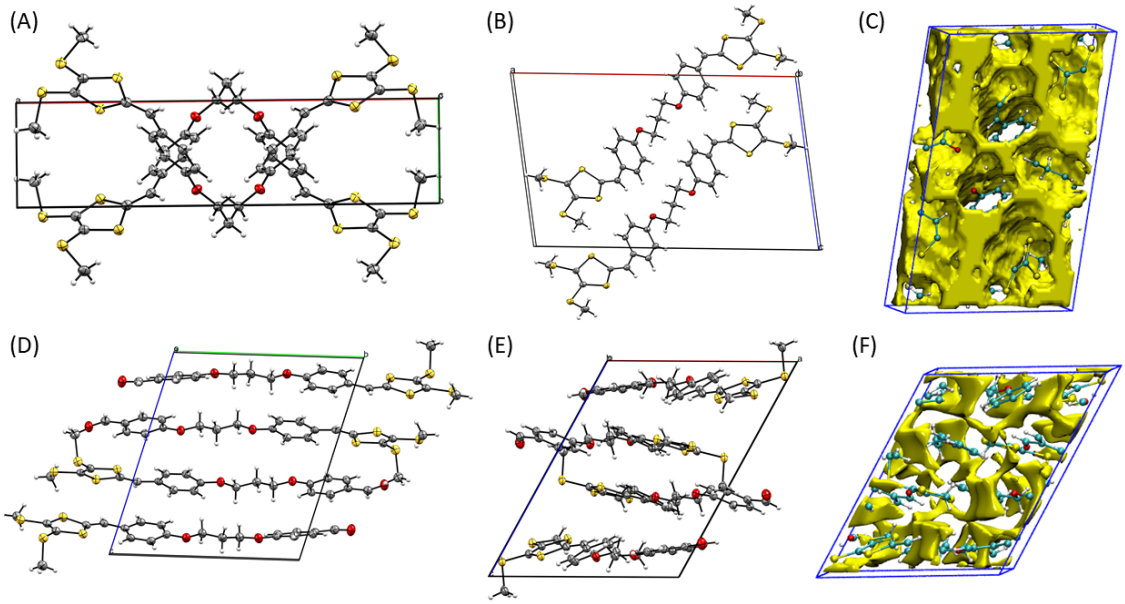

Figure 3.4: ORTEP drawings (50% probability ellipsoids) of the unit cells of (A) **5** viewed along the *c* axis, (B) **5** viewed along the *b* axis, (D) **6** viewed along the *a* axis, and **6** viewed along the *b* axis. Plots of the unit cells of (C) **5** and (F) **6** with free space highlighted by yellow-colored isosurface. CCDC numbers: 2157962 (**5**) and 2158002 (**6**.

Figure 3.4A and B show the X-ray structure of bola-bis(DTF) **5** in the unit cell. Compound **5** crystallizes in the monoclinic space group P/c, with two molecules in the unit cell. In each of the molecules, the central O–C–C–C–O skeleton adopts an all-gauche conformation, rendering the molecule a wedge-like molecular shape. This conformation is similar to that reported for the crystal structure of compound **3**.[294] The crystal packing of compound **5** is hence dominated by a herringbone-shaped stacking as depicted in Figure 3.5. Various non-covalent forces come into play in this type of assembly. Figure 3.5 highlights the C–H$\cdots\pi$ interactions between phenyl rings and their adjacent OCH_2 groups. The stacking distance is 3.55 Å, which is slightly longer than the van der Waals diameter of carbon. Viewing from the edge of this stack, one can notice significant intermolecular S$\cdots$H and S$\cdots$C interactions (Figure 3.5B). The S$\cdots$H contact occurs between two CH_3 groups in proximity, with an S$\cdots$H distance at 2.88 Å and an S$\cdots$H–C angle at 157.4°. These geometric features suggest weak hydrogen bonding interactions. The S$\cdots$C contact shows a distance of 3.46 Å and an S$\cdots$C–S angle of 160.9°. The origin of this contact can be attributed to the orbital interactions between the lone pair orbital of sulfur (donor) and the antibonding orbital of the adjacent C–S bond (acceptor).[295,296] These noncovalent forces enable the wedge-shaped molecules of **5** to pack efficiently in the crystalline state. Figure 3.4C depicts the distribution of free space within the unit cell of **5**, which contributes to 28.93% of the total volume of the unit cell.

The molecular structure of mono-DTF derivative **6** determined in the crystal structure shows a very different conformation in comparison to its bola-bis(DTF) counterpart. As can be seen from Figure 3.4D and E, the crystal structure of of **6** takes a triclinc $P-1$ group space with four molecules in the unit cell. Each of the

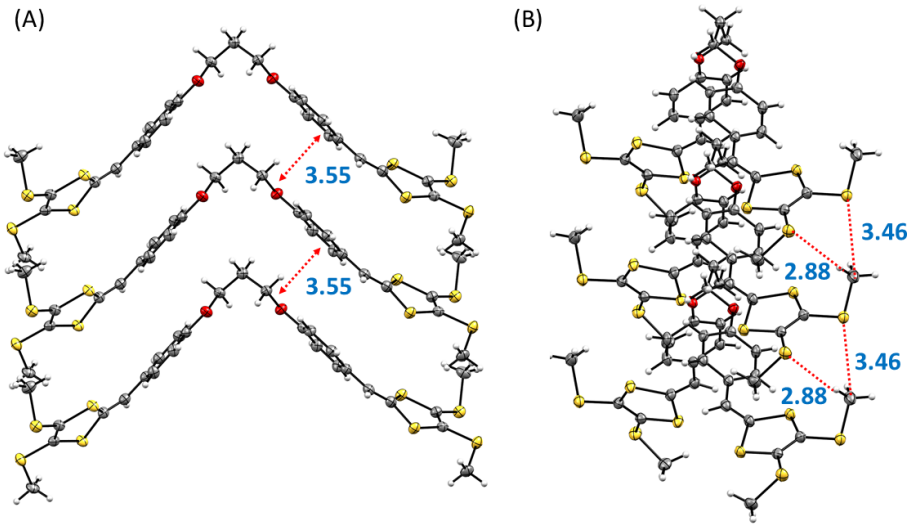

Figure 3.5: (A) Front view and (B) side view of the herringbone-shaped stacking in the crystal packing of **5**. Intermolecular distances are highlighted in Å.

molecules adopts a linear conformation, in which the central O–C–C–C–O tether is in an all-anti (zig-zag) arrangement. In the crystal packing, adjacent molecules of **6** are in an anti-parallel orientation. The free space in the unit cell accounts for 28.15% of the total volume (see Figure 3.4F), which is slightly lower than that of bio-bis(DTF) **5**. Close examination of the crystal packing properties reveals intimate intermolecular C–H$\cdots$O contacts between a pair of anti-parallelly oriented molecules of **6**. As shown in Figure 3.6A, the O$\cdots$H contact between phenyl C–H and phenolic oxygen gives a distance of 2.70 Å, while the methylthio C–H and aldehyde oxgen atom interacts at a distance of 2.60 Å. Both types of O$\cdots$H interactions can be viewed as very weak hydrogen bonding. It is interesting to see that the aldehyde oxygen shows a close intermolecular interaction with one of the SCH_3 groups in an adjacent molecule (Figure 3.6B), indicating an orbital interaction between the oxygen lone pair orbital (donor) and the S–C antibonding orbital (acceptor).[297,298] This donor–acceptor orbital

interaction drives the two interacting molecules into a linear arrangement.

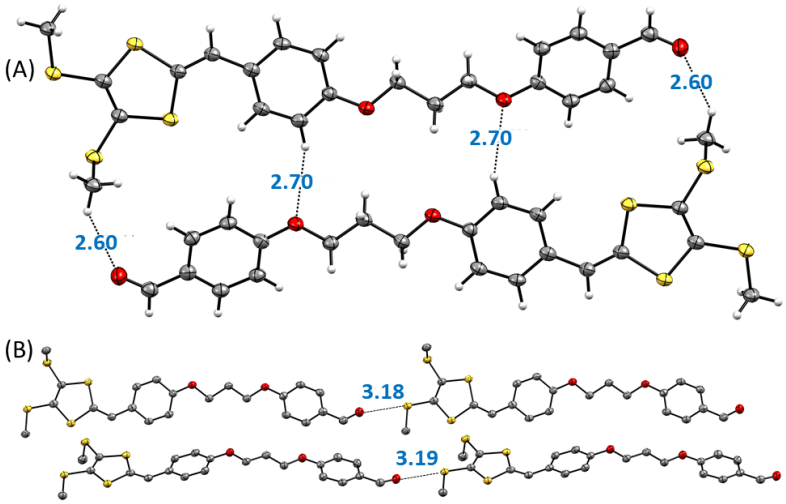

Figure 3.6: (A) Anti-parallel packing of two adjacent molecules of **6** driven by intermolecular O···H interactions. (B) Linear arrangements of the molecules **5** through intermolecular S···S–C contacts. Intermolecular distances are highlighted in Å.

3.2.3 Electronic absorption and molecular orbital properties

The electronic absorption properties of bola-bis(DTF) **5** and its mono-DTF substituted counterpart **6** were determined by UV-Vis spectral analysis. Figure 3.7 compares the normalized UV-Vis absorption spectra of both compounds measured in CH_2Cl_2. Compound **5** shows two absorption bands at 340 nm and 270 nm, while the spectrum of **6** gives two bands at 338 nm and 255 nm. The origin of the low-energy absorption band in each absorption spectrum can be assigned to the $S_\circ \rightarrow S_1$ transition. Since compounds **5** and **6** carry different π-chromophore groups, it is kind of interesting to observe that their low-energy absorption bands are of nearly

identical energy (340 nm for **5** and 338 nm for **6**). Time-dependent density functional theory (TD-DFT) calculations offered a deep insight into their electronic transition properties. Calculated at the M06-2X/DEF2SVP level of theory,[299,300] the $S_\circ \rightarrow S_1$ transition energy for **5** is 3.788 eV (327.3 nm), while the $S_\circ \rightarrow S_1$ transition energy for **6** is 3.781 eV (327.9 nm). These results agree well with the experimental UV-Vis data. Detailed contributions of frontier molecular orbitals (FMO) to the $S_\circ \rightarrow S_1$ transitions for **5** and **6** are summarized in Figures 3.8 and 3.9, respectively.

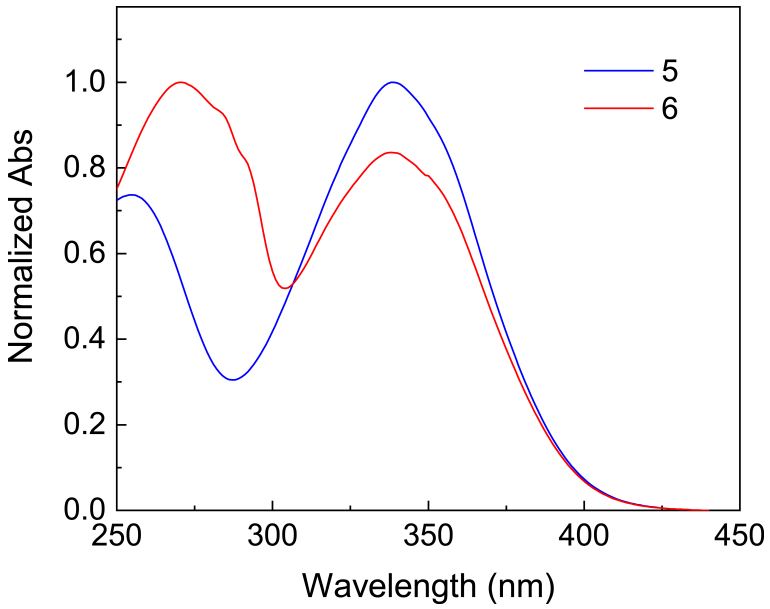

Figure 3.7: Normalized UV-vis absorption spectra of compounds **5** and **6** measured in CH_2Cl_2 at room temperature.

As shown in Figure 3.8, the the $S_\circ \rightarrow S_1$ transition is due to $H - 1 \rightarrow$ LUMO (48%), $H - 1 \rightarrow L + 6$ (10%), and HOMO $\rightarrow$ LUMO (20%). The bonding and antibonding orbitals that participate in the electronic transition show significant spatial overlap at one of the DTF groups (i.e., symmetry allowedness). The $S_\circ \rightarrow S_1$ transition for **6**, as can be seen in Figure 3.9, is contributed by $H - 7 \rightarrow$ LUMO

(83%) and H − 7 → L + 10 (15%). In the molecule of **6**, the HOMO is distributed on the electron-donating phenyl-DTF, while the LUMO is at the electron-accepting benzaldehyde unit. Interestingly, the HOMO → LUMO transition has no contribution to the $S_\circ \rightarrow S_1$ band, because they are spatially separated (i.e., symmetry forbidden transition). The benzaldehyde unit appears to be the chormophore group that gives rise to the $S_\circ \rightarrow S_1$ band of **6**, the transition energy of which is nearly identical to that of **5** by coincidence.

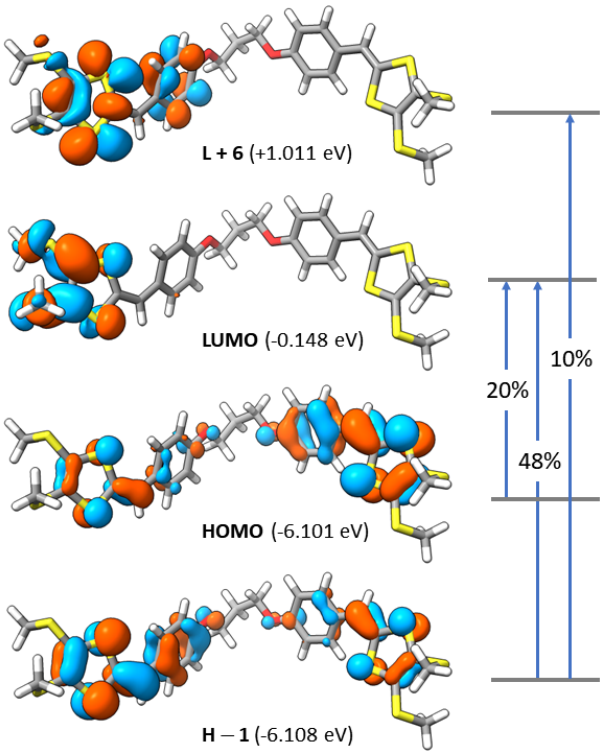

Figure 3.8: Plots and energies of the FMOs of **5** that are involved in the $S_\circ \rightarrow S_1$ transition. Calculations done at the M06-2X/DEF2SVP level, and isovalue of orbital plots is set as 0.03 au.

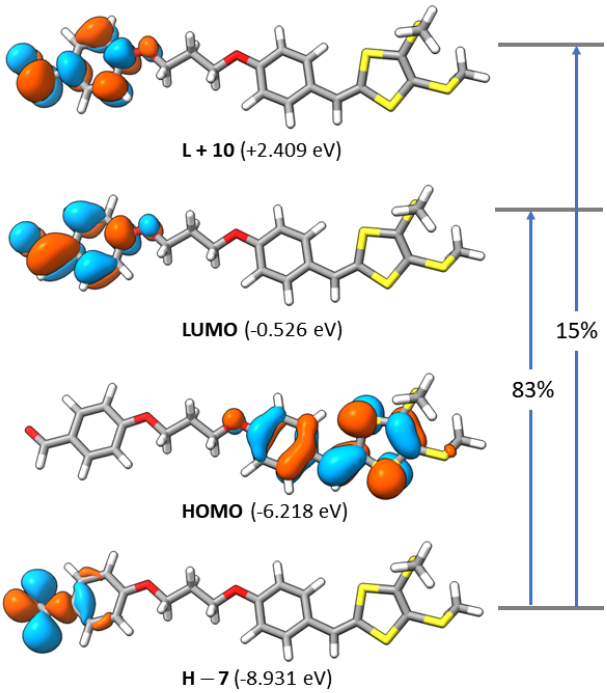

Figure 3.9: Plots and energies of the FMOs of **6** that are involved in the $S_\circ \rightarrow S_1$ transition. Calculations done at the M06-2X/DEF2SVP level, and isovalue of orbital plots is set as 0.03 au.

3.2.4 Electrochemical properties and redox reactivity

The electrochemical redox properties of compounds **5** and **6** were examined by cyclic voltammetric (CV) analysis. Figure 3.10 shows their cyclic voltammograms obtained from multiple-cycle CV scans in the positive potential window. For comparison purposes, the cyclic voltammogram of a bis(DFT) derivative **7**[262,286] was also measured under the same experimental conditions. Compound **7** represents a structurally rigid DTF–π–DTF molecular dumbbell, in which the two DTF groups are connected through a linear π-conjugated butadiynylene bridge.

In our previous studies, the electrochemical redox properties and reactivity of bis(DTF) **7** were fully examined.[262,286,290] As shown in its voltammogram, the first cycle of CV scan resulted in an anodic peak at $E_{\mathrm{pa}} = +0.83$ V, which can be attributed to the simultaneous oxidation (i.e., two electron transfer) taking place on the two DTF groups. The electrochemical behavior of **7** follows an EC mechanism, in which the oxidized **7** undergoes DTF coupling reactions on the electrode surface, resulting in the formation of TTFV-based polymer film. This is clearly evidenced by the growing quasi-reversible redox couple at $E_{\mathrm{pa}} = +0.69$ V and $E_{\mathrm{pc}} = +0.58$ V, which is the redox characteristic of TTFV.[262,286,290]

The cyclic voltammogram of bola-bis(DTF) **5** shows a pattern similar to that of bis(DTF) dumbbell **7**, indicating the occurrence of electrochemical polymerization during the multiple-cycle CV scans as a result of DTF coupling reactions. Nevertheless, the anodic and cathodic peaks of **5** are markedly shifted to the lower potential direction in comparison with those of **7**. In the first cycle of the CV scan, the anodic peak of **5** is observed at $E_{\mathrm{pa}} = +0.64$ V, while the resulting TTFV redox couple

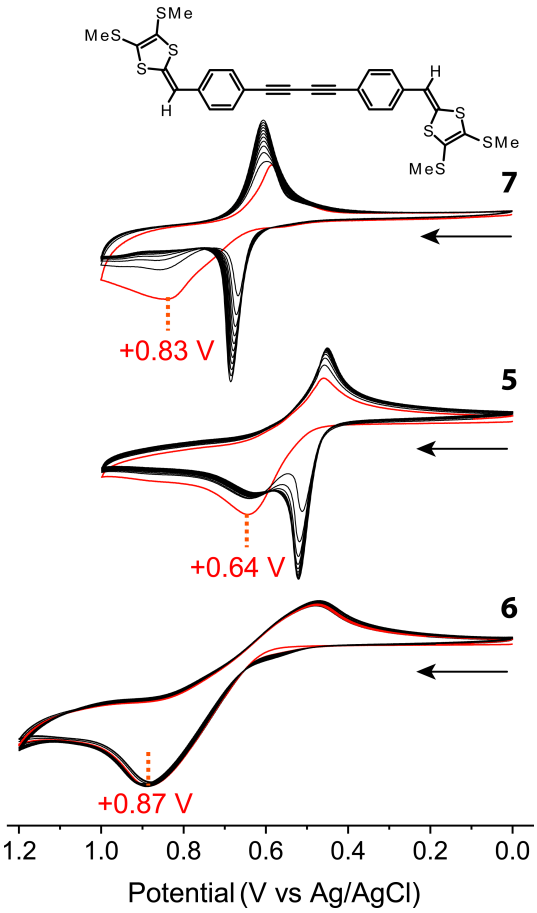

Figure 3.10: Cyclic voltammograms of compounds **5**–**7**. Experimental conditions: Bu_4NBF_4 (0.10 M) as the electrolyte, CH_2Cl_2/CH_3CN (5:1, v/v) as the solvent, glassy carbon as the working electrode, Pt wire as the couter electrode, Ag/AgCl as the reference electrode, scan rate = 100 mV/s.

appears at E_{pa} = +0.52 V and E_{pc} = +0.45 V. For mono-DTF substituted **6**, the cyclic voltammogram shows little change during multiple-cycle scans; the anodic peak consistently appears at E_{pa} = +0.87 V and the cathodic peak at E_{pc} = +0.49 V. These feature suggest that the DTF group in **6** lacks the reactivity towards oxidative coupling, and only shows a quasi-reversible redox pattern due to the DTF group.[301]

Comparison of the three voltammograms in Figure 3.10, one would come up with

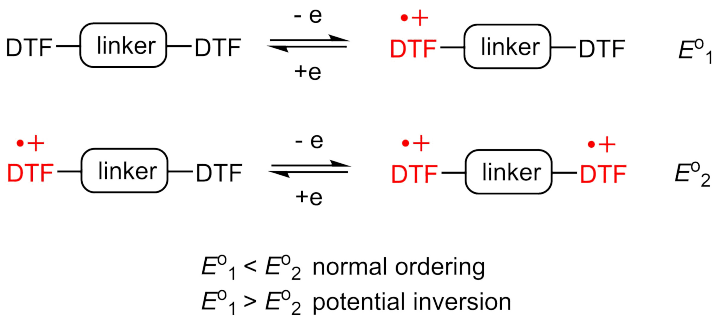

Figure 3.11: Normal ordering and potential inversion scenarios for the oxidation of a bis(DTF) system.

a question; that is, why are the redox potentials of bio-bis(DTF) **5** shifted to much less positive values than the others? To address this question, we need to examine the bis(DTF) oxidation mechanism. As illustrated in Figure 3.11, the oxidation of a bis(DTF) system involves two steps of single electron transfer occurring on each redox-active DTF moiety, respectively. If the linker group induces a certain degree of electron communication, the oxidation of the second DTF group should be more difficult than the first step of oxidation, making the second oxidation potential greater than the first oxidation potential (i.e., $E^\circ_2 - E^\circ_1 > 0$). This situation is called normal ordering,[302] for which two separate steps of single electron transfer should be seen in the CV analysis. On the other hand, if the electron-transfer reactions are accompanied by significant structural variations, the second oxidation potential may become lower than the first oxidation potential ($E^\circ_2 - E^\circ_1 < 0$). This scenario results in the so-called "potential inversion".[302,303] In such a case, the system would undergo simultaneous two-electron transfer at a potential lower than the oxidation of a single DTF group. According to the CV results in Figure 3.10, both of the bis(DTF) compounds **5** and **7** show one anodic peak in the first cycle of scan, which are lower in potential than that

of mono-DTF **6**. So, it is clear that both bis(DTF) derivatives undergo a simultaneous two-electron transfer upon oxidation due to potential inversion. Compound **7** is structurally more rigid than bola-bis(DTF) **5**. It is therefore reasonable to predict that **5** would undergo a much higher degree of structural changes associated with the redox process. Our results here clearly demonstrate that the structural flexibility of the linker group in a bis(DTF) system has a pronounced effect on its redox potentials. This property deserves serious consideration in the design of bis(DTF) precursors for functional TTFV-based polymers.

3.2.5 Electropolymerization and application in phenol sensing

The multiple-cycle CV experiments of bola-bis(DTF) **5** and rigid bis(DTF) **7** both ended with the formation of a polymer thin film on the surface of the working (glassy carbon) electrode. The polymerization reactions are described in Figure 3.12A and (B), respectively. Both polymers contain TTFV units in their backbones, which deliver redox activity to their thin films. The structurally rigid bis(DTF) **7** upon electropolymerization yielded a robust thin film that showed excellent stability to solvent rinsing and multiple CV scans after preparation. In contrast, the polymer thin film generated from flexible bola-bis(DTF) **5** afforded poor stability and could be easily detached by solvent rinsing. The intimate $\pi - \pi$ stacking among the molecular chains of poly-[**7**] is believed to be the main reason for the excellent stability of its polymer film. Taking advantage of this property, we previously developed a two-layer electrodeposition strategy,[304] in which dendritic poly(DFT) precursors were

electrochemically polymerized on the surface of poly-[**7**] to generate double-layered electrochemical thin film sensors for nitroaromatic compounds (e.g., TNT). In this work, we employed this strategy to have the polymer of bola-bis(DTF) **5** grafted onto the surface of poly-[**7**] through the stepwise electropolymerization approach illustrated in Figure 3.12C.

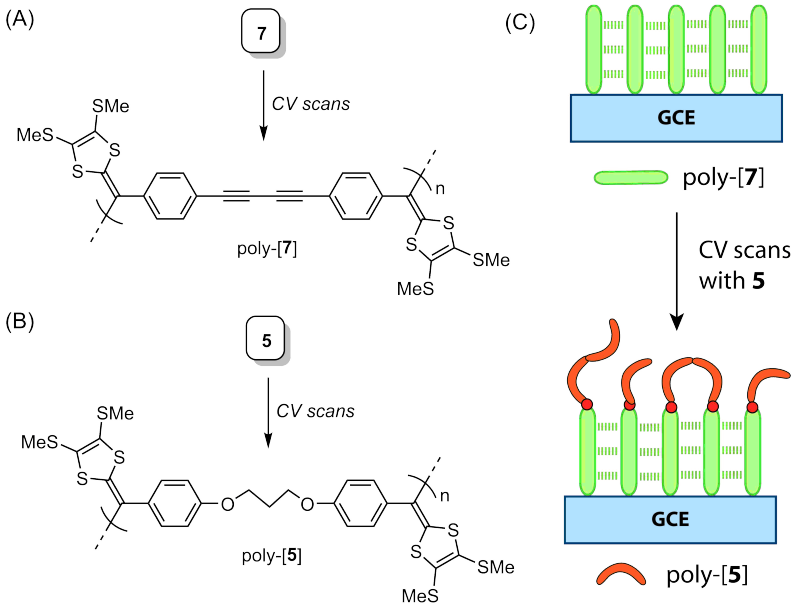

Figure 3.12: Polymerization reactions of (A) bis(DTF) **5** and (B) **7** under electrochemical conditions. (C) Schematic illustration of electrodeposition of two layers of polymers on the surface of glassy carbon electrode (GEC) using **7** and **5** as monomeric precursors.

In our experiments, a poly-[**7**] thin film was first generated on the surface of a glassy carbon working electrode by performing 48 cycles of CV scans of a solution of bis(DTF) **7** in CH_2Cl_2/CH_3CN with Bu_4NBF_4 as the electrolyte. A robust polymer film was formed, showing excellent redox-activity as depicted in Figure 3.13A. The

CV profile of the thin film of poly-[**7**] shows a reversible redox couple at E_{pa} = +0.69 V and E_{pa} = +0.61 V, respectively. This redox feature arises from the TTFV moieties present in the molecular structure of poly-[**7**]. The poly-[**7**]-modified glassy carbon electrode was further subjected to multiple cycles of CV scans in a solution of bola-bis(DTF) **5** under the same experimental conditions used for the generation of poly-[**7**] thin film. As illustrated in Figure 3.13B, the first forward CV scan of **5** with poly-[**7**]-coated glassy carbon electrode gives an anodic peak at E_{pa} = +0.71 V, which mainly reflects the redox-activity of the thin film of poly-[**7**]. In the reverse scan, the voltammogram shows two cathodic peaks at $E^1{}_{pc}$ = +0.43 V and $E^2{}_{pc}$ = +0.57 V, which contrasts the one cathodic peak observed for the pristine poly-[**7**] film. Starting from the second cycle of CV scans, the anodic peak at +0.71 V completely vanishes and the voltammograms show two reversible redox couples at $E^1{}_{pa}$ = +0.50 V/$E^1{}_{pc}$ = +0.43 V and $E^2{}_{pa}$ = +0.62 V/$E^2{}_{pc}$ = +0.57 V, respectively. This observation indicates that the surface of the poly-[**7**] film is significantly modified after one CV cycle. The current intensity of the first redox couple continues to grow with increasing CV scans, but the second redox couple changes insignificantly. These outcomes suggest that the first redox couple is due to the formation of a poly-[**5**] layer on top of the poly-[**7**] thin film. The second redox couple can be ascribed to the redox features of the layer of poly-[**7**], and its redox potentials are significantly shifted to the less positive direction. This shift can be rationalized by the fact that poly-[**5**] is covalently linked to the terminal end of poly-[**7**] during the electrodeposition process (as schematically illustrated in Figure 3.12C). With this functionalization, the intramolecular $\pi - \pi$ stacking of poly-[**7**] is attenuated and the flexibility of the polymer backbone is increased. As discussed previously, the gained structural

flexibility enhances the potential inversion scenario and hence results in lowered redox potentials.

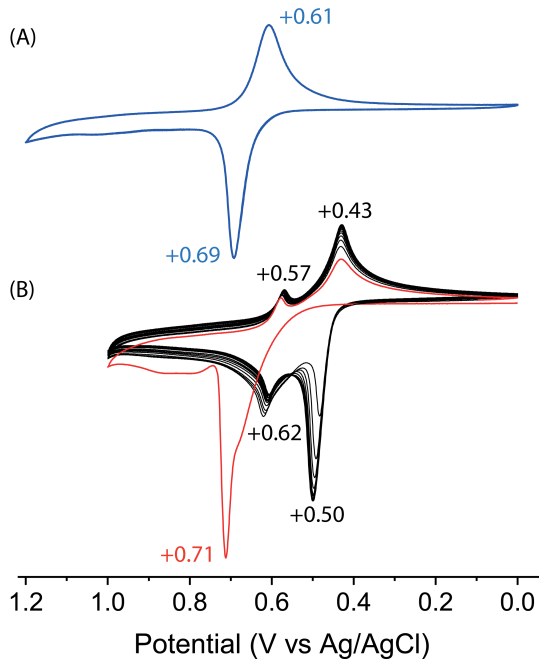

Figure 3.13: (A) CV scan of poly-[**7**] thin film-coated glassy carbon electrode measured in a solution of Bu_4NBF_4 (0.1 M) in CH_3CN/CH_2Cl_2 (5:1, v/v). (B) Voltammograms monitoring 24 cycles of CV scans of bola-DTF **5** in a solution of Bu_4NBF_4 (0.1 M) in CH_3CN/CH_2Cl_2 (5:1, v/v) using poly-[**7**]-coated glassy carbon as the working electrode. The first cycle of scans is highlighted in red color.

After the above-mentioned two-stage CV scan experiments, a double-layer thin film, namely poly-[**5**]//poly-[**7**], was deposited on the glassy carbon working electrode. This polymer-modified electrode showed redox activity when subjected to CV scans in an electrolyte solution. For instance, in a solution of 0.1 M Bu_4NBF_4 in CH_3CN), multiple CV scans gave two redox couples at $E^1_{pa} = +0.53$ V/$E^1_{pc} = +0.49$ V $E^2_{pa} = +0.64$ V$E^1_{pa} = +0.60$ V, respectively (see the red-color trace in Figure 3.14A). The

cyclic voltammograms showed nearly unchanged profiles after multiple cycles of CV scans, indicating good consistency and stability of the double-layer film generated. Interestingly, the poly-[**5**]//poly-[**7**] film exhibited very significant CV responses to the presence of phenol or phenol derivatives in the electrolyte solution.

Changes in the CV profiles were observed. In our experiment, three representative phenolic compounds–phenol, catechol, and cannabidiol–were examined. Figure 3.14A depicts the CV responses of the poly-[**5**]//poly-[**7**] thin film to the gradual titration of cannabidiol.

Phenolic compounds are widely present in the environment, owing to their extensive application in medicine, pesticides, plastics, food, and dyes.[305–308] Also there are abundant natural products containing phenolic groups in their molecular structures. Many phenolic compounds are toxic, teratogenic, or carcinogenic. Rapid and cost-effective detection methods for these compounds are therefore urgently needed. The commonly used detection methods for phenolic compounds are based on spectrometric and chromatographic analyses, which are time-consuming and unsuitable for in situ analysis and monitoring. Recently, the use of electrochemical sensors for phenolic compounds has captured growing interest owing to their advantages of easiness to use, fast response, high sensitivity/selectivity, and low costs.[309–312] In our experiments, three representative phenolic compounds–phenol, catechol, and cannabidiol–were investigated as analytes for the poly-[**5**]//poly-[**7**] thin film. Figure 3.14 illustrates the results of CV titration with cannabidiol. As can bee seen, the two redox couples show continuous attenuation in current intensity with increasing concentration of cannabidiol. The anodic peaks are slightly shifted to the most positive direction, while the cathodic peaks shift to the less positive

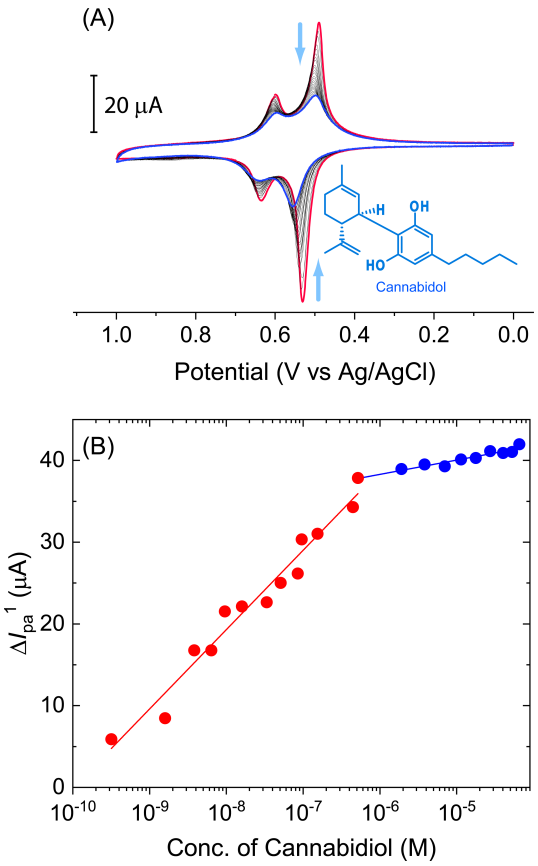

Figure 3.14: (A) CV scans monitoring the responses of the poly-[**5**]//poly-[**7**] thin film to the titration of cannabidiol (0 to 6.54 $\times 10^{-5}$ M) in CH_3CN with Bu_4NBF_4 (0.1 M) as the electrolyte. (B) Correlation of changes in the intensity of the first anodic peak with the concentration of cannabidiol.

direction as the titration progresses. Examination of the correlation of the cannadidiol concentration with the current intensities of the anodic and cathodic peaks show two stages of changes. As illustrated in Figure 3.14B, the current change at the first anodic peak is plotted against the logarithm of cannabidiol concentration. Herein the current change ($\Delta I_{\mathrm{pa}}{}^{1}$) is calculated by the following equation, $\Delta I_{\mathrm{pa}}{}^{1} = I_{\mathrm{pa}}{}^{1}(0) - I_{\mathrm{pa}}{}^{1}(\mathrm{m})$, where $I_{\mathrm{pa}}{}^{1}(0)$ is the current intensity of the first andoic peak before titration, and $I_{\mathrm{pa}}{}^{1}(\mathrm{m})$ is the current intensity of the first anodic peak measured at the mth step

of titration. The plot shows that when the concentration of cannabidol is below 5.67 $\times 10^{-7}$ M, the $\Delta {I_{\mathrm{pa}}}^{1}$ shows a nearly linear correlation with the logarithm of the cananbidiol concentration. When the concentration of cannabidiol is higher than $\times 10^{-7}$ M, the thin film shows very weak responses, indicating the saturation.

In a control experiment, the thin film made of only poly-[**5**] was subjected to CV titrations with the three phenolic compounds and it showed quite insignificant responses to these analytes. The results validate that the CV responses of the double-layer thin film to phenolic compounds are due to the interactions of the phenolic analytes with poly-[**5**] layer. It can reasoned that the phenolic ether moieties in the structure of poly-[**5**] can attract phenol analytes through hydrogen bonding, $\pi - \pi$ stacking, and van der Waals forces. When complexed with the phenol analytes, the conformation and rigidity of the molecular backbone of poly-[**5**] are changed, which in turn result in the observed CV responses. In the CV analysis, the peak current can be described by the Randles–Sevcik equation,

$$I_p = 0.4463^{3/2} F^{3/2} A \frac{D^{1/2} C v^{1/2}}{(RT)^{1/2}}$$

where: I_p is the peak current, F is the Faraday constant 96485 C·mol^{-1}), A is the working electrode surface area, D is the diffusion coefficient of the redox-active species, C is the molar concentration of the redox-active species, v is scan rate, R is the gas constant (8.31 J·K^{-1}·mol^{-1}), and T is the temperature. According to this equation, the peak current variation during the titration process can be mainly attributed to the changes in the diffusion coefficient of the redox-active TTFV moieties in poly-[**5**] as a result of their binding with phenolic analytes. After the titration with

cannabidiol, poly-[**5**]//poly-[**7**] film was thoroughly rinsed with CH_2Cl_2 and then subjected to another round of CV scans in CH_3CN with Bu_4NBF_4. The CV profile determined remained the same as that of the last stage of the cannabidiol titration (see Appendix), suggesting that cannabidiol can be so strongly trapped inside the poly-[**5**] layer that the regeneration of free polymer film cannot be achieved by solvent rinsing. Overall, our CV studies indicated that the poly-[**5**]//poly-[**7**] double-layer film can be used to rapidly and sensitively detect the presence of phenolic species at sub-μM concentrations in organic media. The reusability of the double-layer polymer film is poor, but this is offset by its easy and low-cost generation. The CV titration results of phenol and catechol show similar trends of redox changes to those for the cannabidiol titration (see Appendix), indicating that the poly-[**5**]//poly-[**7**] polymer film would act as a universal and disposable electrochemical sensor for various phenolic compounds.

3.2.6 Molecular Dynamic Simulations

According to our CV titration experiments, the layer of poly-[**5**] shows significant affinity for phenolic compounds, which in turn leads to detectable electrochemical responses. To gain a deeper insight into the interactions of poly-[**5**] and phenolic compounds at the molecular level, molecular dynamic (MD) simulations were carried out using a tetramer of bola-DTF **5** as a model polymer. In our simulation studies, the tetramer was first set with a non-folded conformation (see the snapshot at 0 ns in Figure 3.15B) and allowed to evolve in an aqueous medium at 298 K. It was found that the conformation of the non-folded tetramer undergoes dramatic changes in the first 4 ns of evolution, which can be seen from the root-mean-square deviation

(RMSD) trace in Figure 3.15B.

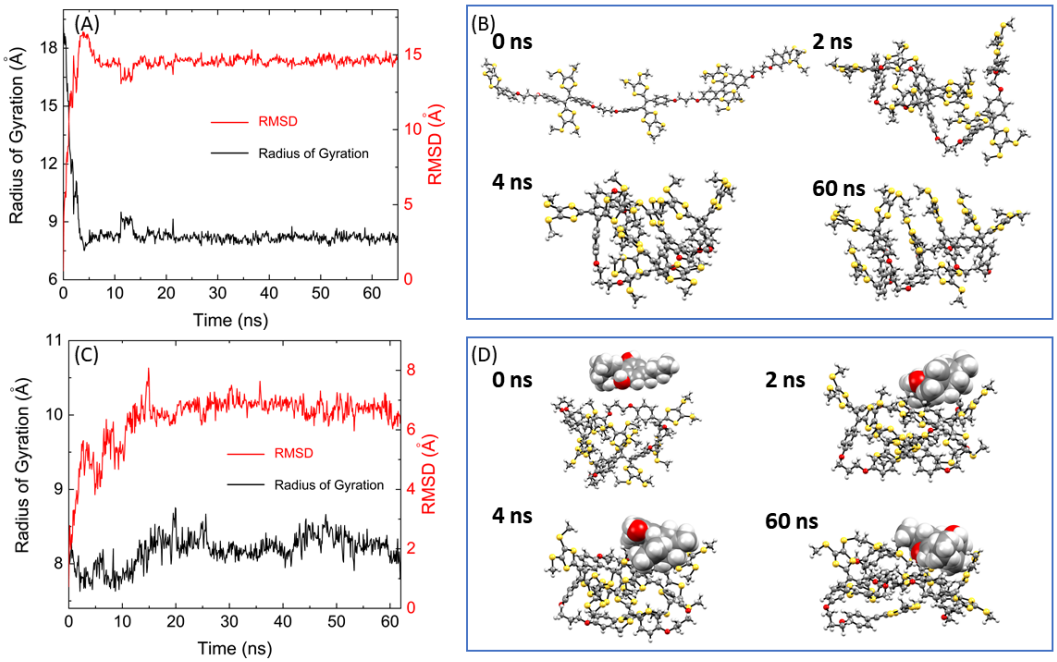

Figure 3.15: Molecular geometry of the 1:1 complex of a tetramer of **5** (drawn in the wireframe style) and cannabidiol (blue-color capped sticks) optimized by MM calculations. Close intermolecular O$\cdots$S distances are highlighted.

Examination of the snapshots of the molecular structures during this period of simulation time reveal a folding process that is dictated by the $\pi - \pi$ stacking among the arene groups with the tetramer. The radius of gyration of the tetramer is also reduced from 19 Å to 8 Å. After 4 ns, the conformation of the tetramer becomes fully folded and remains stable, which is reflected by the insignificantly fluctuated RMSD and radius of gyration traces (Figure 3.15B). The simulation results of the tetramer suggest that the polymer of bola-bis(DTF) can readily fold owing to its flexible molecular backbones. From the above MD simulations, a stable folded conformer of the model tetramer was extracted. In the vicinity of its major groove, a molecule of

cannabidiol was placed. This molecular ensemble (see the snapshot at 0 ns in Figure 3.15D) was then subjected to MD simulations in water to examine the dynamics of their intermolecular interactions. As shown in Figure 3.15C, the RMSD trace shows some fluctuations in the first 20 ns and then becomes stable. The radius of gyration trace shows insignificant fluctuations during the entire simulation time (62 ns). Analysis of the snapshots of the MD simulations shows that the cannabidiol molecule is drawn close to the groove of the folded tetramer within the first few ns. As the simulations continue, the tetramer adapts to have the cannabidiol molecule partially engulfed through various intermolecular interactions, in which the O$\cdots$S interactions between the oxygen atoms of cannabidiol and the sulfur atoms of the tetramer play an important role. Hydrogen bonding interactions between the phenolic oxygen atoms of the tetramer and the cannabidiol hydroxy groups, however, are not observed during the MD simulations. The complex of the tetramer with cannabidiol appears to be quite stable throughout the entire simulation period, which concurs with the significant affinity of poly-[**5**] with phenolic compounds observed in our experiments.

The stable tetramer–cannabidiol complex evolved from the MD simulations was further subjected to molecular mechanics (MM) calculations using the MMFF force field in water. The MM optimized structure is shown in Figure 3.16, in which three intimate intermolecular O$\cdots$S contacts can be seen. The binding energy (ΔG°, at 298 K) of this complex is calculated as 6.287 kcal/mol. Intermolecular O$\cdots$S interactions are commonly seen in biological systems and have been know to exhibit strength comparable to typical hydrogen bonding interactions.[313] Our modeling study herein disclose a molecular origin of the favored binding of poly-[**5**] with various phenolic

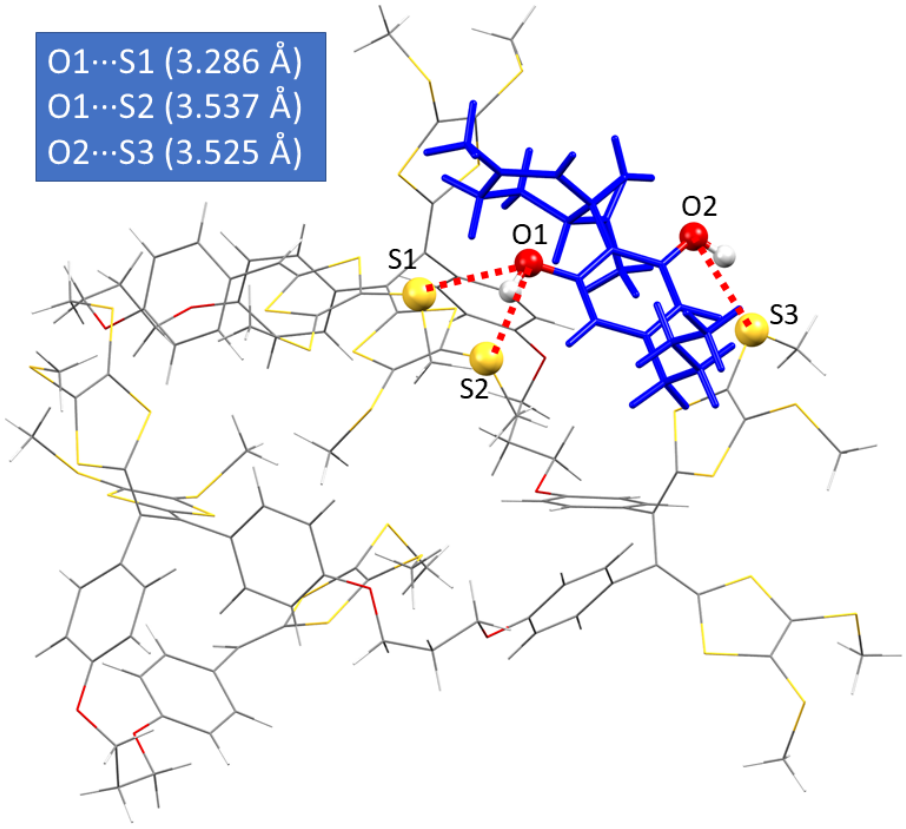

Figure 3.16: Molecular geometry of the 1:1 complex of a tetramer of **5** (drawn in the wireframe style) and cannabidiol (blue-color capped sticks) optimized by MM calculations. Close intermolecular O···S distances are highlighted.

compounds.

3.3 Experimental section

3.3.1 Materials and instrumentation

All starting materials and reagents were acquired from commercial sources and used directly without purification. Compound **3** was prepared following the procedure reported by Saeed *et al.*[314], and compound **4** was made following our previously

reported method.[301] All reactions were conducted in standard, dry glassware. Evaporation and concentration were carried out with a rotary evaporator. Flash column chromatography was performed with 240-400 mesh silica gel, and thin-layer chromatography (TLC) was carried out with silica gel F254 covered on plastic sheets and visualized by UV light. Melting points (m.p.) were measured using an SRS OptiMelt melting point apparatus and are uncorrected. ^{1}H and ^{13}C NMR spectra were measured on a Bruker Avance III 300 MHz multinuclear spectrometer. Chemical shifts (δ) are reported in ppm downfield relative to the signals of the internal reference $SiMe_4$ or residual solvents ($CHCl_3$: δ_H = 7.24 ppm, δ_C = 77.2 ppm). Coupling constants (J) are given in Hz. Infrared spectra (IR) were recorded on a Bruker Alfa spectrometer. High-resolution APPI-TOF MS analysis was done on a GCT premier Micromass Technologies instrument. UV-Vis absorption spectra were measured on a Cary 6000i spectrophotometer.

Cyclic voltammetric (CV) analysis was carried out in a standard three-electrode setup controlled by a BASi Epsilon potentiostat. Glassy carbon electrode was used as the working electrode, and its surface was polished by 1.0 micron alumina prior to CV scans. A Pt wire was used as the counter electrode, and the reference electrode was Ag/AgCl (3.0 M NaCl). All CV experiments were performed in CH_2Cl_2 and/or CH_3CN media with Bu_4NBF_4 as the electrolyte.

Single crystal X-ray diffraction (SCXRD) analyses were performed on a XtaLAB Synergy-S, Dualflex, HyPix-6000HE diffractometer at 100(2) K, using Cu K_α radiation (λ = 1.5406 Å). The data collection and reduction were processed within *CrysAlisPro* (Rigaku OD, 2019). For the single crystal of **5**, a multi-scan absorption correction was applied to the collected reflections. Using the software package,

Olex2,[315] the structure was solved with the *ShelXT* structure solution program using Intrinsic Phasing and refined with the *ShelXL* refinement package using Least Squares minimisation. For the single crystal of **6**, two-component non-merohedral twin was found in and the twin law was identified as the matrix -1 0 0 0 -1 0 1.254 0.663 0.955. An empirical absorption correction using spherical harmonics (ABSPACK in $CrysAl^{isPro}$) was applied to the collected reflections. The structure was solved from a detwinned HKLF 4 reflection file with the ShelXT[316] structure solution program using Intrinsic Phasing. The structure was refined from the HKLF 5 reflection file with the *ShelXL* refinement package[317] using Least Squares minimisation. All non-hydrogen atoms were refined anisotropically, and the organic hydrogen atoms were generated geometrically.

3.3.2 Computational analysis

In our DFT computational studies, molecular structures of **5** and **6** were optimized using the M06-2X density functional[299] in conjunction with the DEF2SVP basis set.[300] The optimized structures were then subjected to TD-DFT analysis (nstates = 10) at the same level of theory. All of these calculations were performed using the methods implemented in the Gaussian 16 software package.[318] Assessment of the free space in the crystal unit cells of **5** and **6** was performed using the **Multiwfn** software package,[319] and the isosurface of calculated free space was rendered by the *VMD* program.[320]

3.3.3 Synthetic procedures

To a round-bottom flask (50 mL) were added compound **3** (1.00 g, 3.52 mmol), compound **4** (2.39 g, 10.6 mmol), and $P(OMe)_3$ (8 mL). The mixture was heated at 120 °C for 3 h with an oil bath. After that, the reaction mixture was subjected to vacuum distillation at the same temperature to quickly remove unreacted $P(OMe)_3$. The residue was purified through silica gel flash column chromatography using hexanes/CH_2Cl_2 (7:3, v/v) as the eluent. The separation resulted in two products. Compound **5** (1.03 g, 1.61 mmol mmol, 46%) as a yellow pale crystalline solid. m.p: 114.1–115.1 °C; ^{1}H NMR (300 MHz, $CDCl_3$) δ 7.14 (d, J = 8.9 Hz, 4H), 6.90 (d, J = 8.9 Hz, 4H), 6.42 (s, 2H), 4.16 (t, J = 6.1 Hz 4H), 2.43 (s ,6H), 2.41 (s, 6H), 2.25 (quintet, J = 6.0 Hz, 2H) ppm; ^{13}C NMR (75 MHz, $CDCl_3$) δ 157.2, 129.5, 128.4, 127.8, 126.7, 123.9, 114.6, 114.2, 64.1, 28.4, 19.1, ppm; FTIR (neat) 2960, 2359, 1739, 1568, 1505, 1426, 1368, 1224, 1116, 1069, 972, 892, 827, 754 cm^{-1}; HRMS (APPI, positive) *m/z* calcd for $C_{27}H_{29}O_2S_8$ 640.9933, found, 640.9948 $[M + H]^+$. Compound **6** (0.57 g, 0.89 mmol, 25%) as a yellow crystalline solid . m.p.: 90.1–92.0 °C; ^{1}H NMR (300 MHz, $CDCl_3$) δ 9.89 (s, 1H), 7.83 (d, J = 8.7 Hz, 2H), 7.14 (d, J = 8.8 Hz , 2H), 7.01 (d, J = 8.7 Hz , 2H), 6.90 (d, J = 8.8 Hz , 2H), 6.43 (s, 1H), 4.26 (t, J = 6.1 Hz, 2H), 4.18 (t, J = 5.9 Hz, 2H), 2.43 (s, 3H), 2.41 (s, 3H), 2.30 (quintet, J = 6.0 Hz, 2H) ppm; ^{13}C NMR (75 MHz, $CDCl_3$) δ 190.3, 163.7, 156.8, 131.6, 129.8, 129.1, 128.8, 127.7, 126.3, 114.6, 113.6, 64.8, 63.8, 29.6, 28.5, 18.8 ppm; FTIR (neat) 3084, 2915, 1586, 1548, 1494, 1479, 1317, 1102, 725, 852, 742, 681 cm^{-1}; HRMS (APPI, positive) m/z calcd for $C_{22}H_{23}O_3S_4$ 463.0530, found, 463.0517 $[M+H]^+$.

3.4 Conclusions

In conclusion, a new bola-type bis(DTF) compound **5** and its mono-DTF-substituted precursor **6** were synthesized and characterized in this work. Our crystallographic and UV-Vis absorption spectral analyses have clearly elucidated their molecular conformations, solid-state packing, and electronic transition properties. The structural flexibility of the bola-DTF was convincingly identified as an important factor influencing the redox properties; in particular, significant potential inversion took place in the bola-bis(DTF) system, making the redox potentials considerably shifted to the less positive direction in comparison with those of its structurally rigid analogues. This finding points to a new design approach for DTF and TTFV-based redox-active molecular devices (e.g., electrochemical sensors). A double-layer thin film was generated through sequential electropolymerization of a structurally rigid bis(DTF) **7** and bola-bis(DTF) **5** on a glassy carbon electrode. CV analyses showed that this hybrid film showed sensitive redox responses to phenolic compounds in organic media. Our findings disclosed in this work not only cast insight into the fundamental properties of the intriguing class of bola-bis(DTF) derivatives, but recommend new polymer materials suitable for the development of sensitive and cost-effective polymer-based electrochemical sensors. We envision that further exploration of the bola-bis(DTF) systems will broaden their application in multiple disciplines (e.g., environmental monitoring, food chemistry, and pharmaceutical industry), where rapid and sensitive detection methods for various phenolic compounds are highly desired.

Chapter 4

Conclusions and Future Work

In this MSc thesis, two experimetal projects have been successfully accomplished to investigate the fundamental properties and application potential of new DTF-based organic molecular materials. The long-term objective of this thesis work is to explore the applications of DTF-based π-conjugated polymers in optoelectronic devices (e.g., electrochemical sensors). In this light, the findings of this work have pointed to a very promising prospect. The significance of each research project in this thesis is outlined as follows.

In the first project (Chapter 2), a series of reactions such as phosphite-promoted olefination, alkylation, and oxidative coupling have been carried out to prepare new DTF and TTFV derivatives substituted with different donor (methoxyphenyl)/acceptor (nitrophenyl) groups. Following the synthetic work, a series of advanced instrumental analyses have been conducted, including NMR, mass spectrometry, IR, UV-Vis absorption spectroscopy, X-ray single crystallography, and cyclic voltammetry (CV). These studies systematically examined the structural,

electronic, and redox properties of these new redox-active compounds. Among the experimental results, the observation of close intermolecular DTF/nitrobenzene stacking in the X-ray single crystal structure is remarkable and inspirational, which offers strong theoretical evidence for the use of DTF as a building block in the design of chemical sensors for nitroaromatic compounds, which are an important class of pollutants in the environment. Moreover, the intramolecular electron push–pull effects in the acceptor-substituted DTF and TTFV compounds were found to result in relatively narrow electronic bandgaps and significantly shifted oxidation potentials. Given the excellent crystallinity exhibited by these compounds, intriguing intramolecular and intermolecular charge-transfer properties are expected for the co-crystals of these compounds with other functional organic π-molecules. This crystal engineering approach should lead to the discovery of new organic crystalline materials useful for optoelectronic applications such as nonlinear optics and small-molecule organic semi-conductors. More explorations along these directions are warranted in our future study.

In the second project (Chapter 3), an object-oriented molecular design was conducted, aiming at developing new redox-active polymers useful for electrochemical sensing. The choice of using 1,3-diphenoxypropane as a flexible linker in a bis(DTF) system led to a novel bola-type bis(DTF) compound. This type of bis(DTF)s have been rarely reported in the literature, mainly due to the perception that a flexible, non-conjugated linker group is not beneficial to electronic and redox activity. Our comparative analyses of the structural and electrochemical properties of this compound, on the other hand, clearly points to the opposite. The finding that the bola-bis(DTF) shows a significantly lowered oxidation potential than its

structurally rigid, fully π-conjugated counterpart suggests that the linker flexibility is indeed an important molecular factor that controls the redox properties of bis(DTF) or poly(DTF) systems. The lowered oxidation potential of the bola-bis(DTF) is comparable with those of TTFs and TTFVs, which are excellent organic π-donors. This property points out a potential to new redox-active ligands with a high-degree of structural adaptability. To demonstrate this, prototype polymer thin film sensors have been prepared by electropolymerization. The double-layer thin film has shown a potential in electrochemical sensing for various phenolic compounds. Rapid and cost-effective detection of these compounds have extensive applications in environmental control as well as food and pharmaceutical industries. At this juncture, the electrochemical sensing function only works well in polar organic media (e.g., CH_3CN). Whether this polymer film can be applied to detect phenolic pollutants in aqueous media (e.g., seawater) is a question worthy of more active studies.

According to the results obtained from the two research projects, a number of future directions can be envisioned as follows:

(1) Design and synthesis of bola-bis(DTF) with various alkyl liner groups should be conducted to better understand the effects of linker flexibility and intramolecular distances of DTF groups on redox properties.

(2) The synthesis of some analogues of bola-bis(DTF) with star and tree-like (dendritic) molecular shapes are appealing synthetic targets that are worth investigating. These types of compounds allow the multi-DTF effects to be explored, and they are also expected to generate complex, microporous polymer networks through electropolymerization.

(3) Fundamental studies of the detailed mechanisms for the absorption of phenols

on the TTFV polymer films are a new direction to pursue. Better understanding these properties will help improve the sensitivity/selectivity of the polymer films towards certain phenol derivatives.

(4) Improvement on the compatibility of the TTFV polymers with other solvents, particularly water, will greatly enhance the applicability in environmental sensing. So far, the oxidation of DTF or TTFV in water has been observed to cause structural degradation. Most likely, the cations of DTF and TTFV can readily react with water molecules. A reasonable way to avoid this problem is to coat a hydrophobic membrane layer on top of the double-layer polymer film.

Bibliography

[1] Batsanov, A. S. Tetrathiafulvalene revisited. *Acta Crystallogr. C* **2006**, *62*, o501–o504.

[2] Narita, M.; Pittman Jr, C. U. Preparation of tetrathiafulvalenes (TTF) and their selenium analogs-tetraselenafulvalenes (TSeF). *Synthesis* **1976**, *1976*, 489–514.

[3] Krief, A. Syntheses of tetraheterofulvalenes and of vinylene triheterocarbonates-strategy and practice. *Tetrahedron* **1986**, *42*, 1204–1252.

[4] Adam, M.; Müllen, K. Oligomeric tetrathiafulvalenes: extended donors for increasing the dimensionality of electrical conduction. *Adv. Mater.* **1994**, *6*, 439–459.

[5] Jørgensen, T.; Hansen, T. K.; Becher, J. Tetrathiafulvalenes as building-blocks in supramolecular chemistry. *Chem. Soc. Rev.* **1994**, *23*, 41–51.

[6] Bryce, M. R. Current trends in tetrathiafulvalene chemistry: Towards increased dimensionality. *J. Mater. Chem.* **1995**, *5*, 1481–1496.

[7] Blanchard, P.; Sallé, M.; Duguay, G.; Jubault, M.; Gorgues, A. 2-Mono or

2,3-bis(hydroxymethyl)-6,7-ethylenedithio-tetrathiafulvalenes: New potential precursors of organic metals endowed with hydrogen bonds. *Tetrahedron Lett.* **1992**, *33*, 2685–2688.

[8] Garín, J. The reactivity of tetrathiafulvalene. *Adv. Heterocycl. Chem.* **1995**, 249.

[9] Wudl, F.; Smith, G. M.; Hufnagel, E. J. Bis-1,3-dithiolium chloride: an unusually stable organic radical cation. *J. Chem. Soc. D* **1970**, 1453–1454.

[10] Coffen, D. L.; Chambers, J. Q.; Williams, D. R.; Garrett, P.; Canfield, N. Tetrathioethylenes. *J. Am. Chem. Soc.* **1971**, *93*, 2258–2268.

[11] Deuchert, K.; Hünig, S. Multistage organic redox systems–a general structural principle. *Angew. Chem. Int. Ed. Engl.* **1978**, *17*, 875–886.

[12] Aumüller, A.; Erk, P.; Klebe, G.; Hünig, S.; von Schütz, J. U.; Werner, H.-P. A radical anion salt of 2,5-dimethyl-N,N-dicyanoquinonediimine with extremely high electrical conductivity. *Angew. Chem. Int. Ed. Engl.* **1986**, *25*, 740–741.

[13] Ferraris, J.; Cowan, D.; Walatka, V.; Perlstein, J. Electron transfer in a new highly conducting donor-acceptor complex. *J. Am. Chem. Soc.* **1973**, *95*, 948–949.

[14] Andrieux, A.; Duroure, C.; Jérome, D.; Bechgaard, K. The metallic state of the organic conductor TMTSF-DMTCNQ at low temperature under pressure. *J. Phys. Lett.* **1979**, *40*, 381–383.

[15] Jérome, D.; Mazaud, A.; Ribault, M.; Bechgaard, K. Superconductivity in a synthetic organic conductor (TMTSF)2PF6. *J. Phys. Lett* **1980**, *41*, 95–98.

[16] Ashton, P. R.; Balzani, V.; Becher, J.; Credi, A.; Fyfe, M. C.; Mattersteig, G.; Menzer, S.; Nielsen, M. B.; Raymo, F. M.; Stoddart, J. F., et al. A three-pole supramolecular switch. *J. Am. Chem. Soc.* **1999**, *121*, 3951–3957.

[17] Balzani, V.; Credi, A.; Mattersteig, G.; Matthews, O. A.; Raymo, F. M.; Stoddart, J. F.; Venturi, M.; White, A. J.; Williams, D. J. Switching of pseudorotaxanes and catenanes incorporating a tetrathiafulvalene unit by redox and chemical inputs. *J. Org. Chem.* **2000**, *65*, 1924–1936.

[18] Aviram, A.; Ratner, M. A. Molecular rectifiers. *Chem. Phys. Lett.* **1974**, *29*, 277–283.

[19] Segura, J. L.; Martín, N. New concepts in tetrathiafulvalene chemistry. *Angew. Chem. Int. Ed.* **2001**, *40*, 1372–1409.

[20] Perepichka, D. F.; Bryce, M. R.; Pearson, C.; Petty, M. C.; McInnes, E. J.; Zhao, J. P. A covalent tetrathiafulvalene–tetracyanoquinodimethane diad: extremely low HOMO–LUMO gap, thermoexcited electron transfer, and high-quality Langmuir–Blodgett films. *Angew. Chem. Int. Ed.* **2003**, *42*, 4636–4639.

[21] Ho, G.; Heath, J. R.; Kondratenko, M.; Perepichka, D. F.; Arseneault, K.; Pézolet, M.; Bryce, M. R. The first studies of a tetrathiafulvalene-σ-acceptor molecular rectifier. *Chem. Eur. J.* **2005**, *11*, 2914–2922.

[22] Leroy-Lhez, S.; Baffreau, J.; Perrin, L.; Levillain, E.; Allain, M.; Blesa, M.-

J.; Hudhomme, P. Tetrathiafulvalene in a perylene-3,4:9,10-bis(dicarboximide)-based dyad: a new reversible fluorescence-redox dependent molecular system. *J. Org. Chem.* **2005**, *70*, 6313–6320.

[23] Luo, Y.; Collier, C. P.; Jeppesen, J. O.; Nielsen, K. A.; DeIonno, E.; Ho, G.; Perkins, J.; Tseng, H.-R.; Yamamoto, T.; Stoddart, J. F., et al. Two-dimensional molecular electronics circuits. *ChemPhysChem* **2002**, *3*, 519–525.

[24] Giacalone, F.; Herranz, M. A.; Grüter, L.; González, M. T.; Calame, M.; Schönenberger, C.; Arroyo, C. R.; Rubio-Bollinger, G.; Vélez, M.; Agraït, N., et al. Tetrathiafulvalene-based molecular nanowires. *Chem. Commun.* **2007**, 4854–4856.

[25] Leary, E.; Higgins, S. J.; van Zalinge, H.; Haiss, W.; Nichols, R. J.; Nygaard, S.; Jeppesen, J. O.; Ulstrup, J. Structure–property relationships in redox-gated single molecule junctions- a comparison of pyrrolo-tetrathiafulvalene and viologen redox groups. *J. Am. Chem. Soc.* **2008**, *130*, 12204–12205.

[26] Liao, J.; Agustsson, J. S.; Wu, S.; Schonenberger, C.; Calame, M.; Leroux, Y.; Mayor, M.; Jeannin, O.; Ran, Y.-F.; Liu, S.-X., et al. Cyclic conductance switching in networks of redox-active molecular junctions. *Nano Lett.* **2010**, *10*, 759–764.

[27] Tour, J. M.; Rawlett, A. M.; Kozaki, M.; Yao, Y.; Jagessar, R. C.; Dirk, S. M.; Price, D. W.; Reed, M. A.; Zhou, C.-W.; Chen, J., et al. Synthesis and preliminary testing of molecular wires and devices. *Chem. Eur. J.* **2001**, *7*, 5118–5134.

[28] Mayor, M.; Weber, H. B.; Reichert, J.; Elbing, M.; Von Hänisch, C.; Beckmann, D.; Fischer, M. Electric current through a molecular rod—relevance of the position of the anchor groups. *Angew. Chem. Int. Ed.* **2003**, *42*, 5834–5838.

[29] Huber, R.; González, M. T.; Wu, S.; Langer, M.; Grunder, S.; Horhoiu, V.; Mayor, M.; Bryce, M. R.; Wang, C.; Jitchati, R., et al. Electrical conductance of conjugated oligomers at the single molecule level. *J. Am. Chem. Soc.* **2008**, *130*, 1080–1084.

[30] Vonlanthen, D.; Mishchenko, A.; Elbing, M.; Neuburger, M.; Wandlowski, T.; Mayor, M. Chemically controlled conductivity: torsion-angle dependence in a single-molecule biphenyldithiol junction. *Angew. Chem. Int. Ed.* **2009**, *48*, 8886–8890.

[31] Kaliginedi, V.; Moreno-García, P.; Valkenier, H.; Hong, W.; García-Suarez, V. M.; Buiter, P.; Otten, J. L.; Hummelen, J. C.; Lambert, C. J.; Wandlowski, T. Correlations between molecular structure and single-junction conductance: a case study with oligo(phenylene-ethynylene)-type wires. *J. Am. Chem. Soc.* **2012**, *134*, 5262–5275.

[32] Frisenda, R.; Perrin, M. L.; Valkenier, H.; Hummelen, J. C.; van der Zant, H. S. Statistical analysis of single-molecule breaking traces. *J. Phys. Status. Solidi. B* . **2013**, *250*, 2431–2436.

[33] Love, J. C.; Estroff, L. A.; Kriebel, J. K.; Nuzzo, R. G.; Whitesides, G. M.

Self-assembled monolayers of thiolates on metals as a form of nanotechnology. *Chem. Rev.* **2005**, *105*, 1103–1170.

[34] Stuhr-Hansen, N.; Sørensen, J. K.; Moth-Poulsen, K.; Christensen, J. B.; Bjørnholm, T.; Nielsen, M. B. Synthetic protocols and building blocks for molecular electronics. *Tetrahedron* **2005**, *61*, 12288–12295.

[35] Müller, T. J.; Bunz, U. H. *Functional organic materials: syntheses, strategies and applications*; John Wiley & Sons, 2007.

[36] Nuzzo, R. G.; Allara, D. L. Adsorption of bifunctional organic disulfides on gold surfaces. *J. Am. Chem. Soc.* **1983**, *105*, 4481–4483.

[37] Strong, L.; Whitesides, G. M. Structures of self-assembled monolayer films of organosulfur compounds adsorbed on gold single crystals: electron diffraction studies. *Langmuir* **1988**, *4*, 546–558.

[38] Kubatkin, S.; Danilov, A.; Hjort, M.; Cornil, J.; Bredas, J.-L.; Stuhr-Hansen, N.; Hedegård, P.; Bjørnholm, T. Single-electron transistor of a single organic molecule with access to several redox states. *Nature* **2003**, *425*, 698–701.

[39] Love, J. C.; Estroff, L. A.; Kriebel, J. K.; Nuzzo, R. G.; Whitesides, G. M. Self-assembled monolayers of thiolates on metals as a form of nanotechnology. *Chem. Rev.* **2005**, *105*, 1103–1170.

[40] Meisner, J. S.; Ahn, S.; Aradhya, S. V.; Krikorian, M.; Parameswaran, R.; Steigerwald, M.; Venkataraman, L.; Nuckolls, C. Importance of direct metal–π

coupling in electronic transport through conjugated single-molecule junctions. *J. Am. Chem. Soc.* **2012**, *134*, 20440–20445.

[41] Trabolsi, A.; Khashab, N.; Fahrenbach, A. C.; Friedman, D. C.; Colvin, M. T.; Cotí, K. K.; Benítez, D.; Tkatchouk, E.; Olsen, J.-C.; Belowich, M. E., et al. Radically enhanced molecular recognition. *Nat. Chem.* **2010**, *2*, 42–49.

[42] Fahrenbach, A. C.; Zhu, Z.; Cao, D.; Liu, W.-G.; Li, H.; Dey, S. K.; Basu, S.; Trabolsi, A.; Botros, Y. Y.; Goddard III, W. A., et al. Radically enhanced molecular switches. *J. Am. Chem. Soc.* **2012**, *134*, 16275–16288.

[43] Erbas-Cakmak, S.; Leigh, D. A.; McTernan, C. T.; Nussbaumer, A. L. Artificial molecular machines. *Chem. Rev.* **2015**, *115*, 10081–10206.

[44] Wang, Y.; Frasconi, M.; Stoddart, J. F. Introducing stable radicals into molecular machines. *ACS Cent. Sci.* **2017**, *3*, 927–935.

[45] Wang, Y.; Frasconi, M.; Stoddart, J. F. Introducing stable radicals into molecular machines. *ACS Cent. Sci.* **2017**, *3*, 927–935.

[46] Cheng, C.; McGonigal, P. R.; Schneebeli, S. T.; Li, H.; Vermeulen, N. A.; Ke, C.; Stoddart, J. F. An artificial molecular pump. *Nanotechnol.* **2015**, *10*, 547–553.

[47] Bruns, C. J.; Frasconi, M.; Iehl, J.; Hartlieb, K. J.; Schneebeli, S. T.; Cheng, C.; Stupp, S. I.; Stoddart, J. F. Redox switchable daisy chain rotaxanes driven by radical–radical interactions. *J. Am. Chem. Soc.* **2014**, *136*, 4714–4723.

[48] Wang, Y.; Frasconi, M.; Liu, W.-G.; Sun, J.; Wu, Y.; Nassar, M. S.; Botros, Y. Y.; Goddard III, W. A.; Wasielewski, M. R.; Stoddart, J. F. Oligorotaxane radicals under orders. *ACS Cent. Sci.* **2016**, *2*, 89–98.

[49] Ziganshina, A. Y.; Ko, Y. H.; Jeon, W. S.; Kim, K. Stable π-dimer of a tetrathiafulvalene cation radical encapsulated in the cavity of cucurbit [8] uril. *Chem. Commun.* **2004**, 806–807.

[50] Zhang, D.-W.; Tian, J.; Chen, L.; Zhang, L.; Li, Z.-T. Dimerization of conjugated radical cations: an emerging non-covalent interaction for self-assembly. *Chem. Asian J.* **2015**, *10*, 56–68.

[51] Skibiński, M.; Gómez, R.; Lork, E.; Azov, V. A. Redox responsive molecular tweezers with tetrathiafulvalene units: synthesis, electrochemistry, and binding properties. *Tetrahedron* **2009**, *65*, 10348–10354.

[52] Fumanal, M.; Capdevila-Cortada, M.; Miller, J. S.; Novoa, J. J. Keys for the existence of stable dimers of bis-tetrathiafulvalene (bis-TTF)-functionalized molecular clips presenting $[TTF^{+}]\cdots[TTF^{+}]$ long, multicenter bonds at room temperature. *J. Am. Chem. Soc.* **2013**, *135*, 13814–13826.

[53] Cotelle, Y.; Allain, M.; Legoupy, S.; Hudhomme, P. Fused glycoluril-tetrathiafulvalene molecular clips as receptors for neutral electron acceptor guests. *Org. Lett.* **2014**, *16*, 2590–2593.

[54] Torrance, J.; Scott, B.; Welber, B.; Kaufman, F.; Seiden, P. Optical properties of the radical cation tetrathiafulvalenium (TTF+) in its mixed-valence and monovalence halide salts. *Phys. Rev. B* **1979**, *19*, 730.

[55] Rosokha, S. V.; Kochi, J. K. Fresh look at electron-transfer mechanisms via the donor/acceptor bindings in the critical encounter complex. *J. Am. Chem. Soc.* **2008**, *41*, 641–653.

[56] Khodorkovsky, V.; Shapiro, L.; Krief, P.; Shames, A.; Mabon, G.; Gorgues, A.; Giffard, M. Do π-dimers of tetrathiafulvalene cation radicals really exist at room temperature? *Chem. Commun.* **2001**, 2736–2737.

[57] Lyskawa, J.; Sallé, M.; Balandier, J.-Y.; Le Derf, F.; Levillain, E.; Allain, M.; Viel, P.; Palacin, S. Monitoring the formation of TTF dimers by Na+ complexation. *Chem. Commun.* **2006**, 2233–2235.

[58] Hasegawa, M.; Daigoku, K.; Hashimoto, K.; Nishikawa, H.; Iyoda, M. Face-to-face dimeric tetrathiafulvalenes and their cation radical and dication species as models of mixed valence and π-dimer states. *Bull. Chem. Soc. Jpn.* **2012**, *85*, 51–60.

[59] Yoshizawa, M.; Kumazawa, K.; Fujita, M. Room-temperature and solution-state observation of the mixed-valence cation radical dimer of tetrathiafulvalene,[(TTF)2^{o+}), within a self-assembled cage. *J. Am. Chem. Soc.* **2005**, *127*, 13456–13457.

[60] Aprahamian, I.; Olsen, J.-C.; Trabolsi, A.; Stoddart, J. F. Tetrathiafulvalene radical cation dimerization in a bistable tripodal [4]rotaxane. *Chem. Eur. J.* **2008**, *14*, 3889–3895.

[61] Spruell, J. M.; Coskun, A.; Friedman, D. C.; Forgan, R. S.; Sarjeant, A. A.; Trabolsi, A.; Fahrenbach, A. C.; Barin, G.; Paxton, W. F.; Dey, S. K., et al.

Highly stable tetrathiafulvalene radical dimers in [3]catenanes. *Nat. Chem.* **2010**, *2*, 870–879.

[62] Coskun, A.; Spruell, J. M.; Barin, G.; Fahrenbach, A. C.; Forgan, R. S.; Colvin, M. T.; Carmieli, R.; Benítez, D.; Tkatchouk, E.; Friedman, D. C., et al. Mechanically stabilized tetrathiafulvalene radical dimers. *J. Am. Chem. Soc.* **2011**, *133*, 4538–4547.

[63] Christensen, M. A.; Parker, C. R.; Sørensen, T. J.; de Graaf, S.; Morsing, T. J.; Brock-Nannestad, T.; Bendix, J.; Haley, M. M.; Rapta, P.; Danilov, A., et al. Mixed valence radical cations and intermolecular complexes derived from indenofluorene-extended tetrathiafulvalenes. *J. Mater. Chem. C.* **2014**, *2*, 10428–10438.

[64] Brunetti, F. G.; López, J. L.; Atienza, C.; Martín, N. π-Extended TTF: a versatile molecule for organic electronics. *J. Mater. Chem.* **2012**, *22*, 4188–4205.

[65] Kamo, H.; Ueda, A.; Isono, T.; Takahashi, K.; Mori, H. Synthesis and properties of catechol-fused tetrathiafulvalene derivatives and their hydrogen-bonded conductive charge-transfer salts. *Tetrahedron Lett.* **2012**, *53*, 4385–4388.

[66] Bao, W.-H.; Wu, C.; Wang, J.-T.; Xia, W.; Chen, P.; Tang, Z.; Xu, X.; He, W.-M. Molecular iodine-mediated synthesis of thiocarbamates from thiols, isocyanides and water under metal-free conditions. *Org. Biomol. Chem.* **2018**, *16*, 8403–8407.

[67] Otón, F.; Lloveras, V.; Mas-Torrent, M.; Vidal-Gancedo, J.; Veciana, J.; Rovira, C. Coupling Tetracyanoquinodimethane to Tetrathiafulvalene: A Fused TCNQ–TTF–TCNQ Triad. *Angew. Chem. Int. Ed.* **2011**, *123*, 11094–11098.

[68] Schröder, H. V.; Hupatz, H.; Achazi, A. J.; Sobottka, S.; Sarkar, B.; Paulus, B.; Schalley, C. A. A divalent pentastable redox-switchable donor–acceptor rotaxane. *Chem. Eur. J.* **2017**, *23*, 2960–2967.

[69] Schröder, H. V.; Sobottka, S.; Nößler, M.; Hupatz, H.; Gaedke, M.; Sarkar, B.; Schalley, C. A. Impact of mechanical bonding on the redox-switching of tetrathiafulvalene in crown ether–ammonium [2]rotaxanes. *Chem. Sci.* **2017**, *8*, 6300–6306.

[70] Schröder, H. V.; Wollschläger, J. M.; Schalley, C. A. Redox-controlled self-inclusion of a lasso-type pseudo [1]rotaxane. *Chem. Commun.* **2017**, *53*, 9218–9221.

[71] Frère, P.; Skabara, P. J. Salts of extended tetrathiafulvalene analogues: relationships between molecular structure, electrochemical properties and solid state organisation. *Chem. Soc. Rev.* **2005**, *34*, 69–98.

[72] Yamada, J.-i.; Sugimoto, T. *TTF chemistry: fundamentals and applications of tetrathiafulvalene*; Springer, 2004.

[73] Wudl, F.; Wobschall, D.; Hufnagel, E. J. Electrical conductivity by the bis(1,3-dithiole)-bis (1,3-dithiolium) system. *J. Am. Chem. Soc.* **1972**, *94*, 670–672.

[74] Wudl, F.; Smith, G.; Hufnagel, E. Bis-1,3-dithiolium chloride: an unusually

stable organic radical cation. *J. Chem. Soc. D., Chem. Commun.* **1970**, 1453–1454.

[75] Wang, C.; Dyar, S. M.; Cao, D.; Fahrenbach, A. C.; Horwitz, N.; Colvin, M. T.; Carmieli, R.; Stern, C. L.; Dey, S. K.; Wasielewski, M. R., et al. Tetrathiafulvalene hetero radical cation dimerization in a redox-active [2]catenane. *J. Am. Chem. Soc.* **2012**, *134*, 19136–19145.

[76] Coskun, A.; Spruell, J. M.; Barin, G.; Fahrenbach, A. C.; Forgan, R. S.; Colvin, M. T.; Carmieli, R.; Benítez, D.; Tkatchouk, E.; Friedman, D. C., et al. Mechanically stabilized tetrathiafulvalene radical dimers. *J. Am. Chem. Soc.* **2011**, *133*, 4538–4547.

[77] Barnes, J. C.; Fahrenbach, A. C.; Dyar, S. M.; Frasconi, M.; Giesener, M. A.; Zhu, Z.; Liu, Z.; Hartlieb, K. J.; Carmieli, R.; Wasielewski, M. R., et al. Mechanically induced intramolecular electron transfer in a mixed-valence molecular shuttle. *Nat. Acad. Sci.* **2012**, *109*, 11546–11551.

[78] Segura, J. L.; Martín, N. New concepts in tetrathiafulvalene chemistry. *Angew. Chem. Int. Ed.* **2001**, *40*, 1372–1409.

[79] Dumur, F.; Gautier, N.; Gallego-Planas, N.; Şahin, Y.; Levillain, E.; Mercier, N.; Hudhomme, P.; Masino, M.; Girlando, A.; Lloveras, V., et al. Novel fused D-A dyad and A-D-A triad incorporating tetrathiafulvalene and p-benzoquinone. *J. Org. Chem.* **2004**, *69*, 2164–2177.

[80] Christensen, C. A.; Batsanov, A. S.; Bryce, M. R. Extreme conformational constraints in π-extended tetrathiafulvalenes: unusual topologies and redox

behavior of doubly and triply bridged cyclophanes. *J. Am. Chem. Soc.* **2006**, *128*, 10484–10490.

[81] Otón, F.; Lloveras, V.; Mas-Torrent, M.; Vidal-Gancedo, J.; Veciana, J.; Rovira, C. Coupling tetracyanoquinodimethane to tetrathiafulvalene: a fused TCNQ–TTF–TCNQ triad. *Angew. Chem. Int. Ed.* **2011**, *123*, 11094–11098.

[82] Lincke, K.; Floor Frellsen, A.; Parker, C. R.; Bond, A. D.; Hammerich, O.; Brøndsted Nielsen, M. A tetrathiafulvalene-functionalized radiaannulene with multiple redox states. *Angew. Chem. Int. Ed.* **2012**, *51*, 6099–6102.

[83] Nelsen, S. F.; Ismagilov, R. F.; Trieber, D. A. Adiabatic electron transfer: Comparison of modified theory with experiment. *Science* **1997**, *278*, 846–849.

[84] Nelsen, S. F. "Almost delocalized" intervalence compounds. *Chem. Eur. J.* **2000**, *6*, 581–588.

[85] Brunschwig, B. S.; Creutz, C.; Sutin, N. Optical transitions of symmetrical mixed-valence systems in the class II–III transition regime. *Chem. Soc. Rev.* **2002**, *31*, 168–184.

[86] Nelsen, S. F.; Trieber, D. A.; Ismagilov, R. F.; Teki, Y. Solvent effects on charge transfer bands of nitrogen-centered intervalence compounds. *J. Am. Chem. Soc.* **2001**, *123*, 5684–5694.

[87] Svenstrup, N.; Becher, J. The organic chemistry of 1, 3-dithiole-2-thione-4, 5-dithiolate (DMIT). *Synthesis* **1995**, *1995*, 215–235.

[88] Takahashi, K.; Ise, T.; Mori, T.; Mori, H.; Tanaka, S. Crystal structures and conducting properties of PF6 and AsF6 salts of a novel benzo[c]furan-extended donor: The role of inter-column interactions. *Chem. Lett.* **1998**, *27*, 1147–1148.

[89] Lyskawa, J.; Le Derf, F.; Levillain, E.; Mazari, M.; Sallé, M.; Dubois, L.; Viel, P.; Bureau, C.; Palacin, S. Univocal demonstration of the electrochemically mediated binding of Pb2+ by a modified surface incorporating a TTF-based redox-switchable ligand. *J. Am. Chem. Soc.* **2004**, *126*, 12194–12195.

[90] Bivaud, S.; Balandier, J.-Y.; Chas, M.; Allain, M.; Goeb, S.; Sallé, M. A metal-directed self-assembled electroactive cage with bis (pyrrolo) tetrathiafulvalene (BPTTF) side walls. *J. Am. Chem. Soc.* **2012**, *134*, 11968–11970.

[91] Bivaud, S.; Goeb, S.; Croué, V.; Dron, P. I.; Allain, M.; Sallé, M. Self-assembled containers based on extended tetrathiafulvalene. *J. Am. Chem. Soc.* **2013**, *135*, 10018–10021.

[92] Narayanaswamy, K.; Venkateswararao, A.; Gupta, V.; Chand, S.; Singh, S. P. NIR absorbing D–π–A–π–D structured diketopyrrolopyrrole–dithiafulvalene based small molecule for solution processed organic solar cells. *Chem. Commun.* **2016**, *52*, 210–213.

[93] Bergkamp, J. J.; Decurtins, S.; Liu, S.-X. Current advances in fused tetrathiafulvalene donor–acceptor systems. *Chem. Soc. Rev.* **2015**, *44*, 863–874.

[94] Dolder, S.; Liu, S.-X.; Guégano, X.; Atanasov, M.; Daul, C. A.; Leiggener, C.; Hauser, A.; Neels, A.; Decurtins, S. Preparation and characterization of 3-(4,5-

ethylenedithio-1, 3-dithiol-2-ylidene) naphthopyranone: a luminescent redox-active donor–acceptor compound. *Tetrahedron* **2006**, *62*, 11106–11111.

[95] Amacher, A. M.; Puigmartí-Luis, J.; Geng, Y.; Lebedev, V.; Laukhin, V.; Krämer, K.; Hauser, J.; Amabilino, D. B.; Decurtins, S.; Liu, S.-X. Coordination-directed self-assembly of a simple benzothiadiazole-fused tetrathiafulvalene to low-bandgap metallogels. *Chem. Commun.* **2015**, *51*, 15063–15066.

[96] Pointillart, F.; Jung, J.; Berraud-Pache, R.; Le Guennic, B.; Dorcet, V.; Golhen, S.; Cador, O.; Maury, O.; Guyot, Y.; Decurtins, S., et al. Luminescence and single-molecule magnet behavior in lanthanide complexes involving a tetrathiafulvalene-fused dipyridophenazine ligand. *Inorg. Chem.* **2015**, *54*, 5384–5397.

[97] Amacher, A.; Yi, C.; Yang, J.; Bircher, M. P.; Fu, Y.; Cascella, M.; Grätzel, M.; Decurtins, S.; Liu, S.-X. A quinoxaline-fused tetrathiafulvalene-based sensitizer for efficient dye-sensitized solar cells. *Chem. Commun.* **2014**, *50*, 6540–6542.

[98] Geng, Y.; Pfattner, R.; Campos, A.; Wang, W.; Jeannin, O.; Hauser, J.; Puigdollers, J.; Bromley, S. T.; Decurtins, S.; Veciana, J., et al. HOMO stabilisation in π-extended dibenzotetrathiafulvalene derivatives for their application in organic field-effect transistors. *Chem. Eur. J.* **2014**, *20*, 16672–16679.

[99] Biaso, F.; Geoffroy, M.; Canadell, E.; Auban-Senzier, P.; Levillain, E.; Fourmigué, M.; Avarvari, N. Intramolecular mixed-valence state through silicon

or germanium double bridges in rigid bis(tetrathiafulvalenes). *Chem. Eur. J.* **2007**, *13*, 5394–5400.

[100] Tanaka, K.; Kunita, T.; Ishiguro, F.; Naka, K.; Chujo, Y. Modulation of morphology and conductivity of mixed-valence tetrathiafulvalene nanofibers by coexisting organic acid anions. *Langmuir* **2009**, *25*, 6929–6933.

[101] Lacroix, J. C.; Chane-Ching, K. I.; Maquère, F.; Maurel, F. Intrachain electron transfer in conducting oligomers and polymers: the mixed valence approach. *J. Am. Chem. Soc.* **2006**, *128*, 7264–7276.

[102] Adam, M.; Müllen, K. Oligomeric tetrathiafulvalenes: extended donors for increasing the dimensionality of electrical conduction. *Adv. Mater.* **1994**, *6*, 439–459.

[103] Iyoda, M.; Hasegawa, M.; Miyake, Y. Bi-TTF, bis-TTF, and related TTF oligomers. *Chem. Rev.* **2004**, *104*, 5085–5114.

[104] Lorcy, D.; Bellec, N.; Fourmigué, M.; Avarvari, N. Tetrathiafulvalene-based group XV ligands: synthesis, coordination chemistry and radical cation salts. *Coord. Chem. Rev.* **2009**, *253*, 1398–1438.

[105] Lahlil, K.; Moradpour, A.; Bowlas, C.; Menou, F.; Cassoux, P.; Bonvoisin, J.; Launay, J.-P.; Dive, G.; Dehareng, D. Intervalence transitions in mixed valence bis(tetrathiafulvalene) compounds. *J. Am. Chem. Soc.* **1995**, *117*, 9995–10002.

[106] Otsubo, T.; Kochi, Y.; Bitoh, A.; Ogura, F. Syntheses and properties of novel

dimeric tetrathiafulvalenes linked with an ethenylene or ethynylene spacer. *Chem. Lett.* **1994**, *23*, 2047–2050.

[107] Iyoda, M.; Hasegawa, M.; Takano, J.-i.; Hara, K.; Kuwatani, Y. Intramolecular charge interaction in the radical cations and dications of conjugated tetrathiafulvalene dimers. *Chem. Lett.* **2002**, *31*, 590–591.

[108] Hara, K.; Hasegawa, M.; Kuwatani, Y.; Enozawa, H.; Iyoda, M. Mono- and bis(tetrathiafulvaleno)hexadehydro[12]annulenes. *Chem. Commun.* **2004**, 2042–2043.

[109] Andersson, A. S.; Kerndrup, L.; Madsen, A. Ø.; Kilså, K.; Nielsen, M. B.; Porta, P. R. L.; Biaggio, I. Synthesis and characterization of tetrathiafulvalene-substituted di-and tetraethynylethenes with p-nitrophenyl acceptors. *J. Org. Chem.* **2009**, *74*, 375–382.

[110] Lincke, K.; Christensen, M. A.; Diederich, F.; Nielsen, M. B. Acetylenic tetrathiafulvalene scaffolds–intramolecular charge-transfer molecules. *Helv. Chim. Acta.* **2011**, *94*, 1743–1753.

[111] Lincke, K.; Floor Frellsen, A.; Parker, C. R.; Bond, A. D.; Hammerich, O.; Brøndsted Nielsen, M. A tetrathiafulvalene-functionalized radiaannulene with multiple redox states. *Angew. Chem., Int. Ed.* **2012**, *51*, 6099–6102.

[112] Jiang, H.; Mazzanti, V.; Parker, C. R.; Broman, S. L.; Wallberg, J. H.; Lušpai, K.; Brincko, A.; Kjaergaard, H. G.; Kadziola, A.; Rapta, P., et al. Interactions between tetrathiafulvalene units in dimeric structures–the influence of cyclic cores. *Beilstein J. Org. Chem.* **2015**, *11*, 930–948.

[113] Parthey, M.; Gluyas, J. B.; Schauer, P. A.; Yufit, D. S.; Howard, J. A.; Kaupp, M.; Low, P. J. Refining the interpretation of near-infrared band shapes in a polyynediyl molecular wire. *Chem. Eur. J.* **2013**, *19*, 9780–9784.

[114] Parthey, M.; Gluyas, J. B.; Fox, M. A.; Low, P. J.; Kaupp, M. Mixed-valence ruthenium complexes rotating through a conformational Robin–Day continuum. *Chem. Eur. J.* **2014**, *20*, 6895–6908.

[115] Iyoda, M.; Kuwatani, Y.; Ueno, N.; Oda, M. Palladium-catalysed coupling of trialkylstannyltetrathiafulvalenes with aryl halides. *J. Chem. Soc., Chem. Commun.* **1992**, 158–159.

[116] Iyoda, M.; Fukuda, M.; Yoshida, M.; Sasaki, S. Multi-tetrathiafulvalene systems. New donors containing two or three tetrathiafulvalene-substituents at 1,3-and 1,3,5-positions of aromatic rings. *Chem. Lett.* **1994**, *23*, 2369–2372.

[117] Vacher, A.; Barrière, F.; Roisnel, T.; Piekara-Sady, L.; Lorcy, D. Electronically coupled tetrathiafulvalene electrophores across a non-innocent acetylide–ruthenium bridge. *Organometallics* **2011**, *30*, 3570–3578.

[118] Misaki, Y.; Matsui, T.; Kawakami, K.; Nishikawa, H.; Yamabe, T.; Shiro, M. 2,5-Bis (1,3-dithiol-2ylidene)-1,3,4,6-tetrathiapentalene and its related unsymmetrical donors. *Chem. Lett.* **1993**, *22*, 1337–1340.

[119] Wu, M.; Li, J.; Zhang, R.; Tian, X.; Han, Z.; Lu, X.; Guo, K.; Liu, Z.; Wang, Z. Synthesis and properties of dithiafulvenyl functionalized spiro[fluorene-9, 9-xanthene] molecules. *Org. Lett.* **2018**, *20*, 780–783.

[120] Fujioka, A.; Kubo, T.; Watanabe, M.; Ueda, M.; Miyamoto, H.; Misaki, Y. Vilsmeier–Haack type formylation on 6-aryl-1,4-dithiafulvenes and syntheses of novel extended tetrathiafulvalene donors. *Synthesis* **2016**, *48*, 845–854.

[121] Keshri, S. K.; Asthana, D.; Chorol, S.; Kumar, Y.; Mukhopadhyay, P. Appending diverse π-extended acceptors with tetrathiafulvalene/dithiafulvalene donors: multistate redox properties, radical ion generation, and mid-IR-absorbing mixed-valence states. *Chem. Eur. J.* **2018**, *24*, 1821–1832.

[122] Balgley, R.; Shankar, S.; Lahav, M.; van der Boom, M. E. Rerouting electron transfer in molecular assemblies by redox-pair matching. *Angew. Chem.* **2015**, *127*, 12634–12639.

[123] Keshri, S. K.; Mandal, K.; Kumar, Y.; Yadav, D.; Mukhopadhyay, P. Naphthalenediimides with high fluorescence quantum yield: bright-red, stable, and responsive fluorescent dyes. *Angew. Chem. Int. Ed.* **2021**, *27*, 6954–6962.

[124] Tseng, H.-R.; Vignon, S. A.; Stoddart, J. F. Toward chemically controlled nanoscale molecular machinery. *Angew. Chem. Int. Ed.* **2003**, *42*, 1491–1495.

[125] Batail, P. Introduction: molecular conductors. 2004.

[126] Sarhan, A. E.-W. A. Synthesis and applications of tetrathiafulvalenes and ferrocene-tetrathiafulvalenes and related compounds. *Tetrahedron* **2005**, *16*, 3889–3932.

[127] Kitamura, T.; Nakaso, S.; Mizoshita, N.; Tochigi, Y.; Shimomura, T.; Moriyama, M.; Ito, K.; Kato, T. Electroactive supramolecular self-assembled

fibers comprised of doped tetrathiafulvalene-based gelators. *J. Am. Chem. Soc.* **2005**, *127*, 14769–14775.

[128] Zheng, Y. B.; Yang, Y.-W.; Jensen, L.; Fang, L.; Juluri, B. K.; Flood, A. H.; Weiss, P. S.; Stoddart, J. F.; Huang, T. J. Active molecular plasmonics: controlling plasmon resonances with molecular switches. *Nano Lett.* **2009**, *9*, 819–825.

[129] Bernhardt, P. V.; Moore, E. G. Functionalized macrocyclic compounds: Potential sensors of small molecules and ions. *Austral. J. Chem.* **2003**, *56*, 239–258.

[130] Jørgensen, T.; Hansen, T. K.; Becher, J. Tetrathiafulvalenes as building-blocks in supramolecular chemistry. *Chem. Soc. Rev.* **1994**, *23*, 41–51.

[131] Hansen, T. K.; Joergensen, T.; Stein, P. C.; Becher, J. Crown ether derivatives of tetrathiafulvalene. 1. *J. Org. Chem.* **1992**, *57*, 6403–6409.

[132] Johnston, B.; Goldenberg, L. M.; Bryce, M. R.; Kataky, R. A tetrathiafulvalene derivative with an acyclic S 4 domain as a voltammetric silver sensor. *J. Chem. Soc.* **2000**, 189–190.

[133] Lyskawa, J.; Le Derf, F.; Levillain, E.; Mazari, M.; Sallé, M.; Dubois, L.; Viel, P.; Bureau, C.; Palacin, S. Univocal demonstration of the electrochemically mediated binding of Pb2+ by a modified surface incorporating a TTF-based redox-switchable ligand. *J. Am. Chem. Soc.* **2004**, *126*, 12194–12195.

[134] Zhao, B.-T.; Blesa, M.-J.; Mercier, N.; Le Derf, F.; Sallé, M. Bis-calix[4]arenes

bridged by an electroactive tetrathiafulvalene unit. *J. Org. Chem.* **2005**, *70*, 6254–6257.

[135] Blesa, M.-J.; Zhao, B.-T.; Allain, M.; Le Derf, F.; Sallé, M. Bis(calixcrown) tetrathiafulvalene receptors. *Chem. Eur. J.* **2006**, *12*, 1906–1914.

[136] Mulla, K.; Zhao, Y. TTFV molecular tweezers with phenylboronic acid and phenylboronate endgroups: modular synthesis and electrochemical responses to saccharides and fluoride ion. *Tetrahedron Lett.* **2014**, *55*, 382–386.

[137] Mulla, K.; Shaik, H.; Thompson, D. W.; Zhao, Y. TTFV-based molecular tweezers and macrocycles as receptors for fullerenes. *Org. Lett.* **2013**, *15*, 4532–4535.

[138] Li, X.; Zhang, G.; Ma, H.; Zhang, D.; Li, J.; Zhu, D. 4,5-Dimethylthio-4‘-[2-(9-anthryloxy)ethylthio] tetrathiafulvalene, a highly selective and sensitive chemiluminescence probe for singlet oxygen. *J. Am. Chem. Soc.* **2004**, *126*, 11543–11548.

[139] Zhang, G.; Li, X.; Ma, H.; Zhang, D.; Li, J.; Zhu, D. A selective and sensitive chemiluminescence reaction of 4,4(5)-bis [2-(9-anthryloxy)ethylthio]tetrathiafulvalene with singlet oxygen. *Chem. Commun.* **2004**, 2072–2073.

[140] Canevet, D.; Sallé, M.; Zhang, G.; Zhang, D.; Zhu, D. Tetrathiafulvalene (TTF) derivatives: key building-blocks for switchable processes. *Chem. Commun.* **2009**, 2245–2269.

[141] Zhang, Y.; Cai, L.-Z.; Wang, C.-Y.; Lai, G.-Q.; Shen, Y.-J. Synthesis and properties of a tetrathiafulvalene–perylene tetracarboxylic diimide–tetrathiafulvalene dyad. *New J. Chem.* **2008**, *32*, 1968–1973.

[142] Zhang, X.; Wang, C.; Lai, G.; Zhang, L.; Shen, Y. Conjugated ethynylene-fluorene polymers with electro-donating TTF as pendant groups: Synthesis, electrochemical and spectroscopic properties. *New J. Chem.* **2010**, *34*, 318–324.

[143] Zhou, Y.; Zhang, D.; Zhu, L.; Shuai, Z.; Zhu, D. Binaphthalene molecules with tetrathiafulvalene units: CD spectrum modulation and new chiral molecular switches by reversible oxidation and reduction of tetrathiafulvalene units. *J. Org. Chem.* **2006**, *71*, 2123–2130.

[144] Setnicka, V.; Urbanova, M.; Bouř, P.; Král, V.; Volka, K. Vibrational circular dichroism of 1,1‘-binaphthyl derivatives: experimental and theoretical study. *J. Phys. Chem. A* **2001**, *105*, 8931–8938.

[145] Huang, T. J.; Brough, B.; Ho, C.-M.; Liu, Y.; Flood, A. H.; Bonvallet, P. A.; Tseng, H.-R.; Stoddart, J. F.; Baller, M.; Magonov, S. A nanomechanical device based on linear molecular motors. *Appl. Phys. Lett.* **2004**, *85*, 5391–5393.

[146] Nguyen, T. D.; Tseng, H.-R.; Celestre, P. C.; Flood, A. H.; Liu, Y.; Stoddart, J. F.; Zink, J. I. A reversible molecular valve. *PNAS* **2005**, *102*, 10029–10034.

[147] Tseng, H.-R.; Vignon, S. A.; Stoddart, J. F. Toward chemically controlled nanoscale molecular machinery. *Angew. Chem. Int. Ed.* **2003**, *42*, 1491–1495.

[148] Kao, J.; Eyermann, C.; Southwick, E.; Leister, D. A systematic approach to calculate molecular properties of organosulfur compounds containing the carbon-sulfur (Csp^2-S) bond. *J. Am. Chem. Soc.* **1985**, *107*, 5323–5332.

[149] Benassi, R.; Taddei, F. Ground-state molecular stabilization of substituted ethylenes. A theoretical mo ab-initio thermochemical study. *J. Mol. Struct.* **2001**, *572*, 169–183.

[150] Nielsen, M. B.; Sauer, S. P. On the aromaticity of tetrathiafulvalene cations. *Chem. Phys. Lett.* **2008**, *453*, 136–139.

[151] Brunetti, F. G.; López, J. L.; Atienza, C.; Martín, N. π-Extended TTF: a versatile molecule for organic electronics. *J. Mater. Chem.* **2012**, *22*, 4188–4205.

[152] Kirmse, W.; Horner, L. Über Lichtreaktionen VIII. photolyse von 1.2.3-thiodiazolen. *Annal. der Chem.* **1958**, *614*, 4–18.

[153] Hartzler, H. D. 2-Benzylidene-1,3-dithioles. Remarkably rapid Wittig reaction. *J. Am. Chem. Soc.* **1971**, *93*, 4961–4962.

[154] Sato, M.; Gonnella, N. C.; Cava, M. P. Synthesis and reactions of (4,5-dicarbomethoxy-1,3-dithiolyl) tributylphosphonium tetrafluoroborate. *J. Org. Chem.* **1979**, *44*, 930–934.

[155] Christensen, C. A.; Batsanov, A. S.; Bryce, M. R. Thiolated π-extended tetrathiafulvalenes: versatile multifunctional π-systems. *J. Org. Chem.* **2007**, *72*, 1301–1308.

[156] Mizuno, M.; Cava, M. P. Organic metals. A study of the Hurtley-Smiles tetrathiafulvalene synthesis. *J. Org. Chem.* **1978**, *43*, 416–418.

[157] Gimbert, Y.; Moradpour, A.; Dive, G.; Dehareng, D.; Lahlil, K. A variable mechanism for the nucleophilic vinylic substitutions in a series of gem-dihalogenated alkenes by a bidentate sulfur nucleophile: an experimental and AM1 theoretical study. *J. Org. Chem.* **1993**, *58*, 4685–4690.

[158] Giguere, J.-B.; Morin, J.-F. Super extended tetrathiafulvalene: synthesis, optoelectronic properties, fullerenes complexation, and photooxidation study. *J. Org. Chem.* **2015**, *80*, 6767–6775.

[159] Broman, S. L.; Andersen, C. L.; Jousselin-Oba, T.; Mansø, M.; Hammerich, O.; Frigoli, M.; Nielsen, M. B. Tetraceno [2,1,12,11-opqra]tetracene-extended tetrathiafulvalene–redox-controlled generation of a large PAH core. *Org. Biomol. Chem.* **2017**, *15*, 807–811.

[160] Parg, R. P.; Kilburn, J. D.; Ryan, T. G. A one-step synthesis of 1,3-dithiol-2-ylphosphonate esters from 1,3-dithiole-2-thiones. *Synthesis* **1994**, *1994*, 195–198.

[161] Ohta, A.; Yamashita, Y. Oxidative intramolecular cyclization of 2,2-bis(1,4-dithiafulven-6-yl)-3,3-bithienyls affording novel bis(1,3-dithiole) electron donors. *J. Chem. Soc.* **1995**, 1761–1762.

[162] Yamashita, Y.; Tomura, M.; Zaman, M. B. Synthesis and properties of novel tetrathiafulvalene vinylogues. *Chem. Commun.* **1998**, 1657–1658.

[163] Müller, H.; Salhi, F.; Divisia-Blohorn, B. Bis-substituted tetrathiapentalenes—Novel building blocks for extended tetrathiafulvalenes and conducting polymers. *Tetrahedron Lett.* **1997**, *38*, 3215–3218.

[164] Massue, J.; Bellec, N.; Guerro, M.; Bergamini, J.-F.; Hapiot, P.; Lorcy, D. Crown ether vinylogous tetrathiafulvalene receptors: complexation interference on the molecular movements triggered by electron transfer. *J. Org. Chem.* **2007**, *72*, 4655–4662.

[165] Lakshmikantham, M.; Cava, M. P.; Carroll, P. J. Novel oxidative rearrangement of o-xylene-α, α'-diylidenebis (4,5-dicarbomethoxy-1,3-dithiole). *J. Org. Chem.* **1984**, *49*, 726–728.

[166] Frère, P.; Gorgues, A.; Jubault, M.; Riou, A.; Gouriou, Y.; Roncali, J. Electrochemically induced intramolecular cyclization of 1,2-bis(1,4-dithiafulven-6-yl) benzenes. *Tetrahedron Lett.* **1994**, *35*, 1991–1994.

[167] Guerro, M.; Roisnel, T.; Pellon, P.; Lorcy, D. Redox-active dithiafulvenyldiphenylphosphine as a mono-or bidentate ligand: intramolecular coupling reaction in the coordination sphere of a metal carbonyl fragment. *Inorg. Chem.* **2005**, *44*, 3347–3355.

[168] Guerro, M.; Pham, N. H.; Massue, J.; Bellec, N.; Lorcy, D. New redox active ligands involving a tetrathiafulvalene vinylogue backbone. *Tetrahedron* **2008**, *64*, 5285–5290.

[169] Gontier, E.; Bellec, N.; Brignou, P.; Gohier, A.; Guerro, M.; Roisnel, T.;

Lorcy, D. Pyridyldithiafulvenes as precursors of coordination-driven self-assembled redox active macrocycle. *Org. Lett.* **2010**, *12*, 2386–2389.

[170] Benahmed-Gasmi, A.; Frère, P.; Roncali, J.; Elandaloussi, E.; Orduna, J.; Garin, J.; Jubault, M.; Gorgues, A. Oxidative dimerization of 2-(1,4-dithiafulven-6-yl) thiophenes: an alternative route towards extensively π-conjugated tetrathiafulvalene analogs. *Tetrahedron Lett.* **1995**, *36*, 2983–2986.

[171] Lorcy, D.; Carlier, R.; Robert, A.; Tallec, A.; Le Maguerès, P.; Ouahab, L. Electrochemical synthesis of extended TTF. *J. Org. Chem.* **1995**, *60*, 2443–2447.

[172] Hascoat, P.; Lorcy, D.; Robert, A.; Carlier, R.; Tallec, A.; Boubekeur, K.; Batail, P. Formation of attractive π-redox cyclophanes. *J. Org. Chem.* **1997**, *62*, 6086–6089.

[173] Hapiot, P.; Lorcy, D.; Tallec, A.; Carlier, R.; Robert, A. Mechanism of dimerization of 1,4-dithiafulvenes into TTF vinylogues. *J. Phys. Chem.* **1996**, *100*, 14823–14827.

[174] Guerro, M.; Lorcy, D. A simple route to novel functionalized tetrathiafulvalene vinylogues. *Tetrahedron Lett.* **2005**, *46*, 5499–5502.

[175] Lakshmikantham, M.; Cava, M. P. Some novel transformations of 1,4-dithiafulvenes. *J. Org. Chem.* **1981**, *46*, 3246–3249.

[176] Sarhan, A. A.; Bolm, C. Iron(III) chloride in oxidative C–C coupling reactions. *Chem. Soc. Rev.* **2009**, *38*, 2730–2744.

[177] Spies, H.; Gewald, K.; Mayer, R. Zur reaktion von natriumphenylacetylid mit schwefel oder selen und heterokumulenen. *J. Praktische Chem.* **1971**, *313*, 804–810.

[178] Mulla, K.; Zhao, Y. When dithiafulvenyl functionalized π-conjugated oligomers meet fullerenes and single-walled carbon nanotubes. *J. Mater. Chem.* **2013**, *1*, 5116–5127.

[179] Fu, H.; Zhao, B.; Zhu, W. Elemental iodine mediated synthesis of thiadiazole-based dithiafulvalene donors via C(sp2)–S formation. *Tetrahedron Lett.* **2019**, *60*, 124–128.

[180] Wang, Y.; Zhao, Y. Dithiafulvenyl-substituted phenylacetylene derivatives: synthesis and structure–property–reactivity relationships. *Org. Biomol. Chem.* **2015**, *13*, 9575–9579.

[181] Wang, C.; Flinn, C.; Zhao, Y. Intramolecular alkyne–dithiolium cycloaddition: a joint experimental and DFT mechanistic study. *RSC Adv.* **2017**, *7*, 36623–36631.

[182] Alévêque, O.; Leriche, P.; Cocherel, N.; Frère, P.; Cravino, A.; Roncali, J. Star-shaped conjugated systems derived from dithiafulvenyl-derivatized triphenylamines as active materials for organic solar cells. *Sol. Energy Mater. Sol. Cells* **2008**, *92*, 1170–1174.

[183] Guo, K.; Yan, K.; Lu, X.; Qiu, Y.; Liu, Z.; Sun, J.; Yan, F.; Guo, W.; Yang, S. Dithiafulvenyl unit as a new donor for high-efficiency dye-sensitized solar cells:

synthesis and demonstration of a family of metal-free organic sensitizers. *Org. Lett.* **2012**, *14*, 2214–2217.

[184] Wu, Y.; Zhang, Q.; Li, J.; Tian, X.; Li, D.; Lu, X.; Xu, B.; Wu, Y.; Guo, K. Regulation of dithiafulvene-based molecular shape and aggregation on TiO 2 for high efficiency dye-sensitized solar cells. *J. Mater. Chem.* **2019**, *7*, 1974–1981.

[185] Wu, M.; Li, J.; Zhang, R.; Tian, X.; Han, Z.; Lu, X.; Guo, K.; Liu, Z.; Wang, Z. Synthesis and properties of dithiafulvenyl functionalized spiro[fluorene-9, 9-xanthene] molecules. *Org. Lett.* **2018**, *20*, 780–783.

[186] Bumm, L.; Arnold, J. J.; Cygan, M.; Dunbar, T.; Burgin, T.; Jones, L.; Allara, D. L.; Tour, J. M.; Weiss, P. Are single molecular wires conducting? *Science* **1996**, *271*, 1705–1707.

[187] Yaliraki, S.; Kemp, M.; Ratner, M. A. Conductance of molecular wires: influence of molecule-electrode binding. *J. Am. Chem. Soc.* **1999**, *121*, 3428–3434.

[188] Leary, E.; La Rosa, A.; González, M. T.; Rubio-Bollinger, G.; Agraït, N.; Martín, N. Incorporating single molecules into electrical circuits. The role of the chemical anchoring group. *Chem. Soc. Rev.* **2015**, *44*, 920–942.

[189] Perrin, M. L.; Burzurí, E.; van der Zant, H. S. Single-molecule transistors. *Chem. Soc. Rev.* **2015**, *44*, 902–919.

[190] Xiang, D.; Wang, X.; Jia, C.; Lee, T.; Guo, X. Molecular-scale electronics: from concept to function. *Chem. Rev.* **2016**, *116*, 4318–4440.

[191] Tanaka, K.; Ishiguro, F.; Chujo, Y. Photoinduced radical generation and self-assembly of tetrathiafulvalene into the mixed-valence state in the poly(vinyl chloride) film under UV irradiation. *Langmuir* **2010**, *26*, 1152–1156.

[192] Coropceanu, V.; Cornil, J.; da Silva Filho, D. A.; Olivier, Y.; Silbey, R.; Brédas, J.-L. Charge transport in organic semiconductors. *Chem. Rev.* **2007**, *107*, 926–952.

[193] Xia, Y.; Yang, P.; Sun, Y.; Wu, Y.; Mayers, B.; Gates, B.; Yin, Y.; Kim, F.; Yan, H. One-dimensional nanostructures: synthesis, characterization, and applications. *Adv. Mater.* **2003**, *15*, 353–389.

[194] Grimsdale, A. C.; Müllen, K. The chemistry of organic nanomaterials. *Angew. Chem. Int. Ed.* **2005**, *44*, 5592–5629.

[195] Kim, Y. I.; Hatfield, W. E. Electrical, magnetic and spectroscopic properties of tetrathiafulvalene charge transfer compounds with iron, ruthenium, rhodium and iridium halides. *Inorg. Chim. Acta* **1991**, *188*, 15–24.

[196] Inoue, M. B.; Inoue, M.; Fernando, Q.; Nebesny, K. W. Highly electroconductive tetrathiafulvalenium salts of copper halides. *Inorg. Chem.* **1986**, *25*, 3976–3980.

[197] Choi, S.-N.; Jung, W.-S.; Lee, M.-J.; Lee, Y.-M.; Kim, Y.-I. Synthesis and physicochemical properties of charge transfer compounds derived from the reaction of tetrathiafulvalene with copper(II). *Polyhedron* **2004**, *23*, 2111–2115.

[198] Sørensen, J. K.; Vestergaard, M.; Kadziola, A.; Kilså, K.; Nielsen, M. B. Syn-

thesis of oligo(phenyleneethynylene)-tetrathiafulvalene cruciforms for molecular electronics. *Org. Lett.* **2006**, *8*, 1173–1176.

[199] Vestergaard, M.; Jennum, K.; Sørensen, J. K.; Kilså, K.; Nielsen, M. B. Synthesis and characterization of cruciform-conjugated molecules based on tetrathiafulvalene. *J. Org. Chem.* **2008**, *73*, 3175–3183.

[200] Jennum, K.; Vestergaard, M.; Pedersen, A. H.; Fock, J.; Jensen, J.; Santella, M.; Led, J. J.; Kilså, K.; Bjørnholm, T.; Nielsen, M. B. Synthesis of oligo (phenyleneethynylene) s with vertically disposed tetrathiafulvalene units. *Synthesis* **2011**, *2011*, 539–548.

[201] Jennum, K.; Nielsen, M. B. Tetrathiafulvalene-based cruciform molecules. *Chem. Lett.* **2011**, *40*, 662–667.

[202] Schou, S. S.; Parker, C. R.; Lincke, K.; Jennum, K.; Vibenholt, J.; Kadziola, A.; Nielsen, M. B. On the phosphite-mediated synthesis of dithiafulvenes and π-extended tetrathiafulvalenes. *Synlett* **2013**, *24*, 231–235.

[203] Wei, Z.; Hansen, T.; Santella, M.; Wang, X.; Parker, C. R.; Jiang, X.; Li, T.; Glyvradal, M.; Jennum, K.; Glibstrup, E., et al. Molecular hterojunctions of oligo(phenylene ethynylene)s with linear to cruciform framework. *Adv. Funct.* **2015**, *25*, 1700–1708.

[204] Parker, C. R.; Leary, E.; Frisenda, R.; Wei, Z.; Jennum, K. S.; Glibstrup, E.; Abrahamsen, P. B.; Santella, M.; Christensen, M. A.; Della Pia, E. A., et al. A comprehensive study of extended tetrathiafulvalene cruciform molecules for

molecular electronics: synthesis and electrical transport measurements. *J. Am. Chem. Soc.* **2014**, *136*, 16497–16507.

[205] Lissau, H.; Frisenda, R.; Olsen, S. T.; Jevric, M.; Parker, C. R.; Kadziola, A.; Hansen, T.; Van Der Zant, H. S.; Brøndsted Nielsen, M.; Mikkelsen, K. V. Tracking molecular resonance forms of donor–acceptor push–pull molecules by single-molecule conductance experiments. *Nature Commun.* **2015**, *6*, 1–8.

[206] Xing, Y.; Wyss, A.; Esser, N.; Dittrich, P. S. Label-free biosensors based on in situ formed and functionalized microwires in microfluidic devices. *Analyst* **2015**, *140*, 7896–7901.

[207] Khadem, M.; Walsh, J. C.; Bodwell, G. J.; Zhao, Y. A macrocyclization of 1,8-bis(dithiafulvenyl)pyrenes. *Org. Lett.* **2016**, *18*, 2403–2406.

[208] Khadem, M.; Zhao, Y. Multivalent dithiafulvenyl functionalization of dendritic oligo(phenylene vinylene)s with an anthraquinodimethane core. *Chem. Commun.* **2017**, *53*, 1821–1824.

[209] Shahrokhi, F.; Zhao, Y. A tetrathiafulvalene vinylogue-based double-layer polymer thin film as a highly sensitive and selective TNT sensor. *New J. Chem.* **2019**, *43*, 5277–5281.

[210] Uemura, T.; Naka, K.; Chujo, Y. *New synthetic methods*; Springer, 2004; pp 81–106.

[211] Salami, F.; Zhao, Y. Synthesis and characterization of bis(dithiafulvenyl)-

substituted fluorenones and fluorenylidene-1,3-dithioles. *New J. Chem.* **2020**, *44*, 9179–9189.

[212] Lorcy, D.; Carlier, R.; Robert, A.; Tallec, A.; Le Maguerès, P.; Ouahab, L. Electrochemical synthesis of extended TTF. *J. Org. Chem.* **1995**, *60*, 2443–2447.

[213] Hapiot, P.; Lorcy, D.; Tallec, A.; Carlier, R.; Robert, A. Mechanism of dimerization of 1,4-dithiafulvenes into TTF vinylogues. *J. Phys. Chem.* **1996**, *100*, 14823–14827.

[214] Moore, A. J.; Bryce, M. R.; Skabara, P. J.; Batsanov, A. S.; Goldenberg, L. M.; Howard, J. A. 1, 4-Dithiafulvene-substituted ferrocenes and their conversion into extended tetrathiafulvalene electron donors: synthetic, electrochemical and X-ray structural studies. *J. Chem. Soc., Perkin Trans. 1* **1997**, 3443–3450.

[215] Wudl, F.; Smith, G.; Hufnagel, E. J. Chem. Soc. D. **1970**,

[216] Wudl, F.; Wobschall, D.; Hufnagel, E. J. Electrical conductivity by the bis (1, 3-dithiole)-bis (1, 3-dithiolium) system. *J. Am. Chem. Soc.* **1972**, *94*, 670–672.

[217] Wudl, F.; Wobschall, D.; Hufnagel, E. J. Electrical conductivity by the bis(1,3-dithiole)-bis(1,3-dithiolium) system. *J. Am. Chem. Soc.* **1972**, *94*, 670–672.

[218] Segura, J. L.; Martín, N. New concepts in tetrathiafulvalene chemistry. *Angew. Chem. Int. Ed.* **2001**, *40*, 1372–1409.

[219] Jeppesen, J. O.; Nielsen, M. B.; Becher, J. Tetrathiafulvalene cyclophanes and cage molecules. *Chem. Rev.* **2004**, *104*, 5115–5132.

[220] Martín, N. Tetrathiafulvalene: the advent of organic metals. *Chem. Commun.* **2013**, *49*, 7025–7027.

[221] Jana, A.; Ishida, M.; Park, J. S.; Bahring, S.; Jeppesen, J. O.; Sessler, J. L. Tetrathiafulvalene-(TTF-) derived oligopyrrolic macrocycles. *Chem. Rev.* **2017**, *117*, 2641–2710.

[222] Wang, H.-Y.; Cui, L.; Xie, J.-Z.; Leong, C. F.; D'Alessandro, D. M.; Zuo, J.-L. Functional coordination polymers based on redox-active tetrathiafulvalene and its derivatives. *Coord. Chem. Rev.* **2017**, *345*, 342–361.

[223] Zhao, Y.; Chen, G.; Mulla, K.; Mahmud, I.; Liang, S.; Dongare, P.; Thompson, D. W.; Dawe, L. N.; Bouzan, S. Tetrathiafulvalene vinylogues as versatile building blocks for new organic materials. *Pure Appl. Chem.* **2012**, *84*, 1005–1025.

[224] Yamashita, Y.; Tomura, M.; Zaman, M. B. Synthesis and properties of novel tetrathiafulvalene vinylogues. *Chem. Commun.* **1998**, 1657–1658.

[225] Tomura, M.; Yamashita, Y. Crystal engineering in π-overlapping stacks: unusual one-and/or two-dimensional stacking of the π-system in the crystal structure of the cation radical salts of tetrathiafulvalene vinylogues. *CrystEngComm* **2000**, *2*, 86–88.

[226] Carlier, R.; Hapiot, P.; Lorcy, D.; Robert, A.; Tallec, A. Electrosynthesis and redox behavior of vinylogous TTF displaying strong conformational changes associated with electron transfers. *Electrochim. Acta* **2001**, *46*, 3269–3277.

[227] Yamashita, Y.; Tomura, M.; Imaeda, K. Hydroxyphenyl substituted tetrathiafulvalene vinylogues affording stable cation radical salts with unusual crystal structures. *Tetrahedron Lett.* **2001**, *42*, 4191–4193.

[228] Mulla, K.; Zhao, Y. TTFV molecular tweezers with phenylboronic acid and phenylboronate endgroups: modular synthesis and electrochemical responses to saccharides and fluoride ion. *Tetrahedron Lett.* **2014**, *55*, 382–386.

[229] Frère, P.; Skabara, P. J. Salts of extended tetrathiafulvalene analogues: relationships between molecular structure, electrochemical properties and solid state organisation. *Chem. Soc. Rev.* **2005**, *34*, 69–98.

[230] Guerro, M.; Pham, N. H.; Massue, J.; Bellec, N.; Lorcy, D. New redox active ligands involving a tetrathiafulvalene vinylogue backbone. *Tetrahedron* **2008**, *64*, 5285–5290.

[231] Bouzan, S.; Dawe, L. N.; Zhao, Y. Bromophenyl substituted dithiafulvenes and tetrathiafulvalene vinylogues: synthesis, structure, and electronic properties. *Tetrahedron Lett.* **2013**, *54*, 4666–4669.

[232] Canevet, D.; Sallé, M.; Zhang, G.; Zhang, D.; Zhu, D. Tetrathiafulvalene (TTF) derivatives: key building-blocks for switchable processes. *Chem. Commun.* **2009**, 2245–2269.

[233] Chen, G.; Bouzan, S.; Zhao, Y. Synthesis and properties of TTFV-hinged molecular tweezers. *Tetrahedron Lett.* **2010**, *51*, 6552–6556.

[234] Mulla, K.; Shaik, H.; Thompson, D. W.; Zhao, Y. TTFV-based molecular

tweezers and macrocycles as receptors for fullerenes. *Org. Lett.* **2013**, *15*, 4532–4535.

[235] Khadem, M.; Zhao, Y. Tetrathiafulvalene vinylogue–fluorene co-oligomers: synthesis, properties, and supramoleclar interactions with carbon nanotubes. *J. Org. Chem.* **2015**, *80*, 7419–7429.

[236] Liang, S.; Chen, G.; Peddle, J.; Zhao, Y. Reversible dispersion and releasing of single-walled carbon nanotubes by a stimuli-responsive TTFV-phenylacetylene polymer. *Chem. Commun.* **2012**, *48*, 3100–3102.

[237] Liang, S.; Chen, G.; Zhao, Y. Conformationally switchable TTFV–phenylacetylene polymers: synthesis, properties, and supramolecular interactions with single-walled carbon nanotubes. *J. Mater. Chem. C* **2013**, *1*, 5477–5490.

[238] Chen, G.; Mahmud, I.; Dawe, L. N.; Zhao, Y. Acetylenic phenyldithiafulvene: a versatile synthon for TTFV-based macromolecules. *Org. Lett.* **2010**, *12*, 704–707.

[239] Nielsen, K. A.; Levillain, E.; Lynch, V. M.; Sessler, J. L.; Jeppesen, J. O. Tetrathiafulvalene porphyrins. *Chem. Eur. J.* **2009**, *15*, 506–516.

[240] Cai, S.; Sun, B.; Li, X.; Yan, Y.; Navarro, A.; Garzon-Ruiz, A.; Mao, H.; Chatterjee, R.; Yano, J.; Zhu, C., et al. Reversible interlayer sliding and conductivity changes in adaptive tetrathiafulvalene-based covalent organic frameworks. *ACS Appl. Mater. Interf.* **2020**, *12*, 19054–19061.

[241] Ishikawa, K.; Akiba, K.-y.; Inamoto, N. Synthesis of 1, 4-benzodithiafulvenes via Wittig reaction. *Tetrahedron Lett.* **1976**, *17*, 3695–3698.

[242] Carlier, R.; Hapiot, P.; Lorcy, D.; Robert, A.; Tallec, A. Electrosynthesis and redox behavior of vinylogous TTF displaying strong conformational changes associated with electron transfers. *Electrochim. Acta* **2001**, *46*, 3269–3277.

[243] Christensen, C. A.; Batsanov, A. S.; Bryce, M. R. Thiolated π-extended tetrathiafulvalenes: versatile multifunctional π-systems. *J. Org. Chem.* **2007**, *72*, 1301–1308.

[244] Guerro, M.; Lorcy, D. A simple route to novel functionalized tetrathiafulvalene vinylogues. *Tetrahedron Lett.* **2005**, *46*, 5499–5502.

[245] Khadem, M.; Walsh, J. C.; Bodwell, G. J.; Zhao, Y. A macrocyclization of 1, 8-bis(dithiafulvenyl)pyrenes. *Org. Lett.* **2016**, *18*, 2403–2406.

[246] Petersen, J. F.; Tortzen, C. G.; Jørgensen, F. P.; Parker, C. R.; Nielsen, M. B. Phosphite-mediated conversion of benzaldehydes into stilbenes via umpolung through a dioxaphospholane intermediate. *Tetrahedron Lett.* **2015**, *56*, 1894–1897.

[247] Ho, P. C.; Wang, J. Z.; Meloni, F.; Vargas-Baca, I. Chalcogen bonding in materials chemistry. *Coord. Chem. Rev.* **2020**, *422*, 213464.

[248] Kolb, S.; Oliver, G. A.; Werz, D. B. Chemistry evolves, terms evolve, but phenomena do not evolve: from chalcogen–chalcogen interactions to chalcogen bonding. *Angew. Chem.* **2020**, *59*, 22306–22310.

[249] D'Andrade, B. W.; Datta, S.; Forrest, S. R.; Djurovich, P.; Polikarpov, E.; Thompson, M. E. Relationship between the ionization and oxidation potentials of molecular organic semiconductors. *Org. Electron.* **2005**, *6*, 11–20.

[250] Shanmugaraju, S.; Mukherjee, P. S. π-Electron rich small molecule sensors for the recognition of nitroaromatics. *Chem. Commun.* **2015**, *51*, 16014–16032.

[251] D'Andrade, B. W.; Datta, S.; Forrest, S. R.; Djurovich, P.; Polikarpov, E.; Thompson, M. E. Relationship between the ionization and oxidation potentials of molecular organic semiconductors. *Org. Electron* **2005**, *6*, 11–20.

[252] Yao, Z.-F.; Wang, J.-Y.; Pei, J. Control of π–π stacking via crystal engineering in organic conjugated small molecule crystals. *Cryst. Growth Des.* **2018**, *18*, 7–15.

[253] Mas-Torrent, M.; Rovira, C. Role of molecular order and solid-state structure in organic field-effect transistors. *Chem. Rev.* **2011**, *111*, 4833–4856.

[254] Abdollahi, M. F.; Zhao, Y. Recent advances in dithiafulvenyl-functionalized organic conjugated materials. *New J. Chem.* **2020**, *44*, 4681–4693.

[255] Katz, E.; Shipway, A. N.; Willner, I. *Nanoscale Mater.*; Springer, 2004; pp 5–78.

[256] Lorcy, D.; Guérin, D.; Boubekeur, K.; Carlier, R.; Hascoat, P.; Tallec, A.; Robert, A. Electrochemical oxidative coupling of 1, 4-bis (1, 4-dithiafulven-6-yl) benzene cyclophanes. *J. Chem. Soc., Perkin Trans. 1* **2000**, 2719–2723.

[257] Hapiot, P.; Lorcy, D.; Tallec, A.; Carlier, R.; Robert, A. Mechanism of

dimerization of 1,4-dithiafulvenes into TTF vinylogues. *J. Phys. Chem.* **1996**, *100*, 14823–14827.

[258] Zhao, Y.; Chen, G.; Mulla, K.; Mahmud, I.; Liang, S.; Dongare, P.; Thompson, D. W.; Dawe, L. N.; Bouzan, S. Tetrathiafulvalene vinylogues as versatile building blocks for new organic materials. *Pure Appl. Chem.* **2012**, *84*, 1005–1025.

[259] Bendikov, M.; Wudl, F.; Perepichka, D. F. Tetrathiafulvalenes, oligoacenenes, and their buckminsterfullerene derivatives: The brick and mortar of organic electronics. *Chem. Rev.* **2004**, *104*, 4891–4946.

[260] Segura, J. L.; Martín, N. New concepts in tetrathiafulvalene chemistry. *Angew. Chem. Int. Ed.* **2001**, *40*, 1372–1409.

[261] Liang, S.; Chen, G.; Peddle, J.; Zhao, Y. Reversible dispersion and releasing of single-walled carbon nanotubes by a stimuli-responsive TTFV-phenylacetylene polymer. *Chem. Commun.* **2012**, *48*, 3100–3102.

[262] Chen, G.; Mahmud, I.; Dawe, L. N.; Zhao, Y. Acetylenic phenyldithiafulvene: a versatile synthon for TTFV-based macromolecules. *Org. Lett.* **2010**, *12*, 704–707.

[263] Goeb, S.; Sallé, M. Electron-rich coordination receptors based on tetrathiafulvalene derivatives: controlling the host–guest binding. *Acc. Chem. Res.* **2021**, *54*, 1043–1055.

[264] Liang, S.; Zhao, Y.; Adronov, A. Selective and reversible noncovalent func-

tionalization of single-walled carbon nanotubes by a pH-responsive vinylogous tetrathiafulvalene–fluorene copolymer. *J. Am. Chem. Soc.* **2014**, *136*, 970–977.

[265] Mulla, K.; Shaik, H.; Thompson, D. W.; Zhao, Y. TTFV-based molecular tweezers and macrocycles as receptors for fullerenes. *Org. Lett.* **2013**, *15*, 4532–4535.

[266] Guerro, M.; Pham, N. H.; Massue, J.; Bellec, N.; Lorcy, D. New redox active ligands involving a tetrathiafulvalene vinylogue backbone. *Tetrahedron* **2008**, *64*, 5285–5290.

[267] Mulla, K.; Zhao, Y. TTFV molecular tweezers with phenylboronic acid and phenylboronate endgroups: modular synthesis and electrochemical responses to saccharides and fluoride ion. *Tetrahedron Lett.* **2014**, *55*, 382–386.

[268] Lorcy, D.; Guerro, M.; Bergamini, J.-F.; Hapiot, P. Vinylogous tetrathiafulvalene based podands: complexation interferences on the molecular movements triggered by electron transfer. *J. Phys. Chem. B.* **2013**, *117*, 5188–5194.

[269] Mulla, K.; Dongare, P.; Thompson, D. W.; Zhao, Y. Click synthesized dianthryl–TTFV: an efficient fluorescent turn-on probe for transition metal ions. *Org. Biomol. Chem.* **2012**, *10*, 2542–2544.

[270] Alías, S.; Andreu, R.; Blesa, M. J.; Franco, S.; Garín, J.; Gragera, A.; Orduna, J.; Romero, P.; Villacampa, B.; Allain, M. Synthesis, structure, and optical properties of 1, 4-dithiafulvene-based nonlinear optic-phores. *J. Org. Chem.* **2007**, *72*, 6440–6446.

[271] Andreu, R.; Aramburo, J.; Cerdán, M. A.; Garín, J.; Orduna, J.; Villacampa, B. Highly polarized dithiafulvenes: synthesis and nonlinear optical properties. *Tetrahedron Lett.* **2006**, *47*, 661–664.

[272] Nielsen, M. B.; Petersen, J. C.; Thorup, N.; Jessing, M.; Andersson, A. S.; Jepsen, A. S.; Gisselbrecht, J.-P.; Boudon, C.; Gross, M. Acetylenic dithiafulvene derived donor–π–acceptor dyads: synthesis, electrochemistry and nonlinear optical properties. *J. Mater. Chem.* **2005**, *15*, 2599–2605.

[273] Moreno-Mañas, M.; Pleixats, R.; Andreu, R.; Garín, J.; Orduna, J.; Villacampa, B.; Levillain, E.; Sallé, M. The first 1,3-dithiol-2-ylidene donor–π–acceptor chromophores containing an azine spacer: synthesis, electrochemical and nonlinear optical properties. *J. Mater. Chem.* **2001**, *11*, 374–380.

[274] Duvva, N.; Chilakamarthi, U.; Giribabu, L. Recent developments in tetrathiafulvalene and dithiafulvalene based metal-free organic sensitizers for dye-sensitized solar cells: a mini-review. *Sustain. Energy Fuels* **2017**, *1*, 678–688.

[275] Shaikh, D. B.; Said, A. A.; Bhosale, R. S.; Chen, W.; Bhosale, S. V.; Puyad, A. L.; Bhosale, S. V.; Zhang, Q. Dithiafulvenyl-naphthalenediimide-based small molecules as efficient non-fullerene electron-transport layer for inverted perovskite solar cells. *J. Org. Chem.* **2018**, *7*, 2294–2301.

[276] Wu, M.; Li, J.; Zhang, R.; Tian, X.; Han, Z.; Lu, X.; Guo, K.; Liu, Z.; Wang, Z. Synthesis and properties of dithiafulvenyl functionalized spiro[fluorene-9, 9-xanthene] molecules. *Org. Lett.* **2018**, *20*, 780–783.

[277] Luo, J.; Wan, Z.; Jia, C.; Wang, Y.; Wu, X.; Yao, X. Co-sensitization of dithiafulvenyl-phenothiazine based organic dyes with N719 for efficient dye-sensitized solar cells. *Electrochim. Acta* **2016**, *211*, 364–374.

[278] Zhang, X.; Gou, F.; Zhao, D.; Shi, J.; Gao, H.; Zhu, Z.; Jing, H. π-Spacer effect in dithiafulvenyl-π-phenothiazine dyes for dye-sensitized solar cells. *J. Power Sources* **2016**, *324*, 484–491.

[279] Wan, Z.; Jia, C.; Wang, Y.; Luo, J.; Yao, X. Significant improvement of phenothiazine organic dye-sensitized solar cell performance using dithiafulvenyl unit as additional donor. *Org. Electron.* **2015**, *27*, 107–113.

[280] Guo, K.; Yan, K.; Lu, X.; Qiu, Y.; Liu, Z.; Sun, J.; Yan, F.; Guo, W.; Yang, S. Dithiafulvenyl unit as a new donor for high-efficiency dye-sensitized solar cells: synthesis and demonstration of a family of metal-free organic sensitizers. *Org. Lett.* **2012**, *14*, 2214–2217.

[281] Inagi, S.; Naka, K.; Chujo, Y. Functional polymers based on electron-donating TTF and derivatives. *J. Mater. Chem,* **2007**, *17*, 4122–4135.

[282] Shahrokhi, F.; Zhao, Y. A tetrathiafulvalene vinylogue-based double-layer polymer thin film as a highly sensitive and selective TNT sensor. *New J. Chem.* **2019**, *43*, 5277–5281.

[283] Khadem, M.; Zhao, Y. Multivalent dithiafulvenyl functionalization of dendritic oligo (phenylene vinylene) s with an anthraquinodimethane core. *Chem. Commun.* **2017**, *53*, 1821–1824.

[284] Khadem, M.; Walsh, J. C.; Bodwell, G. J.; Zhao, Y. A macrocyclization of 1,8-bis(dithiafulvenyl)pyrenes. *Org. Lett.* **2016**, *18*, 2403–2406.

[285] Khadem, M.; Zhao, Y. Tetrathiafulvalene vinylogue–fluorene co-oligomers: synthesis, properties, and supramoleclar interactions with carbon nanotubes. *J. Org. Chem.* **2015**, *80*, 7419–7429.

[286] Chen, G.; Mahmud, I.; Dawe, L. N.; Daniels, L. M.; Zhao, Y. Synthesis and properties of conjugated oligoyne-centered π-extended tetrathiafulvalene analogues and related macromolecular systems. *J. Org. Chem.* **2011**, *76*, 2701–2715.

[287] González, S.; Martín, N.; Sánchez, L.; Segura, J. L.; Seoane, C.; Fonseca, I.; Cano, F. H.; Sedó, J.; Vidal-Gancedo, J.; Rovira, C. Synthesis, X-ray structure, and electrochemical oxidative coupling reactions of 1,5-and 2,6-bis(1,4-dithiafulven-6-yl)naphthalenes. *J. Org. Chem.* **1999**, *64*, 3498–3506.

[288] Naka, K.; Uemura, T.; Chujo, Y. π-Conjugated poly(dithiafulvene) by cycloaddition polymerization of aldothioketene with its alkynethiol tautomer. Polymerization, optical properties, and electrochemical analysis. *Macromolecules* **1999**, *32*, 4641–4646.

[289] Salami, F.; Zhao, Y. Synthesis and characterization of bis(dithiafulvenyl)-substituted fluorenones and fluorenylidene-1, 3-dithioles. *New J. Chem.* **2020**, *44*, 9179–9189.

[290] Wang, Y.; Zhao, Y. Dithiafulvenyl-substituted phenylacetylene derivatives:

synthesis and structure–property–reactivity relationships. *Org. Biomol. Chem.* **2015**, *13*, 9575–9579.

[291] Massue, J.; Ghilane, J.; Bellec, N.; Lorcy, D.; Hapiot, P. Facile electrochemical generation of polyoxyethyl-vinylogous tetrathiafulvalene films. *Electrochem. Commun.* **2007**, *9*, 677–682.

[292] Massue, J.; Bellec, N.; Guerro, M.; Bergamini, J.-F.; Hapiot, P.; Lorcy, D. Crown ether vinylogous tetrathiafulvalene receptors: Complexation interference on the molecular movements triggered by electron transfer. *J. Org. Chem.* **2007**, *72*, 4655–4662.

[293] Christensen, C. A.; Batsanov, A. S.; Bryce, M. R. Thiolated π-extended tetrathiafulvalenes: Versatile multifunctional π-systems. *J. Org. Chem.* **2007**, *72*, 1301–1308.

[294] Ali, Q.; Raza Shah, M.; Ng, S. W. 4, 4-(Propane-1, 3-diyldioxy) dibenzaldehyde. *Acta Crystallogr.* **2010**, *66*, o1620–o1620.

[295] Vogel, L.; Wonner, P.; Huber, S. M. Chalcogen bonding: An overview. *Angew. Chem. Int. Ed.* **2019**, *58*, 1880–1891.

[296] Pascoe, D. J.; Ling, K. B.; Cockroft, S. L. The origin of chalcogen-bonding interactions. *J. Am. Chem. Soc.* **2017**, *139*, 15160–15167.

[297] Vogel, L.; Wonner, P.; Huber, S. M. Chalcogen bonding: An overview. *Angew. Chem. Inter. Ed.* **2019**, *58*, 1880–1891.

[298] Pascoe, D. J.; Ling, K. B.; Cockroft, S. L. The origin of chalcogen-bonding interactions. *J. Am. Chem. Soc.* **2017**, *139*, 15160–15167.

[299] Zhao, Y.; Truhlar, D. G. The M06 suite of density functionals for main group thermochemistry, thermochemical kinetics, noncovalent interactions, excited states, and transition elements: two new functionals and systematic testing of four M06-class functionals and 12 other functionals. *Theor. Chem. Acc.* **2008**, *120*, 215–241.

[300] Weigend, F.; Ahlrichs, R. Balanced basis sets of split valence, triple zeta valence and quadruple zeta valence quality for H to Rn: Design and assessment of accuracy. *Phys. Chem. Chem. Phys.* **2005**, *7*, 3297–3305.

[301] Woolridge, K.; Goncalves, L. C.; Bouzan, S.; Chen, G.; Zhao, Y. Aryl-substituted dithiafulvenes: synthesis, electronic properties, and redox reactivity. *Tetrahedron Lett.* **2014**, *55*, 6362–6366.

[302] Evans, D. H.; Hu, K. Inverted potentials in two-electron processes in organic electrochemistry. *J. Chem. Soc., Faraday Trans.* **1996**, *92*, 3983–3990.

[303] Macías-Ruvalcaba, N. A.; Evans, D. H. Studies of potential inversion in the electrochemical reduction of 11,11,12,12-tetracyano-9,10-anthraquinodimethane and 2,3,5,6-tetramethyl-7,7,8,8-tetracyano-1,4-benzoquinodimethane. *J. Phys. Chem. B* **2006**, *110*, 5155–5160.

[304] Shahrokhi, F.; Zhao, Y. A tetrathiafulvalene vinylogue-based double-layer polymer thin film as a highly sensitive and selective TNT sensor. *New J. Chem.* **2019**, *43*, 5277–5281.

[305] Liu, S.; Wang, J.; Huang, W.; Tan, X.; Dong, H.; Goodman, B. A.; Du, H.; Lei, F.; Diao, K. Adsorption of phenolic compounds from water by a novel ethylenediamine rosin-based resin: interaction models and adsorption mechanisms. *Chemosphere* **2019**, *214*, 821–829.

[306] Adav, S. S.; Chen, M.-Y.; Lee, D.-J.; Ren, N.-Q. Degradation of phenol by Acinetobacter strain isolated from aerobic granules. *Chemosphere* **2007**, *67*, 1566–1572.

[307] Balasundram, N.; Sundram, K.; Samman, S. Phenolic compounds in plants and agri-industrial by-products: Antioxidant activity, occurrence, and potential uses. *Food Chem.* **2006**, *99*, 191–203.

[308] Calace, N.; Nardi, E.; Petronio, B.; Pietroletti, M. Adsorption of phenols by papermill sludges. *Environ. Pollut.* **2002**, *118*, 315–319.

[309] Fu, S.; Zhu, Y.; Zhang, Y.; Zhang, M.; Zhang, Y.; Qiao, L.; Yin, N.; Song, K.; Liu, M.; Wang, D. Recent advances in carbon nanomaterials-based electrochemical sensors for phenolic compounds detection. *Microchem. J.* **2021**, *171*, 106776.

[310] Ge, L.; Li, S.-P.; Lisak, G. Advanced sensing technologies of phenolic compounds for pharmaceutical and biomedical analysis. *J. Pharm. Biomed. Anal.* **2020**, *179*, 112913.

[311] Vasilescu, A.; Fanjul-Bolado, P.; Titoiu, A.-M.; Porumb, R.; Epure, P. Progress in electrochemical (bio)sensors for monitoring wine production. *Chemosensors* **2019**, *7*, 66.

[312] Forzato, C.; Vida, V.; Berti, F. Biosensors and sensing systems for rapid analysis of phenolic compounds from plants: A comprehensive review. *Biosensors* **2020**, *10*, 105.

[313] Zhang, X.; Gong, Z.; Li, J.; Lu, T. Intermolecular sulfur··· oxygen interactions: theoretical and statistical investigations. *J. Chem. Inf. Model.* **2015**, *55*, 2138–2153.

[314] Saeed, A.; Qasim, M.; Hussain, M. Novel bis(2-(5-((5-phenyl-1H-tetrazol-1-yl)methyl)-4H-1,2,4-triazol-3-yl) phenoxy) alkanes: synthesis and characterization. *J. Heterocycl. Chem.* **2015**, *52*, 1114–1118.

[315] Dolomanov, O.; Bourhis, L.; Gildea, R.; Howard, J.; Puschmann, H. SHELXT–integrated space-group and crystal-structure determination. *J. Appl. Crystallogr.* **2009**, *42*, 339–341.

[316] Sheldrick, G. M. SHELXT–integrated space-group and crystal-structure determination. *Acta Crystallogr. A* **2015**, *71*, 3–8.

[317] Sheldrick, G. M. Crystal structure refinement with SHELXL. *Acta Crystallogr. C* **2015**, *71*, 3–8.

[318] Frisch, M. J. et al. Gaussian 16 Revision B.01. 2016; Gaussian Inc. Wallingford CT.

[319] Lu, T.; Chen, F. Multiwfn: a multifunctional wavefunction analyzer. *J. Comput. Chem.* **2012**, *33*, 580–592.

[320] Humphrey, W.; Dalke, A.; Schulten, K. VMD: visual molecular dynamics. *J. Mol. Graph.* **1996**, *14*, 33–38.